ATMOSPHERIC MICROWAVE REFRACTIVITY AND REFRACTION

Eunyoung Yu and D.B. Hodge

Technical Report 712759-1

December 1980

Contract NASW-3393

National Aeronautics and Space Administration Headquarters
Washington, D.C. 20546

TABLE OF CONTENTS

LIST OF TABLES

LIST OF FIGURES

CHAPTER I

INTRODUCTION

Chapter One presents the background and overview of this study. A brief review of the lower atmosphere and its electrical parameter, the complex microwave refractivity, will be given.

A. Overview

As the use of the electromagnetic spectrum has expanded beyond ten GHz, a number of theoretical and experimental studies on the effect of the atmosphere on propagating waves have been performed, and the atmosphere has been found to have a strong influence in this portion of the spectrum. In this high frequency region, the refractive index of the atmosphere can no longer be regarded as a frequency independent quantity in discussions of its influence on radio wave propagation. Microwave signals travelling along atmospheric paths undergo attenuation and refraction due to absorption by atmospheric gases and variations in the refractive index, respectively. After Van Vlecks's pioneering work on microwave absorption theory (1); several models were introduced to develop the microwave refractivity of the clear sky. Based on these works, the microwave refractivity is highly dependent on temperature, pressure, and

and water vapor content which, in turn, are random functions of time and space.

The design of reliable earth-space and terrestrial communication links requires estimates of the deterministic and random changes of these atmospheric effects on radio wave propagation.

Using the extensive meteorological data base available from the National Weather Service, the diurnal and seasonal variability of the surface microwave refractivity has been determined at Columbus, Ohio. The results of this effort make it possible to estimate the variability of the absorption due to atmospheric gases and the refraction effects for a standard atmosphere.

In the following, a standard exponentially tapered atmosphere is assumed and the effects of turbulence are ignored.

B. Atmosphere

The atmosphere that surrounds the earth is a mechanical mixture of many gases. Although the atmosphere is composed of a number of gases, five of them - nitrogen, oxygen, argon, carbon dioxide, and water vapor - make up 99.997 percent of it by volume below 90 km.

A complete description of the physical state of the atmosphere at any moment requires the measurement of dozens of quantities. The analysis of weather is usually centered on several variable characteristics of the atmosphere near the earth's surface: temperature, pressure, humidity, cloud, precipitation, and winds. Among these characteristics temperature, pressure, and humidity are major factors in the determination of the refractive index. Figure 1 shows the vertical distributions of

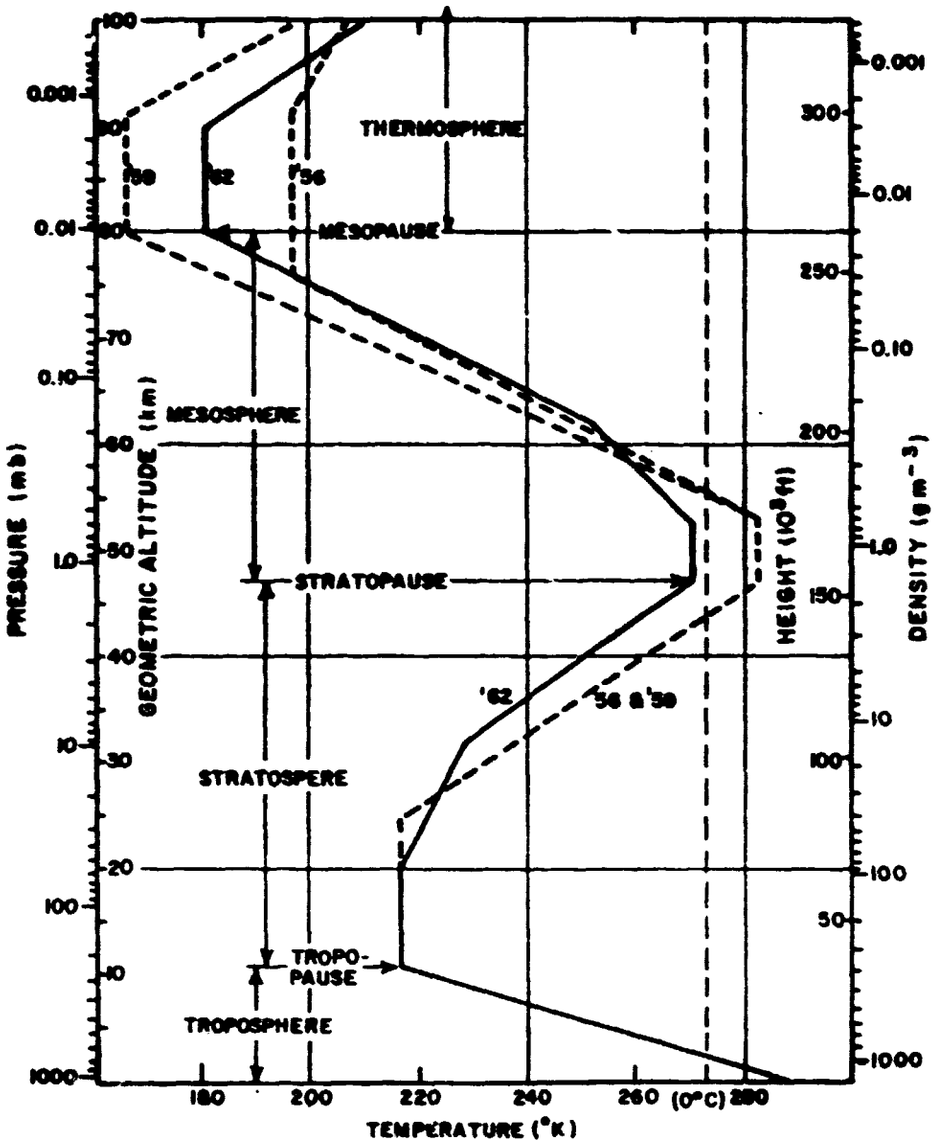

Figure 1. Characteristics of U.S. Standard Atmosphere, 1962, compared to those of ARDC Model Atmospheres, 1956 and 1959. (The 1956 Model agrees with the 1954 "U.S. Extension to the ICAO Standard Atmosphere".) The names shown for atmospheric shells and boundaries are those adopted by the World Meteorological Organization.

temperature, pressure, and density for the U.S. Standard Atmosphere.

1. Temperature

Temperature is a measure of kinetic energy of the molecules present in the air. Temperature varies widely from place to place over the earth's surface as well as through time at a given place. There are two major periodic changes in temperature: the annual and the diurnal.

As shown in Figure 1, the temperature normally decreases with height in the troposphere. An approximate formula which describes the temperature-height dependence in the troposphere is (2):

$$\begin{aligned} T &= 229 - 6.55z \ [°k] \quad ; \quad 0 < h < 11.6 \text{ km} \\ &= 233 \ [°k] \quad ; \quad 11.6 < h < 20 \text{ km} \end{aligned} \qquad (1\text{-}1.1)$$

Where T = temperature at z

z = height above mean sea level [km]

2. Pressure

The pressure exerted at any level is due almost entirely to the weight of the air pressing down from above; this force results from gravitational attraction. As would be expected, the pressure changes rapidly in the vertical direction. The rate of its change is greatest near the surface and decreases at a decreasing rate with height. The pressure-height dependence can be approximated by an exponential law (3):

$$P = P_o \exp[-z/H] \quad [\text{mbar}] \qquad (1\text{-}1.2)$$

Where,
P = total pressure at altitude, z,
P_o = sea level pressure averaged over the earth
$\approx$ 1,013 [mbar]

H = scale height
  ≈ 7 [km]
z = height above mean sea level [km]

Variations of pressure in the horizontal are much smaller than those in the vertical. Near sea level, the change of pressure with distance rarely exceeds 3 mb per 100 km and usually much less than half of this rate (4). Only in the presence of severe storms or exceptionally well developed masses of cold air does the pressure vary more than three percent from the average. Even though the variation in the horizontal is relatively small, this small change in pressure may change the direction and velocity of the wind and can subsequently lead to temperature and moisture changes.

Pressure also changes with time at a single place. Some of these changes are of an irregular nature, caused by occasional invasions of air having a different mean density. But there is also a quite regular diurnal oscillation of the pressure.

3. Water Vapor

The concentration of water vapor in the atmosphere varies from practically zero to as much as four percent by weight. The vertical profile of the averaged density of water vapor, ρ_ω, can be approximately described by an exponential law (2) in a humid atmosphere,

$$\rho_\omega = 20 \exp [-0.12z] \qquad [gm/m^3] \qquad (1\text{-}1.3)$$

while, for a standard atmosphere,

$$\rho_\omega = 5 - \frac{z}{2} \qquad [gm/m^3] \qquad (1\text{-}1.4)$$

The parameter which is in common use for the representation of the water vapor content of the atmosphere is the relative humidity. The

definition of relative humidity, ν, is:

$$\nu = \frac{e}{e_s} \times 100 \quad [\%] \tag{1-1.5}$$

where e is the partial pressure due to water vapor and e_s is the saturation pressure. Starting with the latent heat of vaporization, an expression for the saturation pressure may be derived with the following result:

$$e_s = 6.11 \exp\left[(6{,}830 - 5.14\,\bar{T})\left(\frac{1}{273} - \frac{1}{\bar{T}}\right)\right] \quad [\text{mbar}] \tag{1-1.6}$$

where $\bar{T}$ is temperature [°k].

C. Refractivity

The mathematical formulation for the electric field $\bar{E}$ of a uniform plane wave propagating in a $\hat{l}$-direction can be written:

$$\bar{E} = \bar{E}_o \exp[-j\hat{k}l] \tag{1-2.1}$$

where $\hat{k}$ is the complex wave number. From Maxwell's equations,

$$\hat{k} = \omega\sqrt{\mu_o \varepsilon_o}\sqrt{\hat{\varepsilon}_r} = \frac{2\pi}{c}\sqrt{\hat{\varepsilon}_r} \tag{1-2.2}$$

where $\hat{\varepsilon}_r$ is the complex relative permittivity. The complex index of refraction of the atmosphere is then given by:

$$\hat{n} = \sqrt{\hat{\varepsilon}_r} = n' - jn'' \tag{1-2.3}$$

where the prime and double prime denote real and imaginary parts, respectively. Usually the complex microwave refractivity, N, is used for convenience in practical applications,

$$N = (\hat{n} - 1)\,10^6 = N' - jN'' \quad [\text{ppm}] \tag{1-2.4}$$

There is another propagation parameter in common use: that is the propagation constant:

$$\gamma = j\hat{k} = \alpha_E + j\beta \tag{1-2.5}$$

where, α_E is the specific attenuation of the electric field and β is the phase constant. From equations (1-2.2), (1-2.4) and (1-2.5),

$$\alpha_E = 0.02096\ fN''\ [\text{neper/km}] \tag{1-2.6}$$

$$\beta = 0.02096\ f(10^6 + N')\ [\text{rad/km}] \tag{1-2.7}$$

where f is in [GHz]. The specific power attenuation, α_p, can be defined as:

$$\alpha_p = 10 \log_{10} \frac{P}{P_o} = 10 \log_{10} \{\exp[0.02096 \times 2fN'']\} = 0.182\ fN''\ [\text{dB/km}] \tag{1-2.8}$$

CHAPTER II

METEOROLOGICAL DATA

The weather data used in this report was measured by the National Weather Service at Columbus, Ohio, from 1948 to 1976. Temperature, pressure, relative humidity, wind, and several other meteorological states were observed every hour during the 1949-1958 period, and every three hours during the 1965-1976 period.

The data are stored on two nine-track tapes. The record format consists of fixed blocks each composed of four equal length logical records. Each logical tape record contains six observations and is 495 bytes long. These records consist of fifteen bytes of identification followed by six observations of eighty bytes each. Records always begin with the Local Standard Time hour of ØØLST, Ø6LST, 12LST, or 18LST. Space is always retained on tape for twenty-four observations/day. When no observation is available, the hour is indicated (two bytes) and all other fields are coded blank.

For more detailed information about the format and coding, the reader is referred to Appendix A.

CHAPTER III

STATISTICS OF TEMPERATURE, PRESSURE, AND WATER VAPOR CONTENT

Columbus, Ohio (10), is located in the area of changeable weather. Air masses from central and northwest Canada frequently invade this region. The tropical Gulf air masses often reach central Ohio during the summer and, to a much less extent, in the fall and winter. There are also occasional weather changes brought about by cool outbreaks from the Hudson Bay region of Canada, especially during the spring months. At infrequent intervals the general circulation will bring showers or snows to Columbus from the Atlantic. Although Columbus does not have a "wet" or "dry" season as such, the month of October has a higher frequency of light rainfall than any other month and comes closest to providing a normal dry period.

In this chapter, the statistics of temperature, pressure, and water vapor content are obtained for two ten-year periods: 1949 through 1958, and 1967 through 1976. Note that the weather data were observed every hour during the 1949-1958 period, and every three hours during the 1967-1976 period.

For each weather variable, the probability density, the average diurnal variation on a monthly basis and the daily maximum, average, minimum, and extremes by months are plotted. The maxima and minima are the averages of each year's highest and lowest values. The extremes are the

extreme values observed during the period specified.

A. Temperature

Since the transient periods between summer and winter are relatively short and the two seasons are distinctive, the probability density functions of temperature have a bimodal frequency curve with two maxima at about 31°F and 70°F (see Figures 2 and 3). The diurnal variations of temperature during summer are greater than those of winter (see Figures 4 and 5). But the fluctuation during winter is a little greater than that during summer (see Figures 6 and 7). In all cases, the temperature reaches its minimum value near local sunrise and its maximum at about 3:00 p.m. local time.

B. Pressure

The probability density function has the shape of Gaussian distribution (Figures 8 and 9), and has a peak at 987.14 [mb] in both periods. This value is slightly higher than the value of 978 [mb] predicted by Equation (1-1.2) for the observing station height of 247 [m] above mean sea level.

For the 1949-1958 period, the average is 987.2 [mb], the highest is 1015.62 [mb], and the lowest is 949.24 [mb]. For the period 1967-1976, the average is 987.5 [mb], the highest is 1013.25 [mb], and the lowest is 953.65 [mb].

Figures 10 and 11 show that the diurnal variation of pressure is quite small. But it is interesting to note that there is a quite regular diurnal oscillation of the pressure that causes, on the average, two maxima (at about 10:00 a.m. and 10:00 p.m.) and two minima (at about

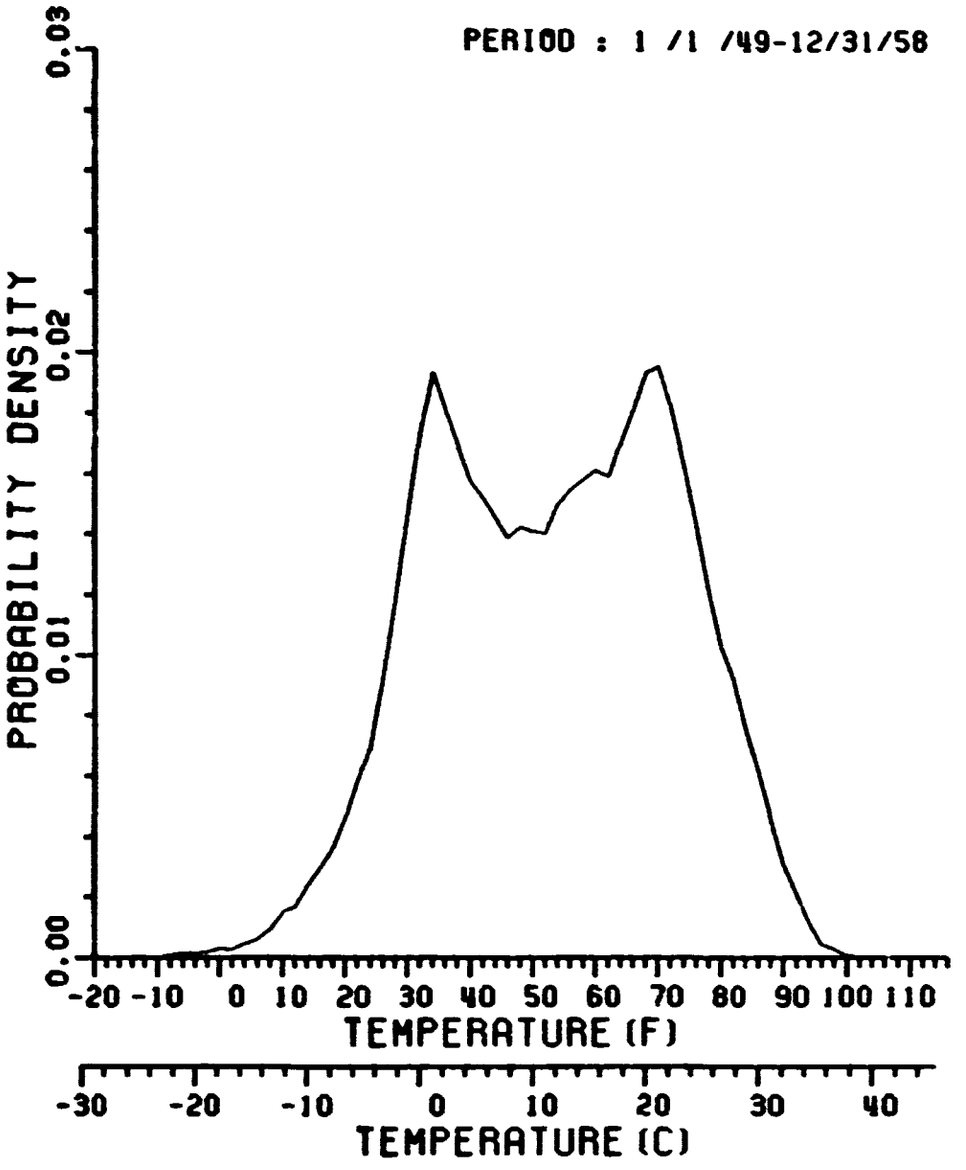

Figure 2. Probability density function of temperature for the period 1949-1958; $\Delta T = 2[°F]$.

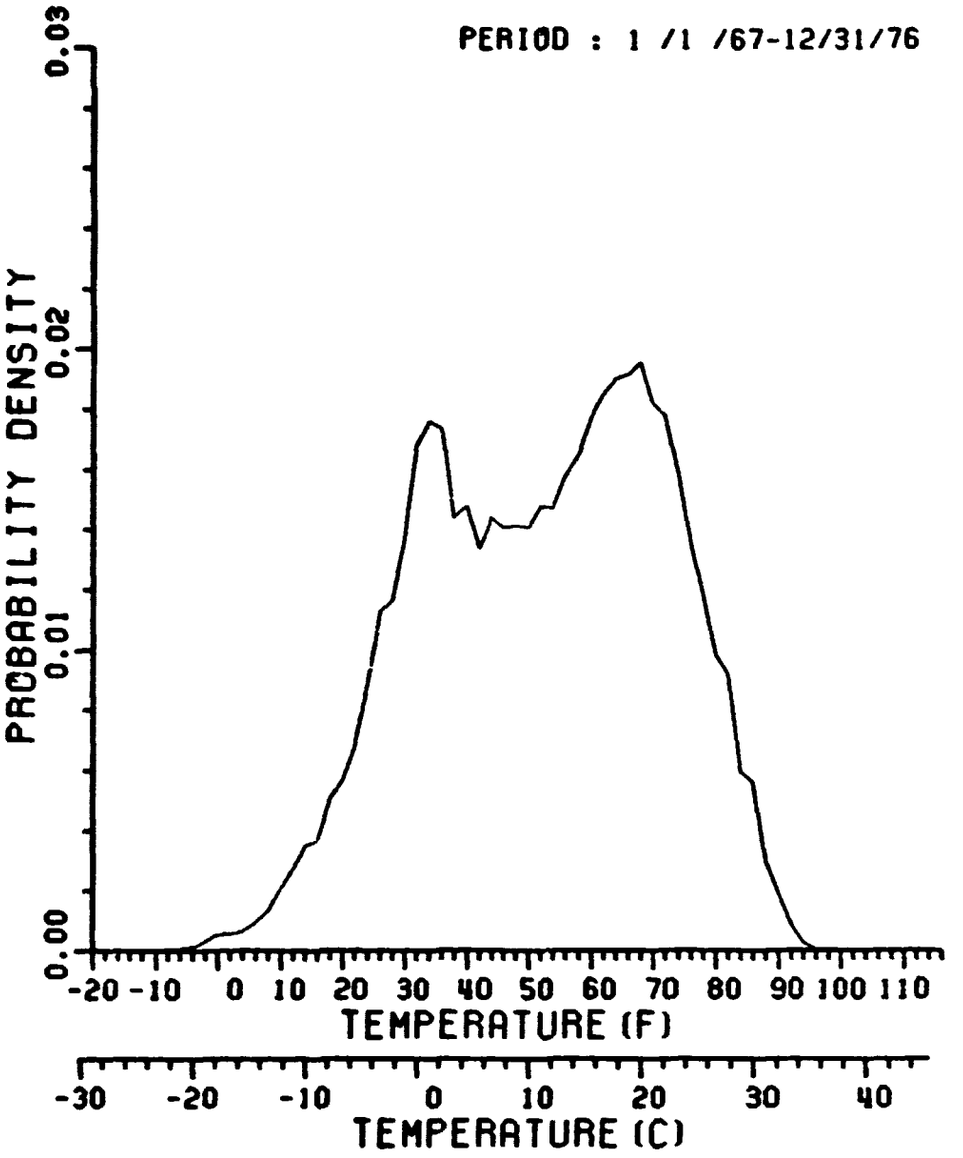

Figure 3. Probability density function of temperature for the period 1967-1976; $\Delta T = 2[°F]$.

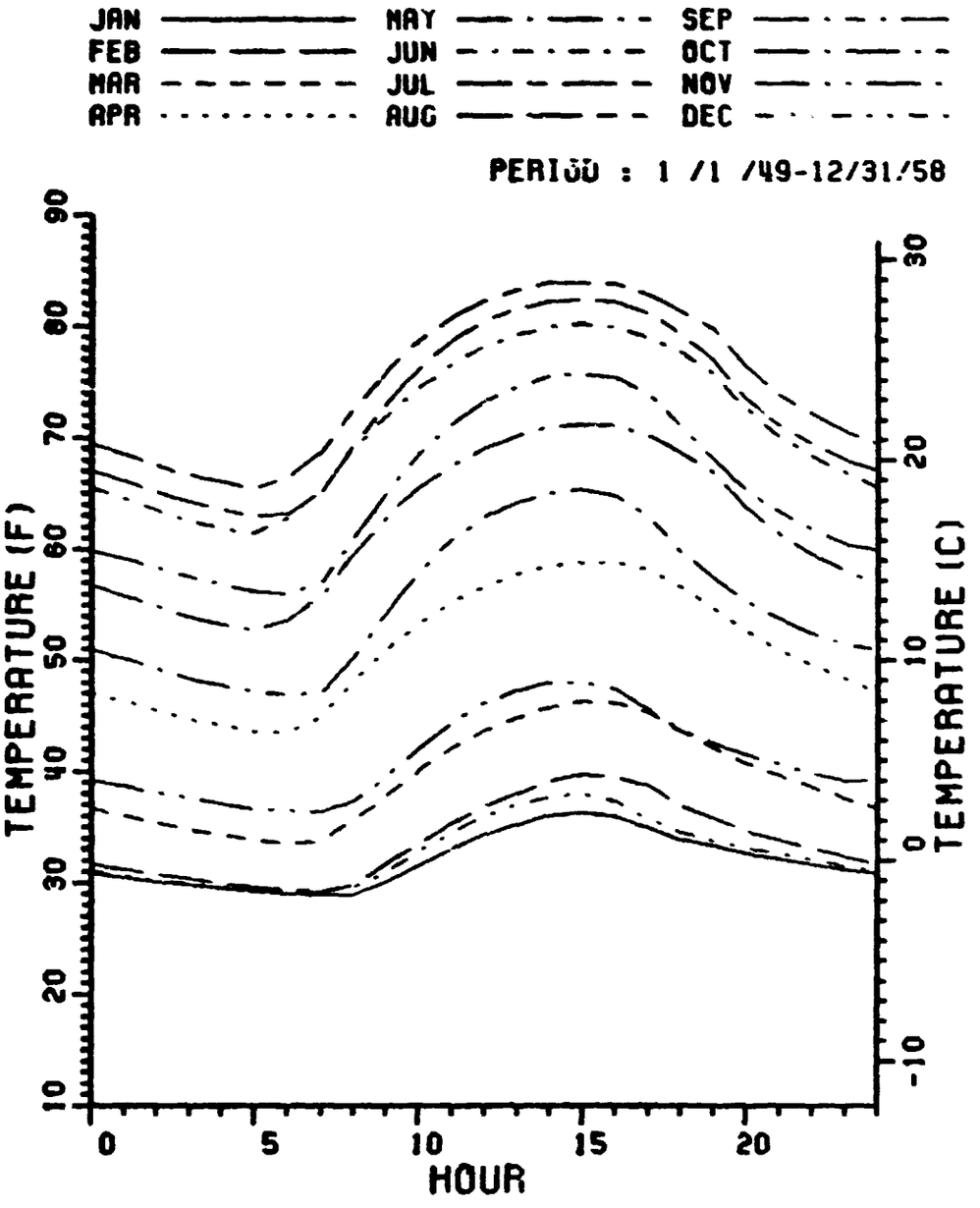

Figure 4. Average diurnal variation of temperature for the period 1949-1958.

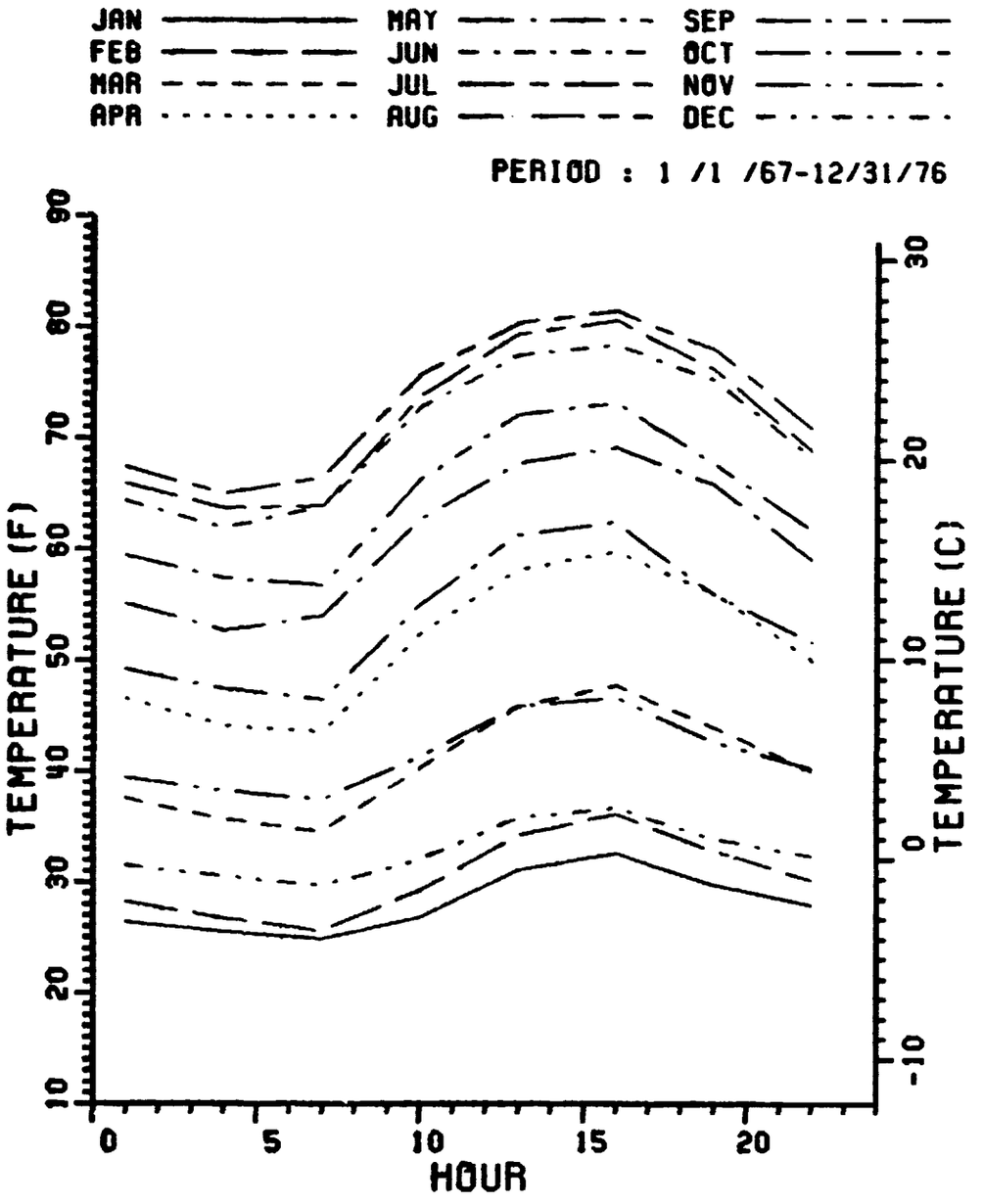

Figure 5. Average diurnal variation of temperature for the period 1967-1976.

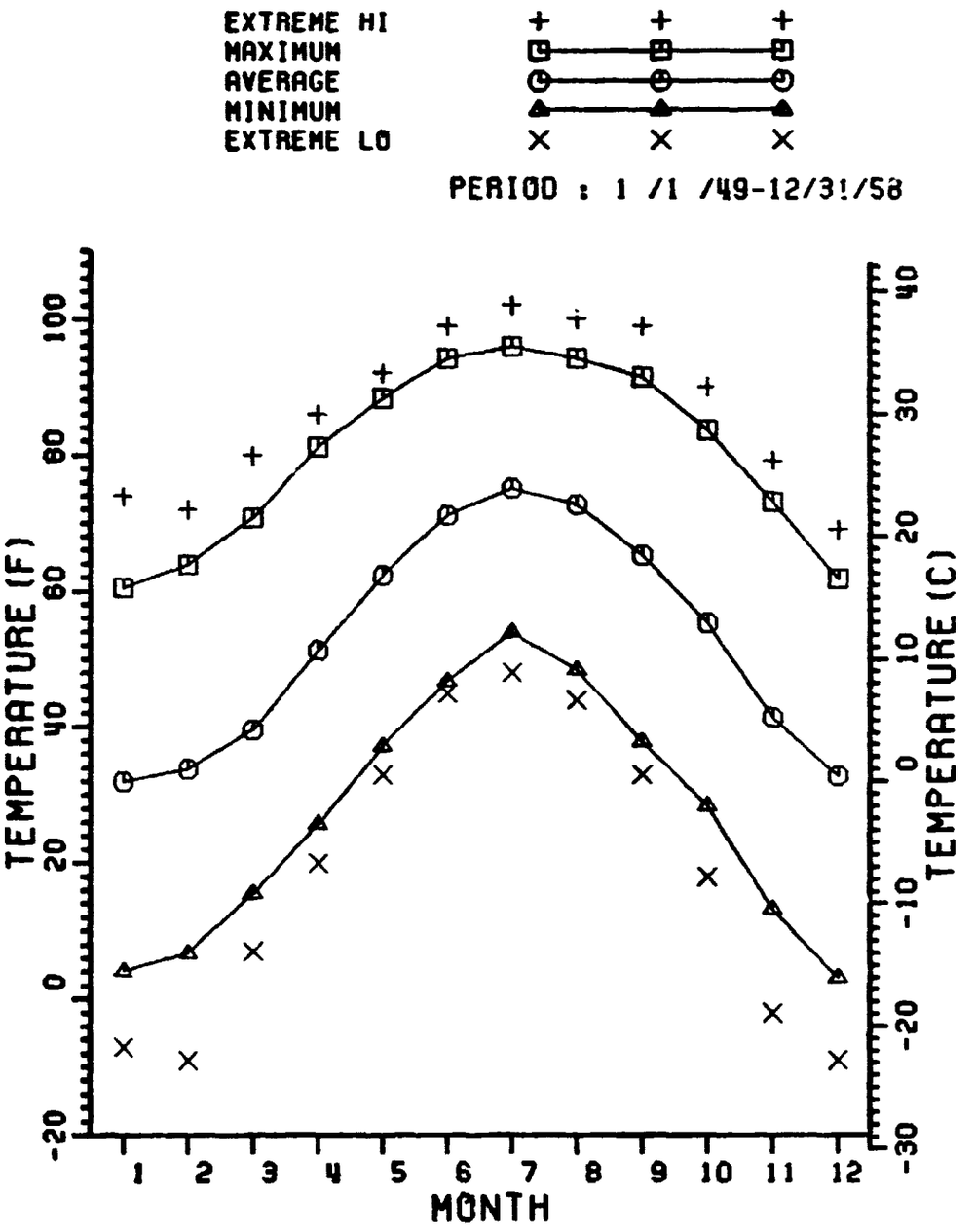

Figure 6. Daily maximum, average, minimum, and extreme temperature by months for the period 1949-1958.

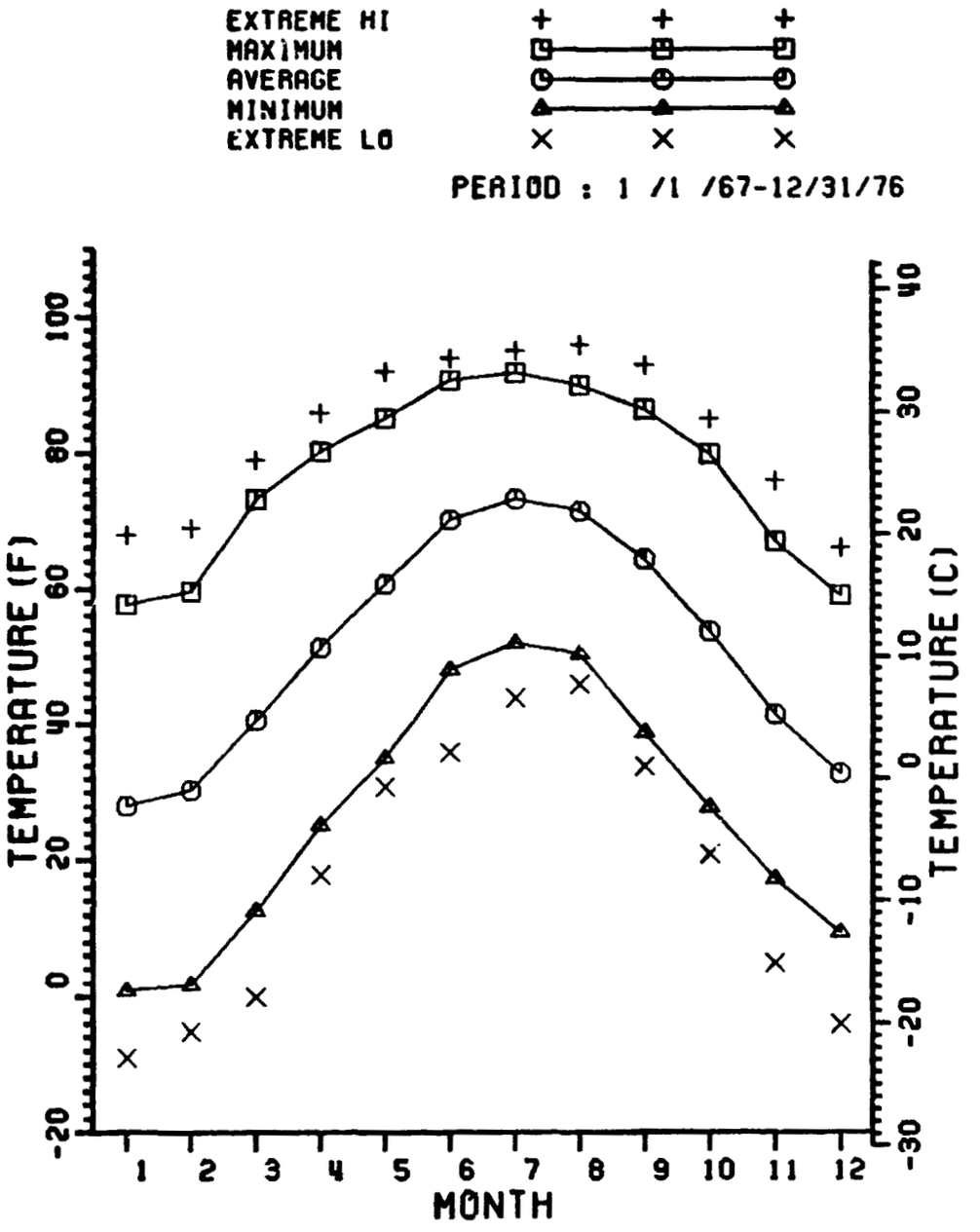

Figure 7. Daily maximum, average, minimum, and extreme temperature by months for the period 1967-1976.

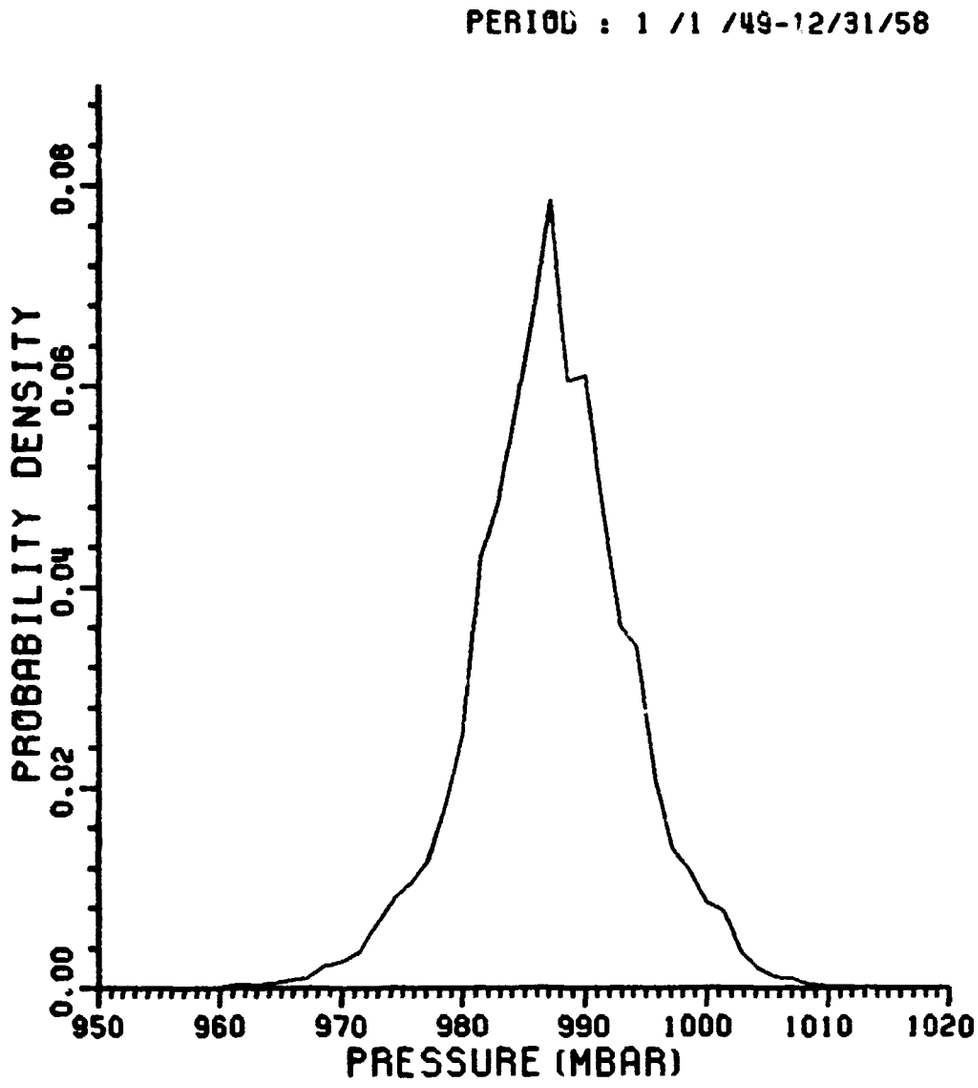

Figure 8. Probability density function of pressure for the period 1949-1958; $\Delta p = 1.43$ [mbar].

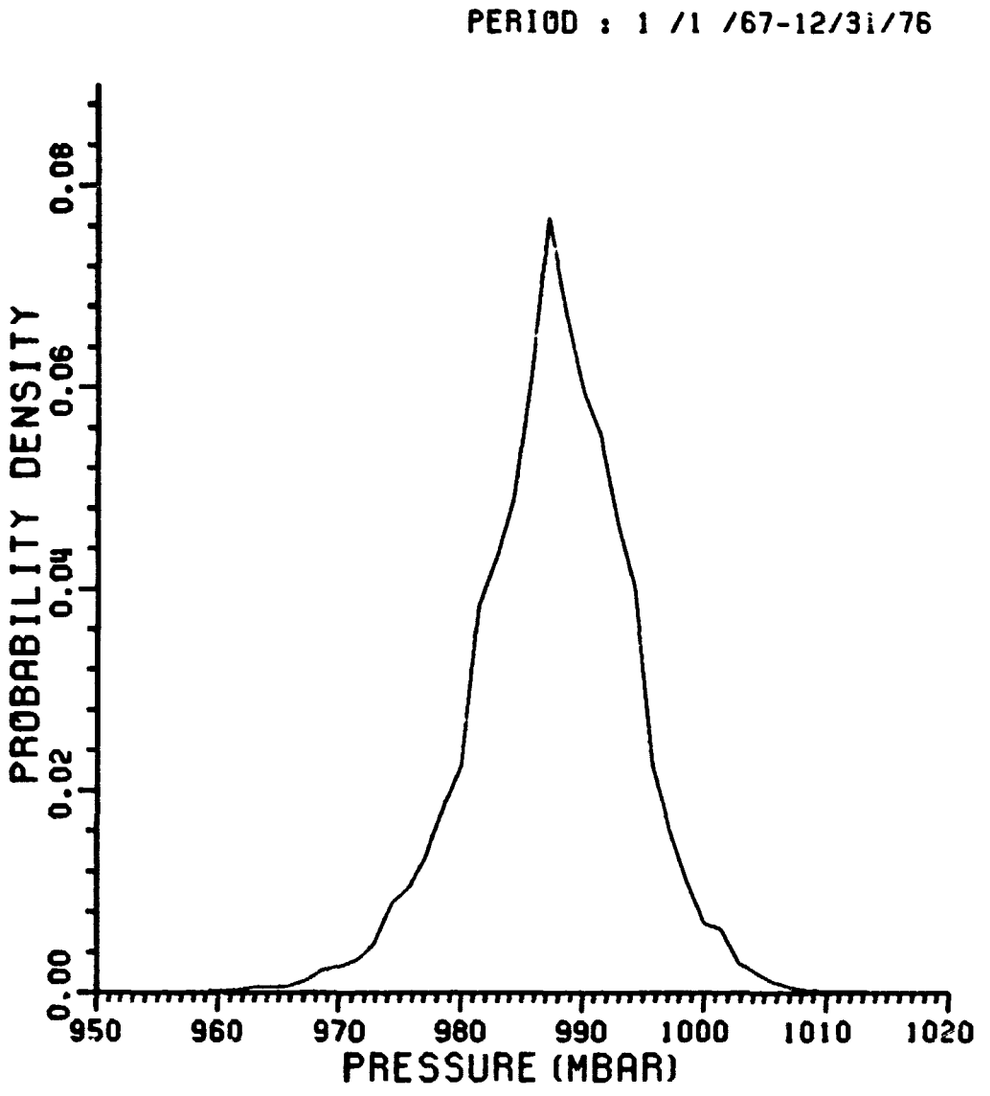

Figure 9. Probability density function of pressure for the period 1967-1976; $\Delta P = 1.43$ [mbar].

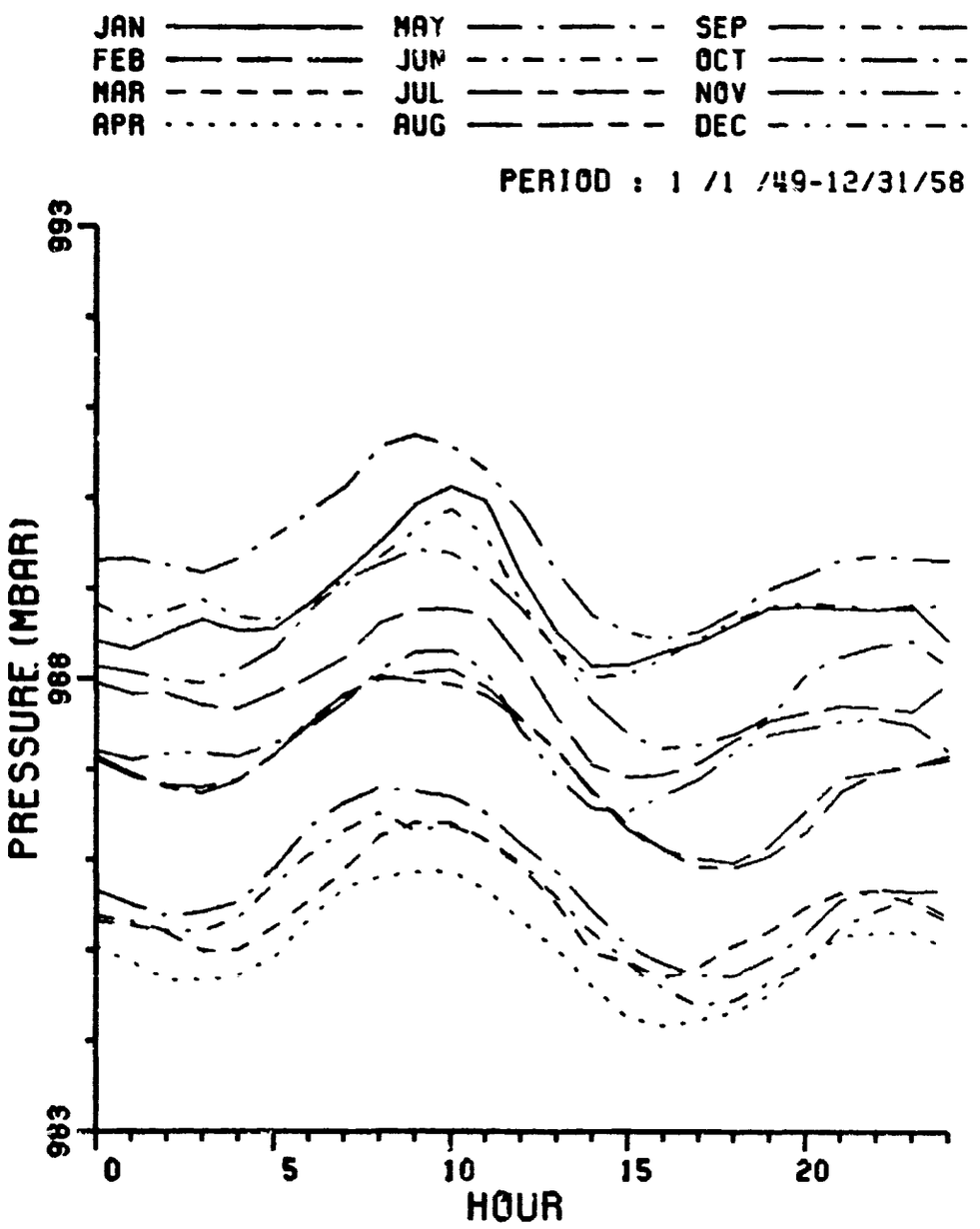

Figure 10. Average diurnal variation of pressure for the period 1949-1958.

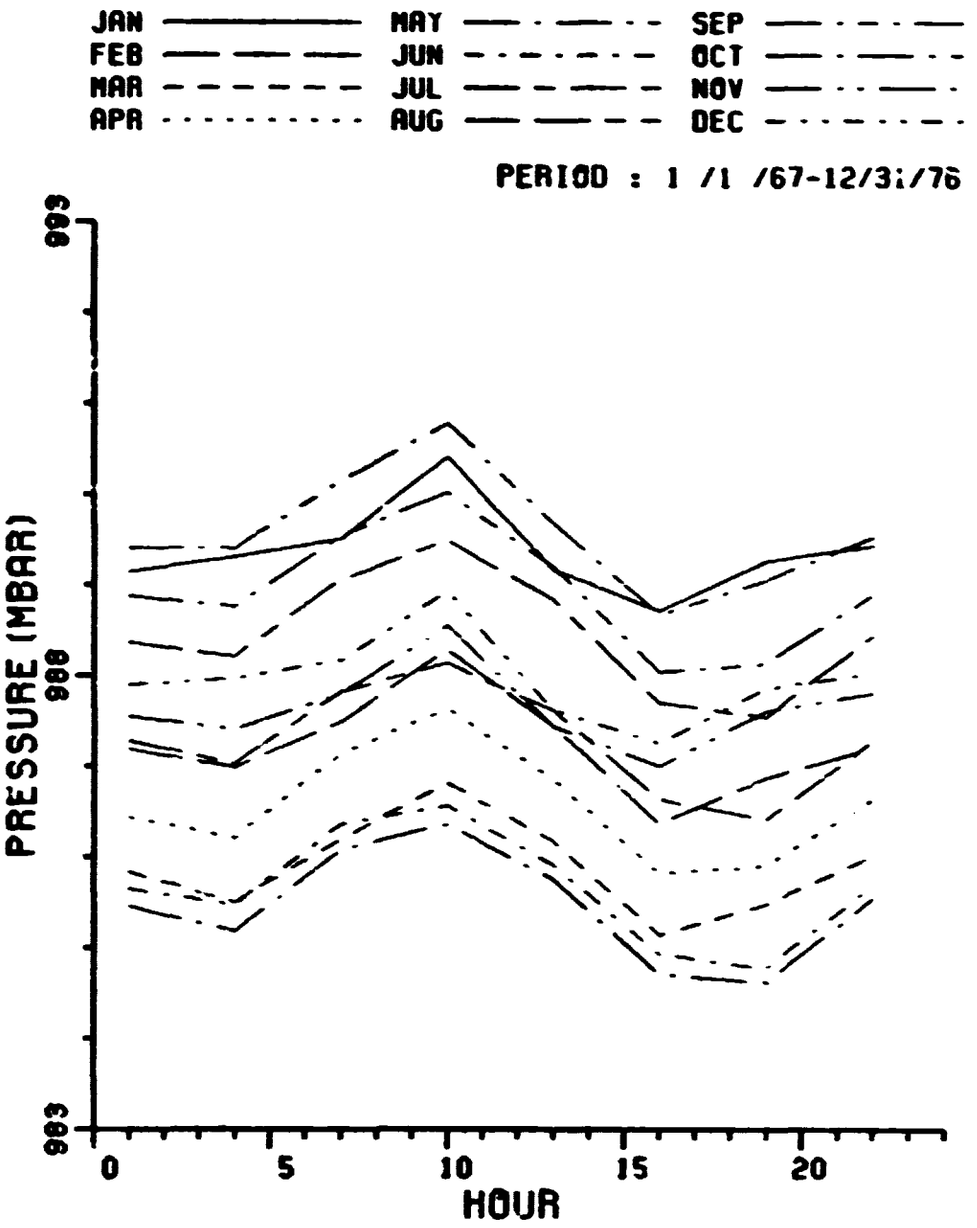

Figure 11. Average diurnal variation of pressure for the period 1967-1976.

4:00 a.m. and 4:00 p.m.). The daily heating and cooling cycle appears to be the dominant cause of the pressure variations. And, the pressure during the spring season tends to be lower than that during the autumn season.

Even though the average pressure does not vary much seasonally, the degree of fluctuation of pressure is dependent on the season (see Figures 12 and 13). The fluctuation of pressure during winter is much greater than during summer.

C. Water Vapor Content

The probability density functions of the relative humidity (Figures 14 and 15) show a strong bias toward values of high relative humidity. The diurnal variation is small during the winter season and large during the summer season (Figures 16 and 17), but the monthly average is the highest in January and December (Figures 18 and 19).

Since the water vapor pressure is dependent on temperature (Equation 1-1.3 and 1-1.4), the shape of its density function (Figures 20 and 21) is quite different from that of relative humidity. The water vapor pressure doesn't vary diurnally, but the monthly average shows a strong seasonal dependence (Figures 22, 23, 24, 25). The average in July is about 20 [mb], and the average in January is about 5 [mb].

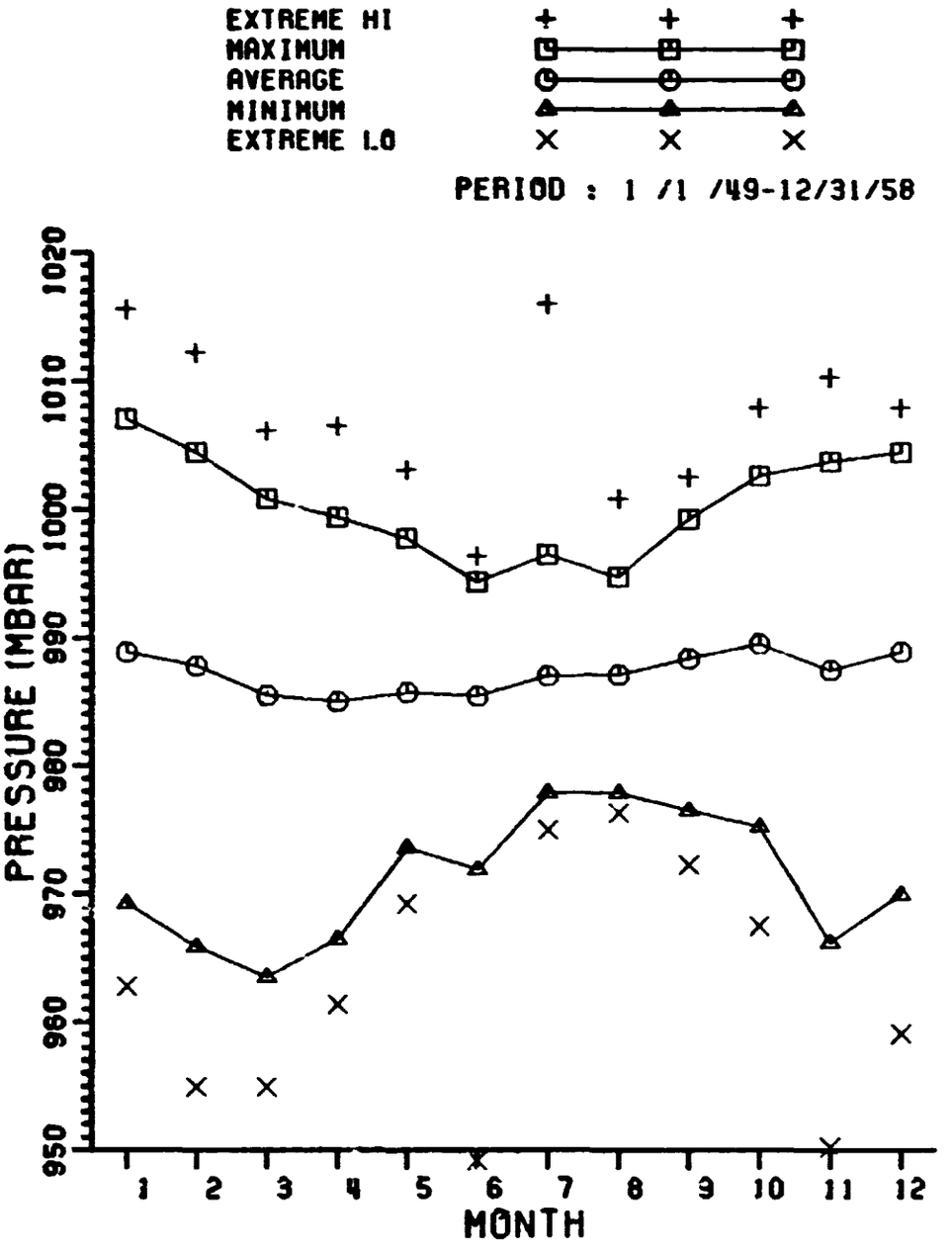

Figure 12. Daily maximum, average, minimum, and extreme pressure by months for the period 1949-1958.

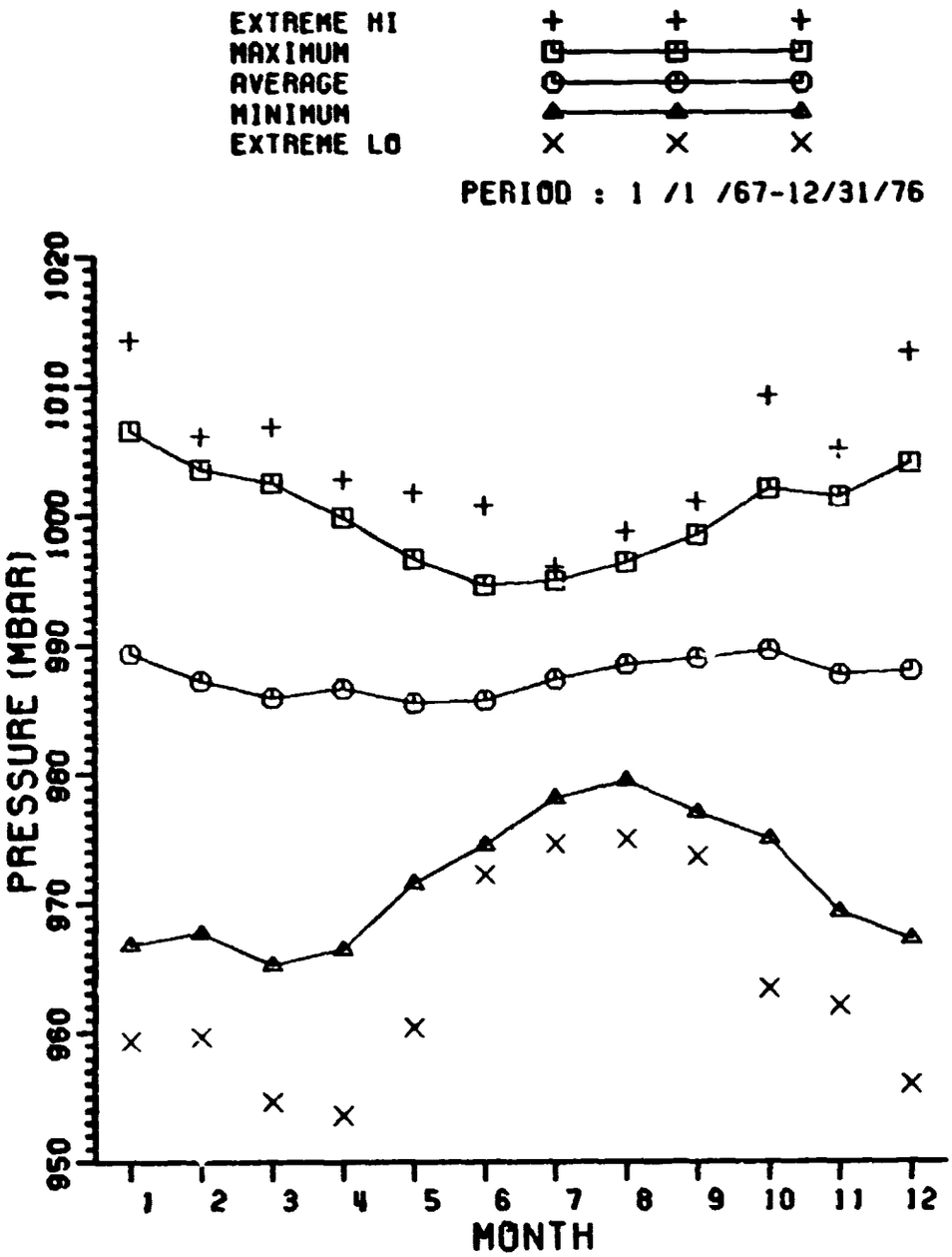

Figure 13. Daily maximum, average, minimum, and extreme pressure by months for the period 1967-1976.

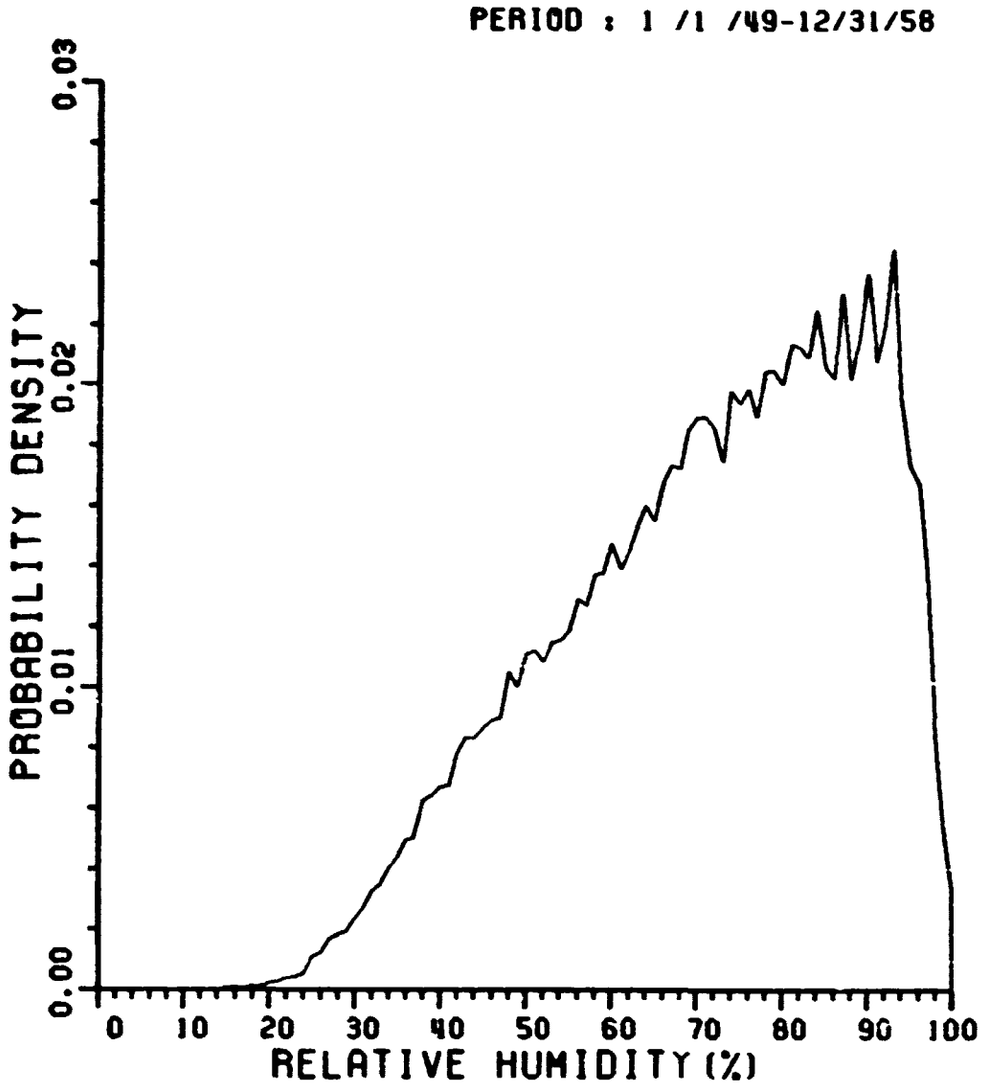

Figure 14. Probability density function of relative humidity for the period 1949-1958; $\Delta v = 1[\%]$.

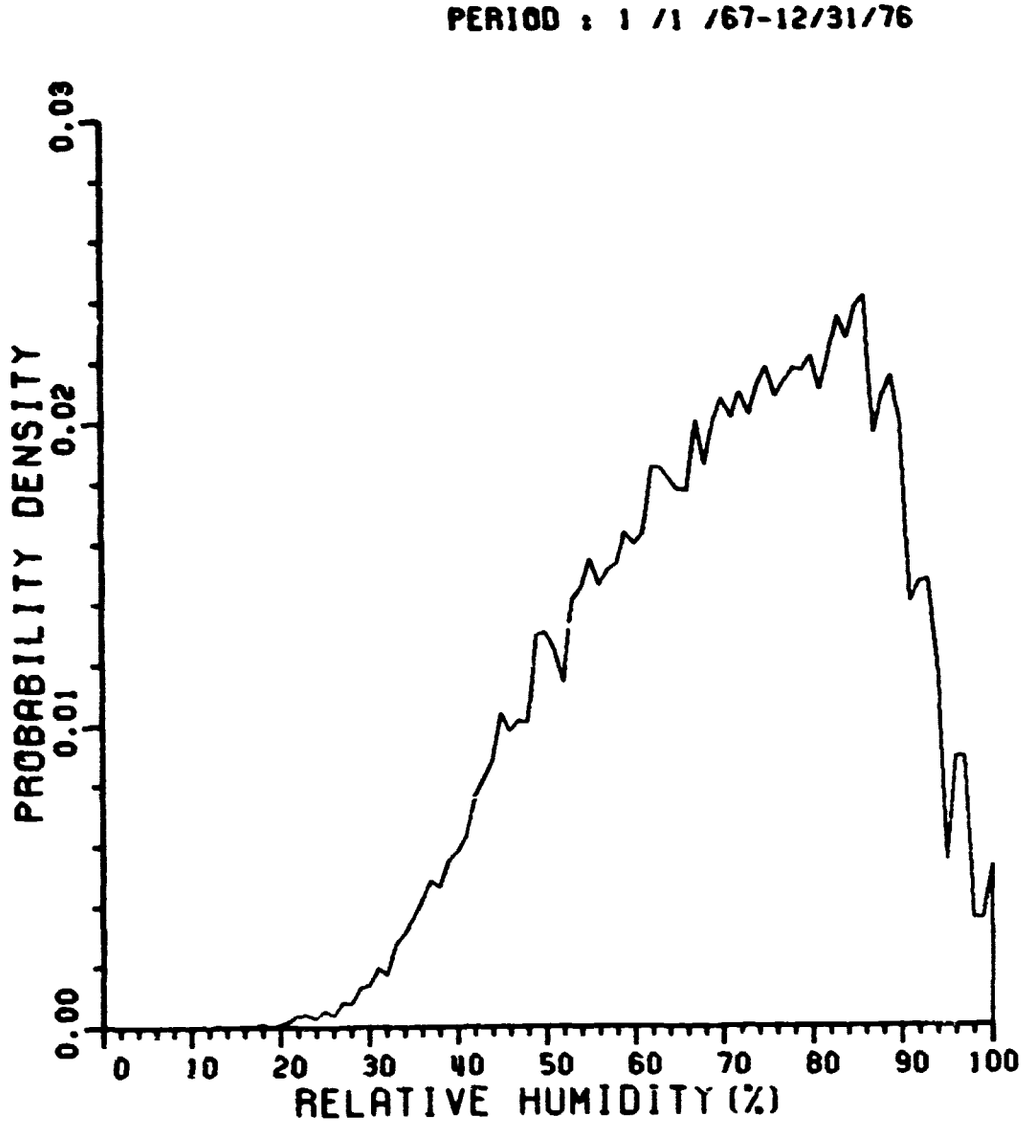

Figure 15. Probability density function of relative humidity for the period 1967-1976; Δv = 1[%].

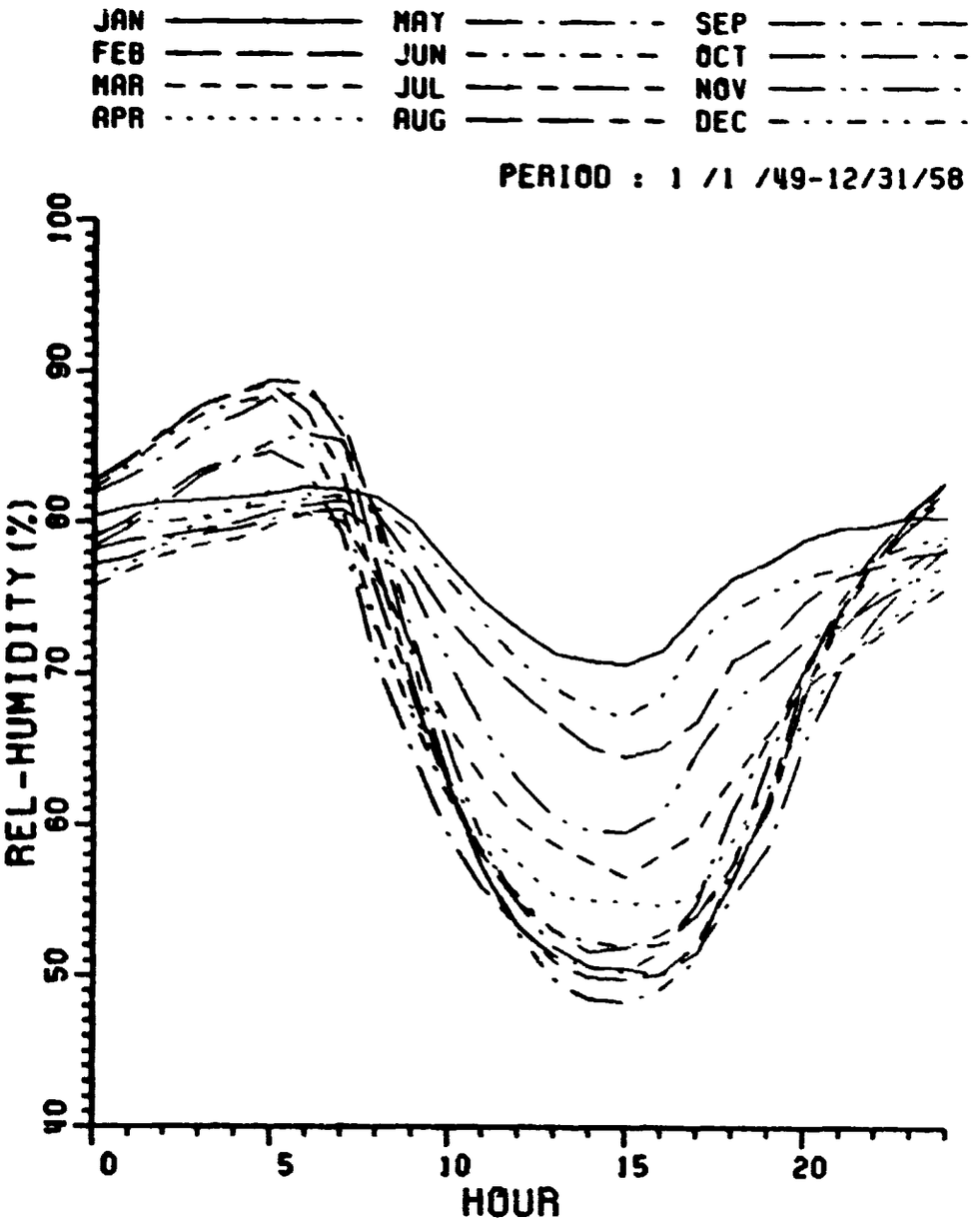

Figure 16. Average diurnal variation of relative humidity for the period 1949-1958.

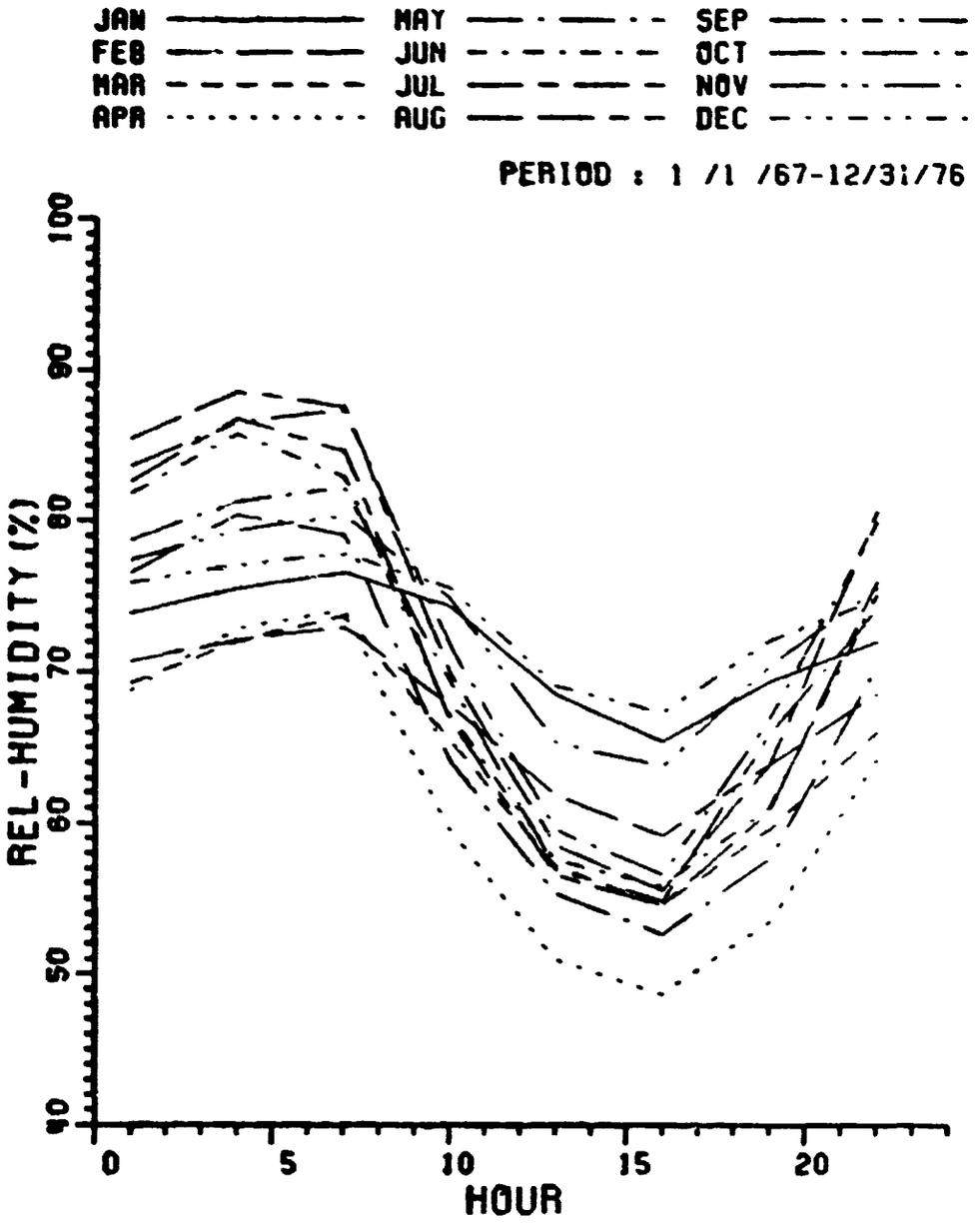

Figure 17. Average diurnal variation of relative humidity for the period 1967-1976.

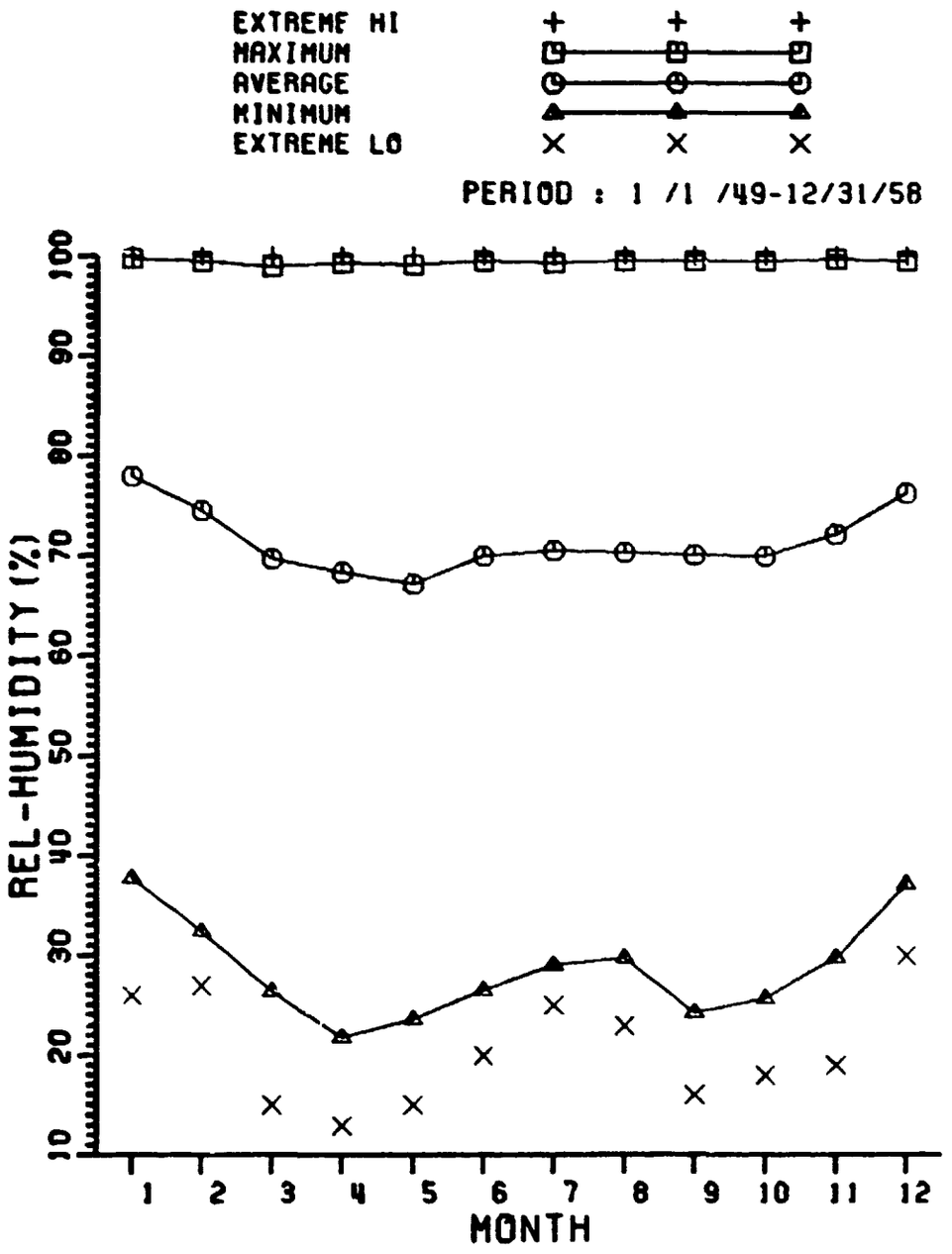

Figure 18. Daily maximum, average, minimum, and extreme relative humidity for the period 1949-1958.

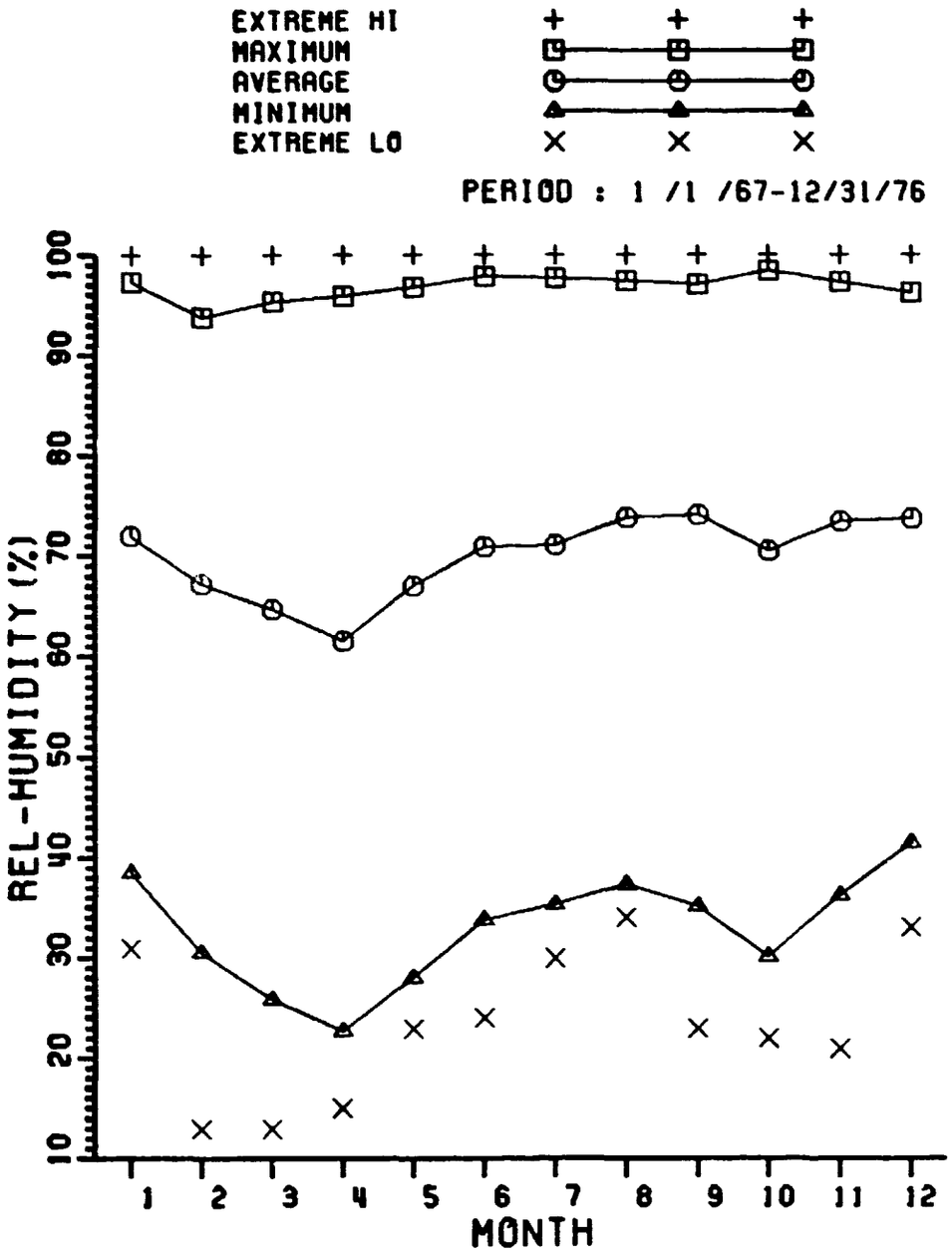

Figure 19. Daily maximum, average, minimum, and extreme relative humidity for the period 1967-1976.

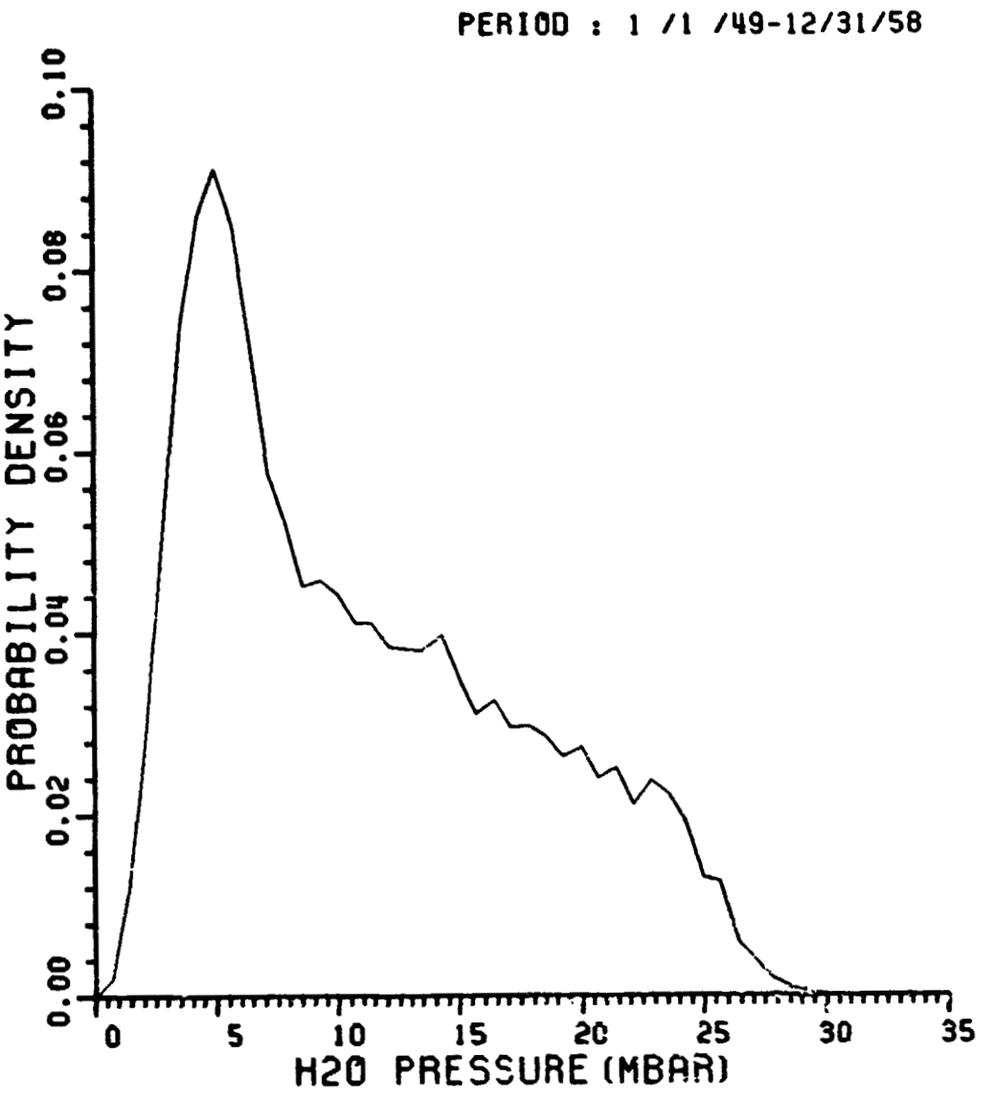

Figure 20. Probability density function of H_2O pressure for the period 1949-1958; Δe = 0.71 [mbar].

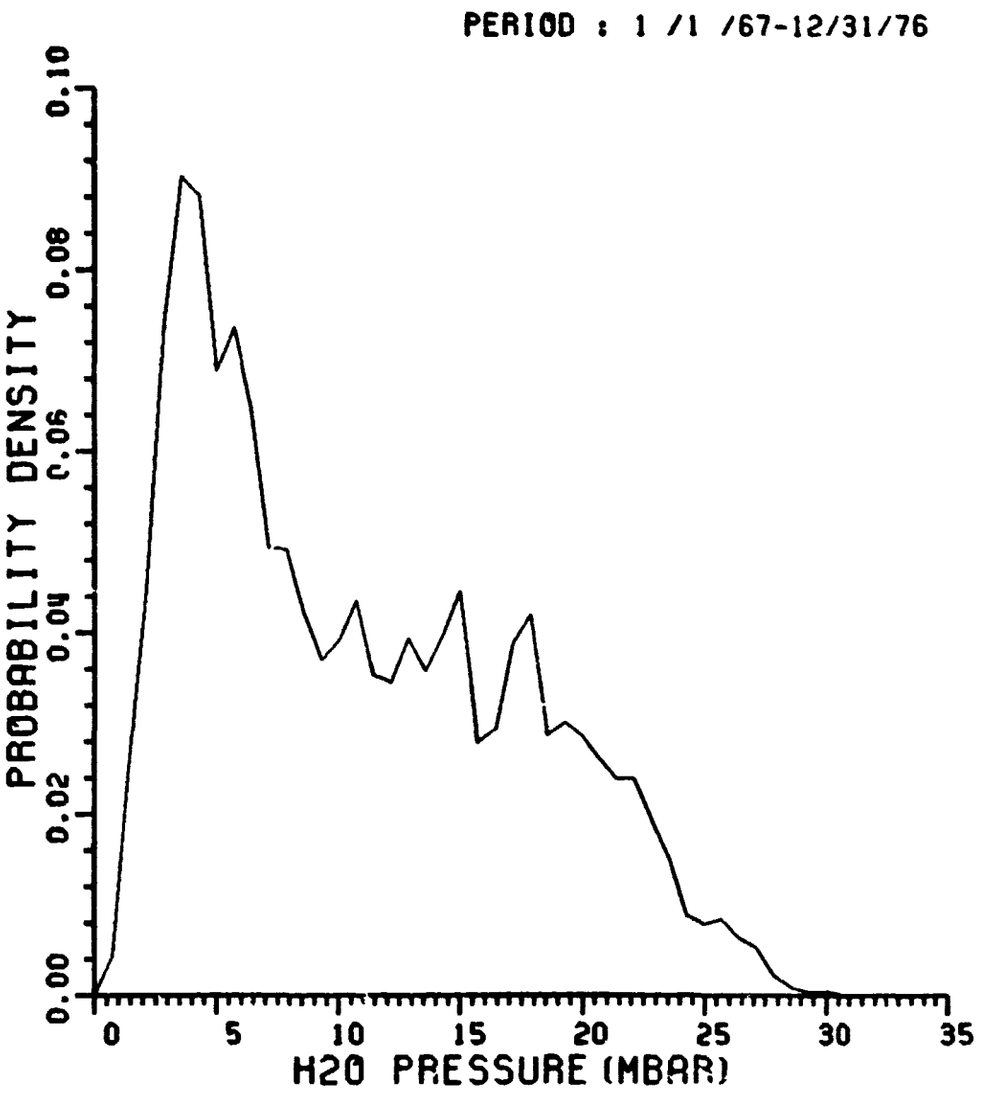

Figure 21. Probability density function of H_2O pressure for the period 1967-1976; Δe = 0.71 [mbar].

Figure 22. Average diurnal variation of H_2O pressure for the period 1949-1958.

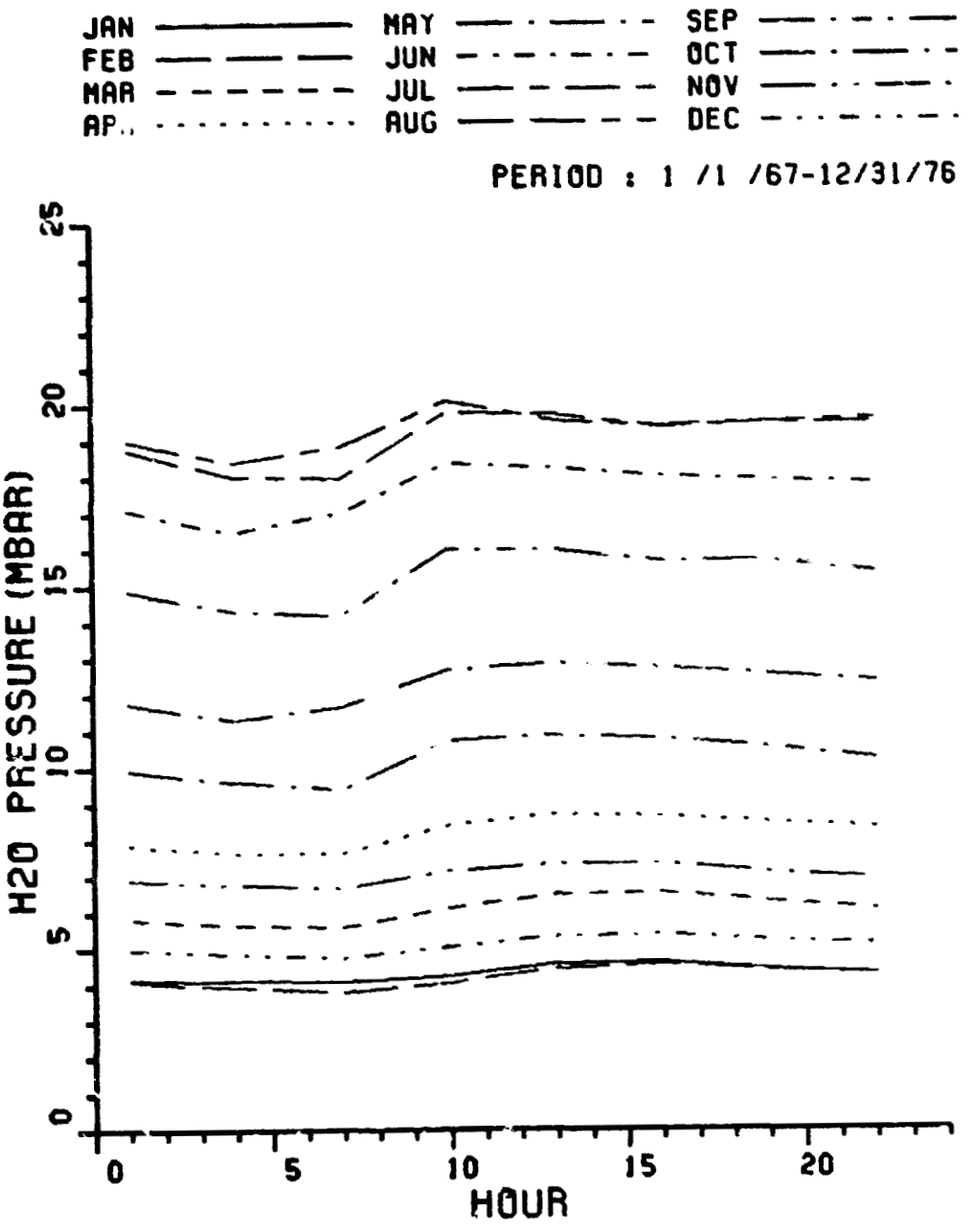

Figure 23. Average diurnal variation of H_2O pressure for the period 1967-1976.

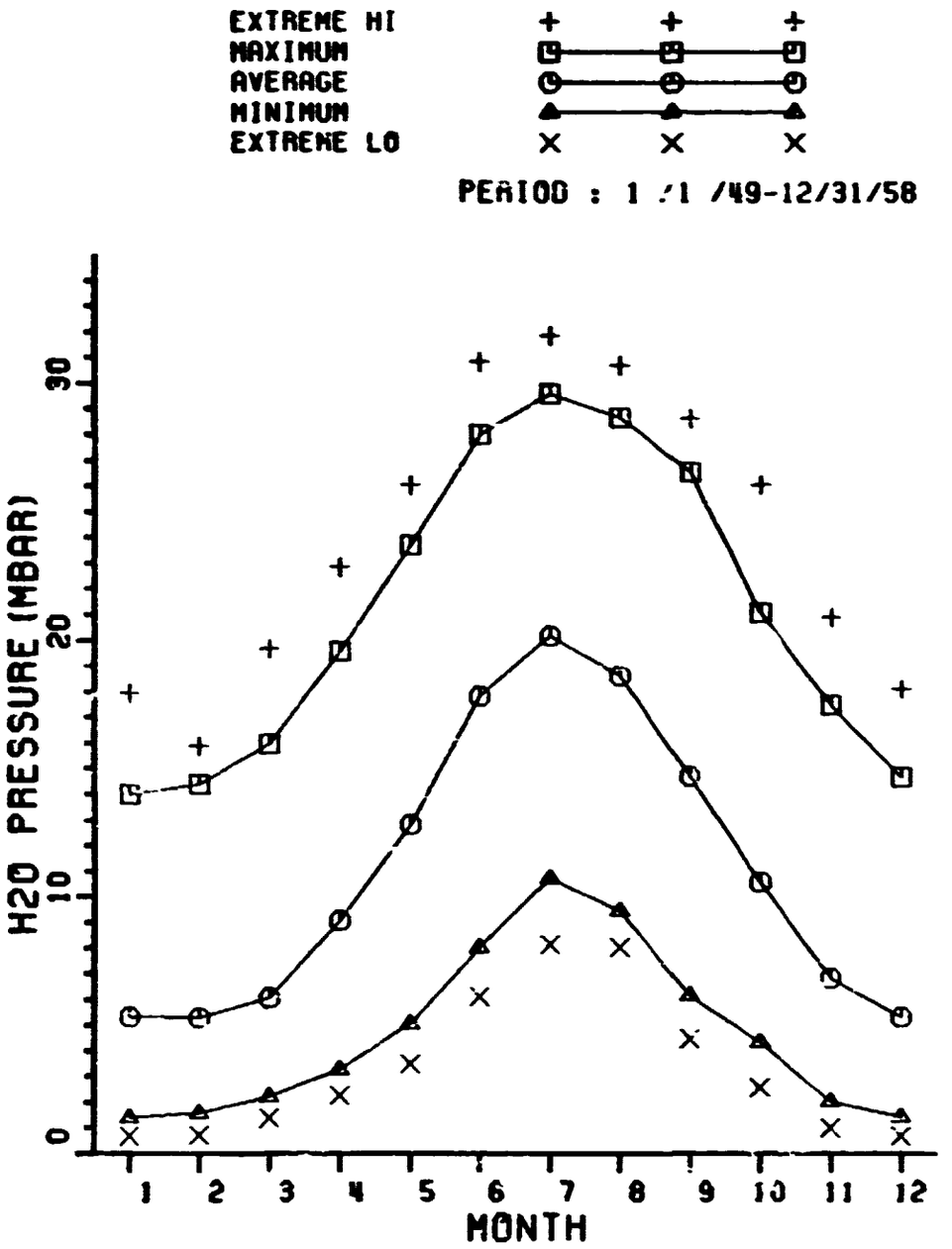

Figure 24. Daily maximum, average, minimum, and extreme H_2O pressure by months for the period 1949-1958.

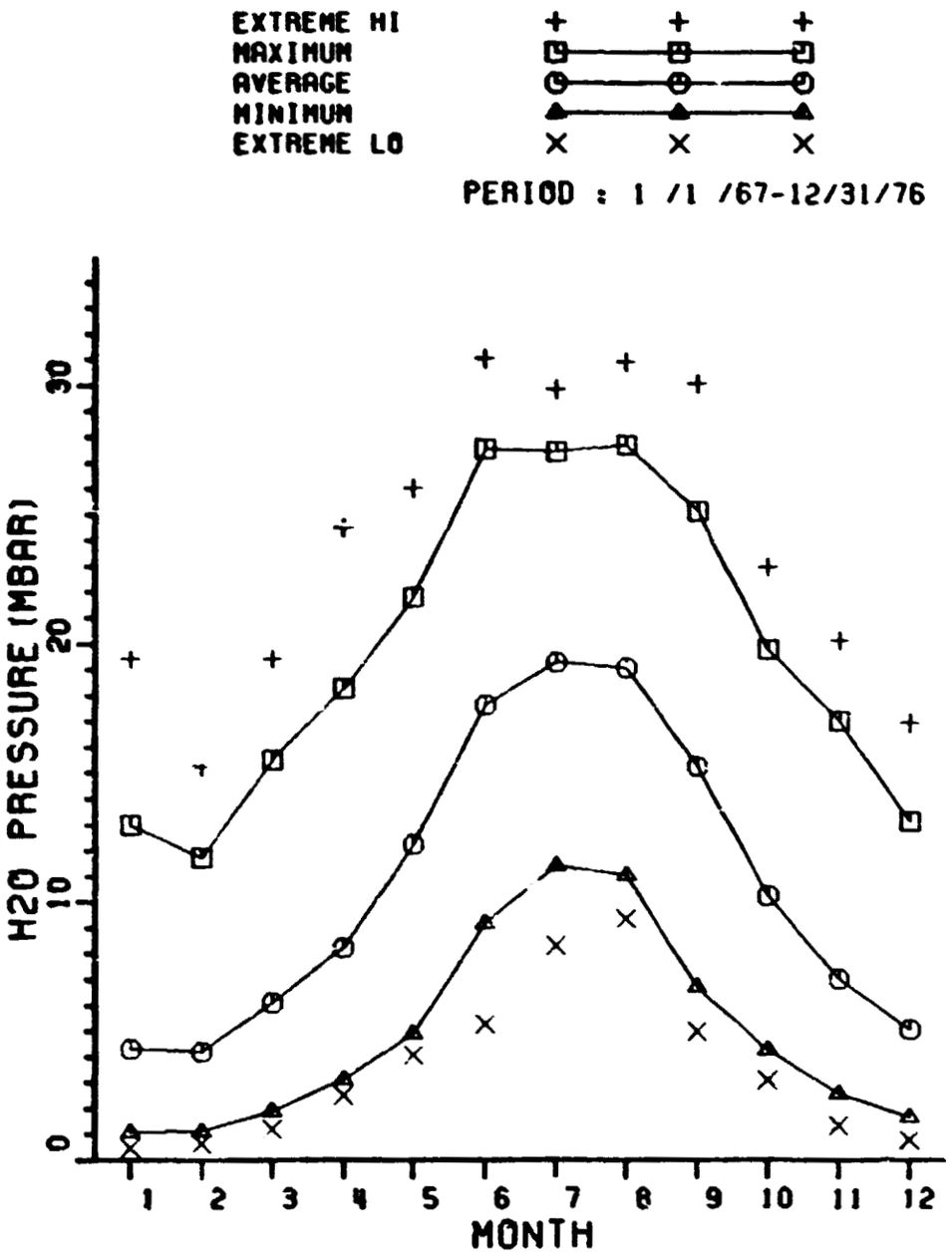

Figure 25. Daily maximum, average, minimum, and extreme H_2O pressure for the period 1967-1976.

CHAPTER IV

ATMOSPHERIC REFRACTIVITY VARIATION

Atmospheric gases having electric or magnetic dipole moments cause absorption and dispersion of electromagnetic waves. In atmospheric propagation, the atmospheric effects are represented by the complex refractivity, N, in parts per million [ppm]. Since the molecular polarization depends upon temperature, pressure, and gas composition, the refractivity varies with the atmospheric state.

In this chapter we will calculate the clear sky refractivity for the meteorological conditions presented in the preceding chapter and its probability distribution and variation for Columbus, Ohio.

A. Calculation

Over the 10-300 GHz frequency range, the spectra of the atmospheric gas molecules lead to a complicated expression for N with several line parameters. The Absorption Line Parameter Compilation (ALPC) (5), which is the most complete account of atmospheric absorption lines, lists more than 10,000 lines for the seven molecules: H_2O, CO_2, O_3, N_2O, CO, CH_4, and O_2. Of these, six water vapor and thirty-six oxygen spectral lines dominate the electromagnetic characteristics of clear air in the EHF range.

Based on Omoura and Hodge's work (6), the complex microwave refractivity, N, can be expressed as the sum of the refractivities due to each

individual absorption line,

$$N = \sum_{i=1} N_i = \sum_{i=1} N_i' - j\sum_{i=1} N_i'' = N_o + \sum_i (N_i' - N_{oi}) - j\sum_i N_i'' = N_o + \sum_i (S_i F_i' - N_{oi}) - j\sum_i S_i F_i'' \quad (4\text{-}1.1)$$

where

$N_o = \sum_i N_{oi}$ is the frequency independent real part of the refractivity of air [ppm],

N_{oi} = the low frequency limit of the i-th line refractivity in [ppm],

S_i = the i-th line strength in [KHz],

F_i' = the dispersion line shape factor of the i-th line in [GHz^{-1}], and

F_i'' = the extinction line shape factor of the i-th line in [GHz^{-1}].

As will be shown in Section (A-1), the low frequency tail can be approximated as:

$$N_{oi} = \lim_{f \to o} S_i F_i' = S_i \lim_{f \to o} F_i' = 2 \frac{S_i}{f_{oi}} \quad (4\text{-}1.2)$$

where f_{oi} is the resonance frequency of i-th line. Therefore, if we neglect the effect of absorption lines other than the six water vapor and thirty-six oxygen lines, the clear air refractivity in the EHF range can be obtained by

$$N' = \left(N_o - \sum_{i=1}^{42} 2 \frac{S_i}{f_{oi}} \right) + \sum_{i=1}^{6} (S_i F_i')_{wt} + \sum_{i=1}^{36} (S_i F_i')_{ox} \quad (4\text{-}1.3)$$

and

$$N'' = \sum_{i=1}^{6} (S_i F_i'')_{wt} + \sum_{i=1}^{36} (S_i F_i'')_{ox} \qquad (4\text{-}1.4)$$

where "wt" stands for water vapor and "ox" stands for oxygen.

The oxygen spectral lines and the water vapor spectral lines with their line parameters are listed in Tables 1 and 2. From Equation (1-2.8) the power attenuation will be given by

$$\alpha_p = 0.182f \left(\sum_{i=1}^{6} (S_i F_i'')_{wt} + \sum_{i=1}^{36} (S_i F_i'')_{ox} \right) \qquad (4\text{-}1.5)$$

where f is in [GHz].

1. Frequency Independent Refractivity

The frequency independent refractivity can be obtained by summing the low frequency limits of all of absorption line refractivities, i.e.

$$N_o = \sum_i N_{oi} \qquad i = \text{all absorption lines} \qquad (4\text{-}1.6)$$

But this is not possible because it requires a full knowledge of all of the absorption lines. Based on experimental work, Bean and Dutton (7) presented the following empirical equation for the frequency independent refractivity of moist air:

$$N_o = 77.6 \frac{P_d}{T} + 72 \frac{e}{T} + 3.75 \times 10^5 \frac{e}{T^2} \qquad (4\text{-}1.7)$$

where

P_d = dry air pressure [mb]

e = partial pressure of water vapor [mb]

T = temperature [°k]

Note that this frequency independent refractivity is purely real. As shown in the next section, the imaginery part of the refractivity is

TABLE 1

OXYGEN SPECTRAL LINES (5)

f_0(GHz)	a [mb^{-1}]	S_0[kHz/mb]	d	γ_0[GHz/mb]
50.9873	5.5×10^{-4}	2.44×10^{-7}	8.69	8.7×10^{-4}
51.50302	5.6×10^{-4}	6.04×10^{-7}	7.74	8.9×10^{-4}
52.02117	5.5×10^{-4}	1.41×10^{-6}	6.84	9.2×10^{-4}
52.54223	5.7×10^{-4}	3.08×10^{-6}	6.00	9.4×10^{-4}
53.0668	5.3×10^{-4}	6.37×10^{-6}	5.22	9.7×10^{-4}
53.59572	5.4×10^{-4}	1.24×10^{-5}	4.48	10.0×10^{-4}
54.12997	4.8×10^{-4}	2.265×10^{-5}	3.81	10.2×10^{-4}
54.67116	4.8×10^{-4}	3.893×10^{-5}	3.19	10.5×10^{-4}
55.22136	4.17×10^{-4}	6.274×10^{-5}	2.62	10.79×10^{-4}
55.78380	3.75×10^{-4}	9.471×10^{-5}	2.11	11.10×10^{-4}
56.26478	7.74×10^{-4}	5.453×10^{-5}	0.0138	16.46×10^{-4}
56.36339	2.97×10^{-4}	1.335×10^{-4}	1.66	11.44×10^{-4}
56.96818	2.12×10^{-4}	1.752×10^{-4}	1.255	11.81×10^{-4}
57.61249	0.94×10^{-4}	2.126×10^{-4}	0.910	12.66×10^{-4}
58.32389	-0.55×10^{-4}	2.369×10^{-4}	0.621	12.66×10^{-4}
58.44660	5.97×10^{-4}	2.0827×10^{-4}	0.0827	14.49×10^{-4}
59.16422	-2.44×10^{-4}	2.387×10^{-4}	0.386	13.19×10^{-4}
59.59098	3.44×10^{-4}	2.097×10^{-4}	0.207	13.6×10^{-4}
60.30604	-4.35×10^{-4}	2.109×10^{-4}	0.207	13.82×10^{-4}
60.43478	1.32×10^{-4}	2.444×10^{-4}	0.386	12.97×10^{-4}
61.15057	-0.36×10^{-4}	2.486×10^{-4}	0.621	12.48×10^{-4}
61.80017	-1.59×10^{-4}	2.281×10^{-4}	0.910	12.07×10^{-4}
62.41122	-2.66×10^{-4}	1.919×10^{-4}	1.255	11.71×10^{-4}
62.48626	-5.03×10^{-4}	1.507×10^{-4}	0.0827	14.68×10^{-4}
62.99800	-3.34×10^{-4}	1.492×10^{-4}	1.66	11.39×10^{-4}
63.56852	-4.17×10^{-4}	1.079×10^{-4}	2.11	11.08×10^{-4}
64.12778	-4.48×10^{-4}	7.281×10^{-5}	2.62	10.78×10^{-4}
64.67892	-5.1×10^{-4}	4.601×10^{-5}	3.19	10.5×10^{-4}

Table 1 (continued)

65.22405 65.76474	-5.1×10^{-4} -5.7×10^{-4}	2.727×10^{-5} 1.52×10^{-5}	3.81 4.48	10.2×10^{-4} 10.0×10^{-4}
66.30206 66.83677	-5.5×10^{-4} -5.9×10^{-4}	7.94×10^{-6} 3.91×10^{-6}	5.22 6.00	9.7×10^{-4} 9.4×10^{-4}
67.36951 67.90073	-5.9×10^{-4} -5.8×10^{-4}	1.81×10^{-6} 7.95×10^{-7}	6.84 7.74	9.2×10^{-4} 8.9×10^{-4}
68.4308 118.75034	-5.7×10^{-4} -0.44×10^{-4}	3.28×10^{-7} 9.341×10^{-5}	8.69 0.0138	8.7×10^{-4} 15.92×10^{-4}

Table 2

WATER VAPOR MICROWAVE SPECTRAL LINES (5)

f_0 (GHz)	S_0 kHz/mbar	d	γ_0 GHz/mbar
22.23508	0.0112	2.143	28.1×10^{-4}
63.052	0.0018	8.75	28.0×10^{-4}
183.31009	0.241	0.653	28.2×10^{-4}
321.22564	0.0044	6.16	22.0×10^{-4}
325.15292	0.159	1.52	29.0×10^{-4}
380.19737	1.240	1.02	28.5×10^{-4}

proportional to the operating frequency for low frequencies and is generally negligible for frequencies below 1 GHz.

2. Line Shape Factors

The frequency variation of the absorption and dispersion of each of the spectral lines is represented by a line shape factor. Three classical line shapes (the Lorentzian, the Van Vleck-Weisskopf, and the Gross) are in common use in atmospheric refractivity studies, but the Gross line shape seems to fit the experimental results better. The three line shape factors and their tails are listed in Tables 3 and 4, respectively.

At low altitudes ($h < 35$km), the effect of pressure broadening causes the absorption lines to overlap. Based on Rosenkranz's work, Liebe (5) used the following line shape factors for the calculation of clear air refractivity in the pressure broadening region ($h < 35$km).

$$F' = \left(\frac{f}{f_o}\right)\left[\frac{(f_o - f) + \gamma I}{(f_o - f)^2 + \gamma^2}\right] - \left[\frac{(f_o + f) + \gamma I}{(f_o + f)^2 + \gamma^2}\right] \qquad (4\text{-}1.8)$$

$$F'' = \left(\frac{f}{f_o}\right)\left[\frac{\gamma - (f_o - f)\, I}{(f_o - f)^2 + \gamma^2}\right] + \left[\frac{\gamma - (f_o + f)\, I}{(f_o + f)^2 + \gamma^2}\right] \qquad (4\text{-}1.9)$$

where f_o is the resonant frequency of the line, f is the operating frequency, γ is the line width, and I is an interference parameter. The interference parameter is negligible in the case of water vapor while it is a function of pressure and temperature for the oxygen molecule (5).

$$I = a\, Pd \left(\frac{300}{T}\right)^2 \qquad (4\text{-}1.10)$$

where

TABLE 3

LINE SHAPE FACTORS (6)

Type	Dispersion F'	Extinction F"
Full Lorentzian (F-L)	$\frac{f_o-f}{(f_o-f)^2+\gamma^2} + \frac{f_o+f}{(f_o+f)^2+\gamma^2}$	$\frac{\gamma}{(f_o-f)^2+\gamma^2} - \frac{\gamma}{(f_o+f)^2+\gamma^2}$
Van Vleck-Weisskopf (VV-W)	$\left(\frac{\gamma^2+f_o(f_o+f)}{(f_o+f)^2+\gamma^2} + \frac{\gamma^2+f_o(f_o-f)}{(f_o-f)^2+\gamma^2}\right)\left(\frac{1}{f_o}\right)$	$\left(\frac{\gamma}{(f_o+f)^2+\gamma^2} + \frac{\gamma}{(f_o-f)^2+\gamma^2}\right)\left(\frac{f}{f_o}\right)$
Gross (G)	$\frac{2f_o(f_o^2-f^2)}{[f_o^2-f^2]^2+4f^2\gamma^2}$	$\frac{4f^2\gamma}{[f_o^2-f^2]^2+4f^2\gamma^2}$

TABLE 4

LINE SHAPE FACTOR TAILS (6)

Type	$f \to 0$		$f \to \infty$	
	F'	F"	F'	F"
F-L	$\frac{2}{f_o}$	$\frac{4\gamma f}{f_o^3}$	$-2\frac{f_o}{f^2}$	$\frac{4\gamma f_o}{f^3}$
VV-W	$\frac{2}{f_o}$	$\frac{2\gamma f}{f_o^3}$	$-2\frac{f_o}{f^2}$	$\frac{2\gamma}{ff_o}$
G	$\frac{2}{f_o}$	$\frac{4\gamma f^2}{f_o^4}$	$-2\frac{f_o}{f^2}$	$\frac{4\gamma}{f^2}$

a = constant

Pd = dry air pressure [mb]

T = temperature [°k]

If $\gamma \ll f_o$ and I is small, the low and high frequency tails are

$$F' \approx \frac{2f^2}{f_o^3} \quad ; \quad F'' \approx \frac{2f(\gamma - f_o I)}{f_o^3} \quad \text{as} \quad f \to 0 \qquad (4\text{-}1.11)$$

$$F' \approx -\frac{2}{f_o} \quad ; \quad F'' \approx \frac{2(\gamma + fI)}{f_o f} \quad \text{as} \quad f \to \infty \qquad (4\text{-}1.12)$$

For comparison, we plot the dispersion and extinction line shape factors of the four lines in Figures 26 and 27 for $\frac{\gamma}{f_o}$ equal to 0.065. The interference parameter is set to 0.06. As shown in Figure 26 and from comparison of low and high frequency tails, Liebe's dispersion line shape factor seems to be shifted downward by $\frac{2}{f_o}$. It should also be noticed that Liebe extinction line shape factor, F", goes below zero if $\frac{\gamma}{f_o} < I$ [see Equation (4-1.11)]. Several oxygen absorption lines satisfy this condition for usual atmospheric states. For these two reasons, the Gross line shape will be used in the following rather than Liebe's more recent result.

The line width and line strength for oxygen can be calculated using the following empirical formulas (5):

$$\gamma = \gamma_o \, [Pd + 1.3e] \left(\frac{300}{T}\right)^{0.9} \qquad [GHz] \qquad (4\text{-}1.13)$$

$$S = S_o Pd \left(\frac{300}{T}\right)^3 \exp\left[d\left(1 - \frac{300}{T}\right)\right] \qquad [KHz] \qquad (4\text{-}1.14)$$

where γ_o, S_o, and d are constants for individual absorption lines (see Table 1).

Figure 26. Comparison of the dispersion line shape factors; $\frac{\gamma}{f_o}$ = 0.065, I = 0.06.

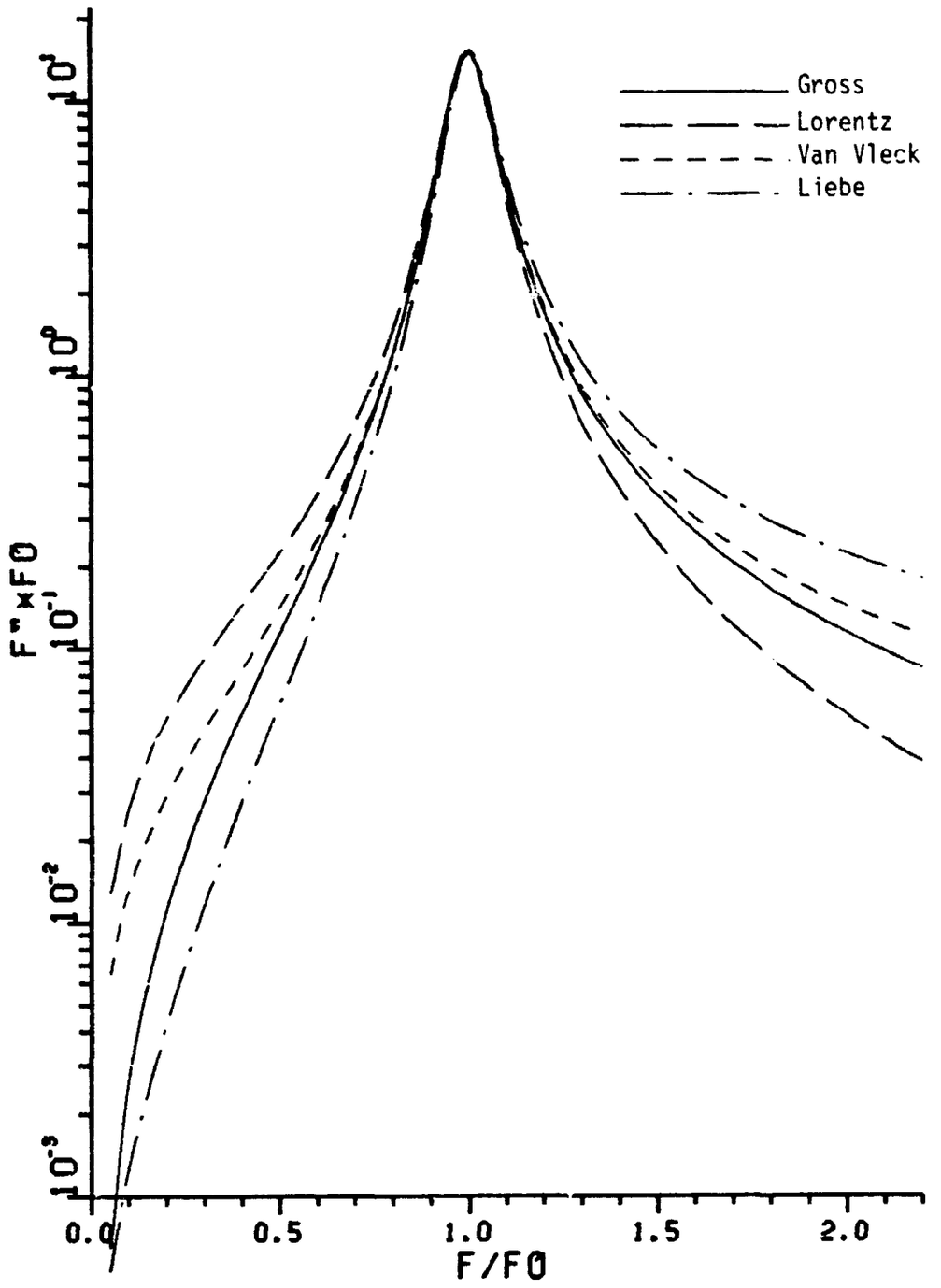

Figure 27. Comparison of the extinction line shape factors; $\frac{\gamma}{f_o} = 0.065$; I = 0.06.

For water vapor the line width and line strength have similar formulas:

$$\gamma = \gamma_o \, [Pd + 4.8e] \left(\frac{300}{T}\right)^{0.6} \qquad [GHz] \qquad (4\text{-}1.15)$$

$$S = S_o e \left(\frac{300}{T}\right)^{3.5} \exp\left[d\left(1 - \frac{300}{T}\right)\right] \qquad [KHz] \qquad (4\text{-}1.16)$$

B. Statistics

To examine the variation of the atmospheric microwave refractivity at the earth's surface, the refractivity was calculated for each meteorological observation using the expressions developed in Section A and the probability density functions, diurnal variations, and seasonal variations were plotted. As was expected, the atmospheric refractivity varies diurnally and seasonally.

1. The Frequency Independent Refractivity

An approximate equation which yields values for N_o within 0.02 percent of those obtained using Equation (4-1.7) is (7):

$$N_o = \frac{77.6}{T}\left(P + \frac{4810}{T} e\right) \qquad (4\text{-}2.1)$$

where P is the total pressure, i.e.

$$P = Pd + e \qquad [mbar]$$

Since pressure does not vary significantly (Figures 8 and 9) and temperature varies within 253-313° [°k] (Figures 2 and 3), the frequency independent refractivity is highly dependent on water vapor pressure. Thus, the shape of the probability density function of N_o is similar to that of water vapor pressure (Figures 28 and 29).

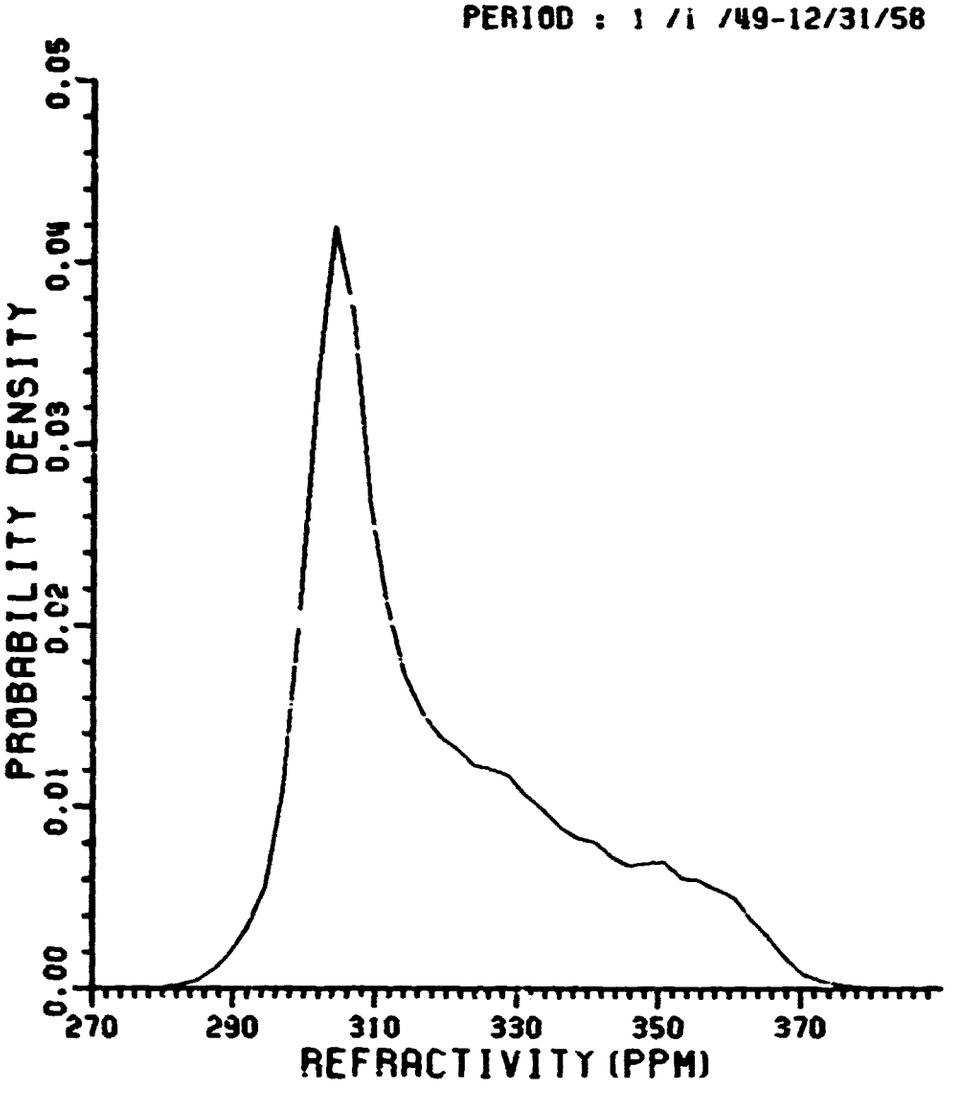

Figure 28. Probability density function of N_s for the period 1949-1958; ΔN = 2.45 [ppm].

Figure 29. Probability density function of N_o for the period 1967-1976; ΔN = 2.45 [ppm].

Even though the diurnal variation of water vapor pressure is very small (Figures 18 and 19), the normal temperature rise and pressure decrease in the afternoon causes N_o to decrease during that period (Figures 30 and 31).

In the summer, the average diurnal variation is about 13 [ppm]. The average monthly variation is about 40 [ppm] during the winter and 80 [ppm] during the summer. The maximum and minimum of the frequency independent refractivity during 1949-1958 and 1967-1976, are 385 [ppm] and 275 [ppm], respectively (Figures 32 and 33).

Figures 34 and 35 show the diurnal and seasonal variation patterns of temperature, pressure, water vapor content, and frequency independent refractivity in a composite display for comparison purposes.

2. Frequency Dependent Refractivity

At low frequencies, the refractivity is simply the frequency independent value which is the summation of the low frequency tails of all of the absorption lines. As the operating frequency increases, the effects of the individual absorption lines are observed; the refractivity goes through dispersion variations as the operating frequency passes through the resonance frequencies of the absorption lines. We plot the mean deviation of the refractivity from its frequency independent value in Figure 36. The dispersion variations at 22, 60, 118, 183, 325, and 380 GHz are shown. Of the water vapor absorption lines, the lines at 68 and 321 GHz are so weak that no significant dispersion is introduced near those frequencies. Note that the dispersion variations at the water vapor absorption lines are very strong during the humid season.

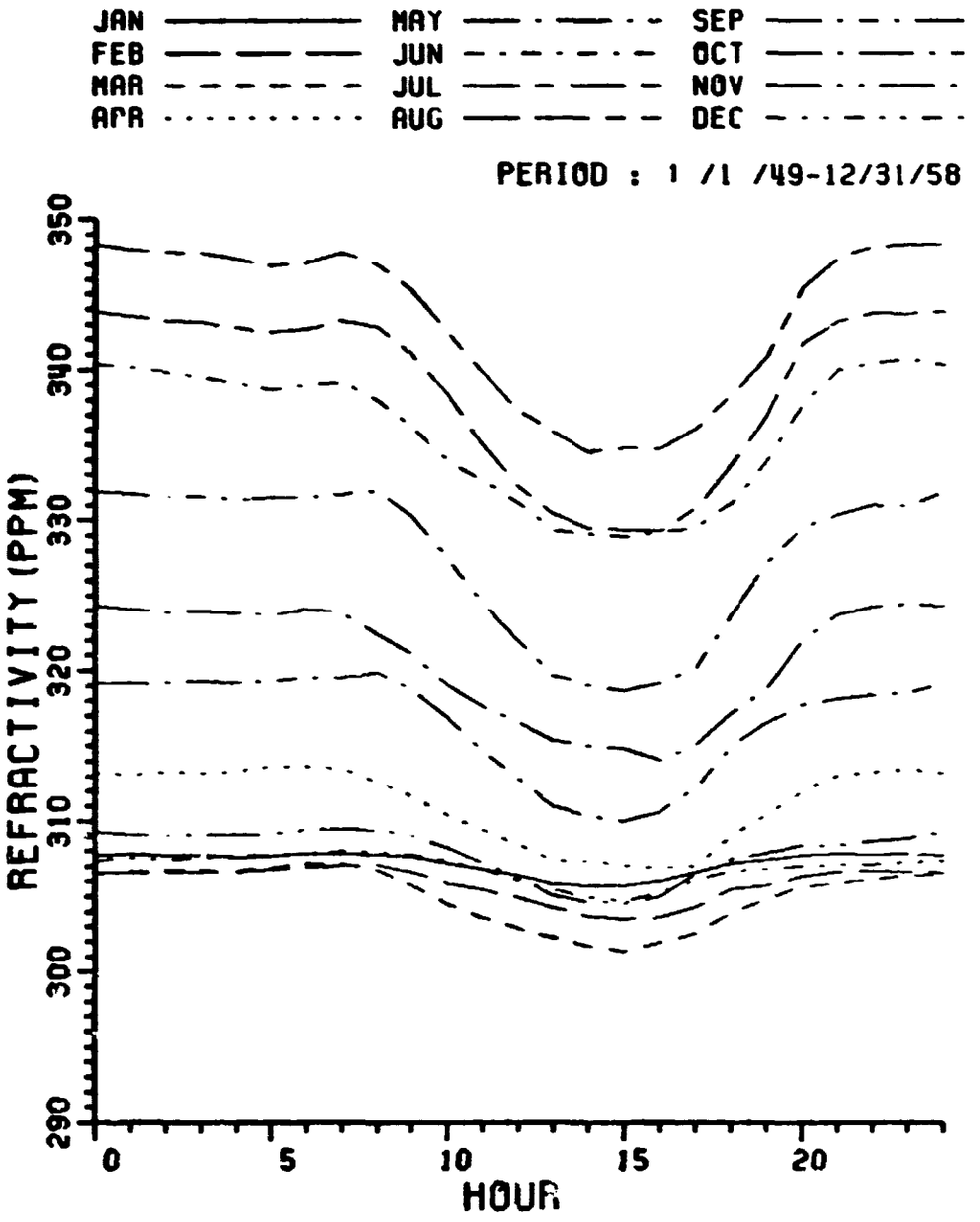

Figure 30. Average diurnal variation of N_o for the period 1949-1958.

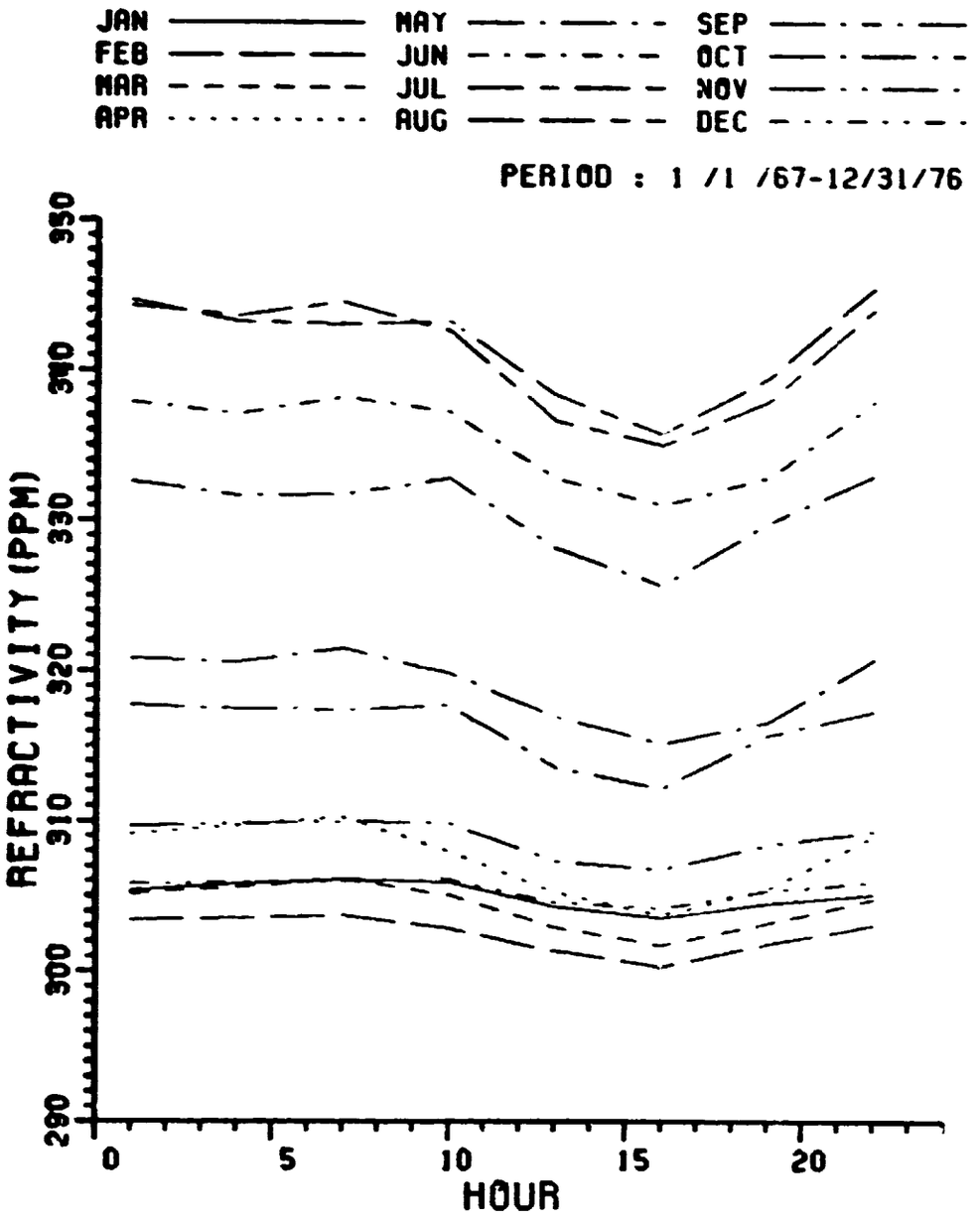

Figure 31. Average diurnal variation of N_o for the period 1967-1976.

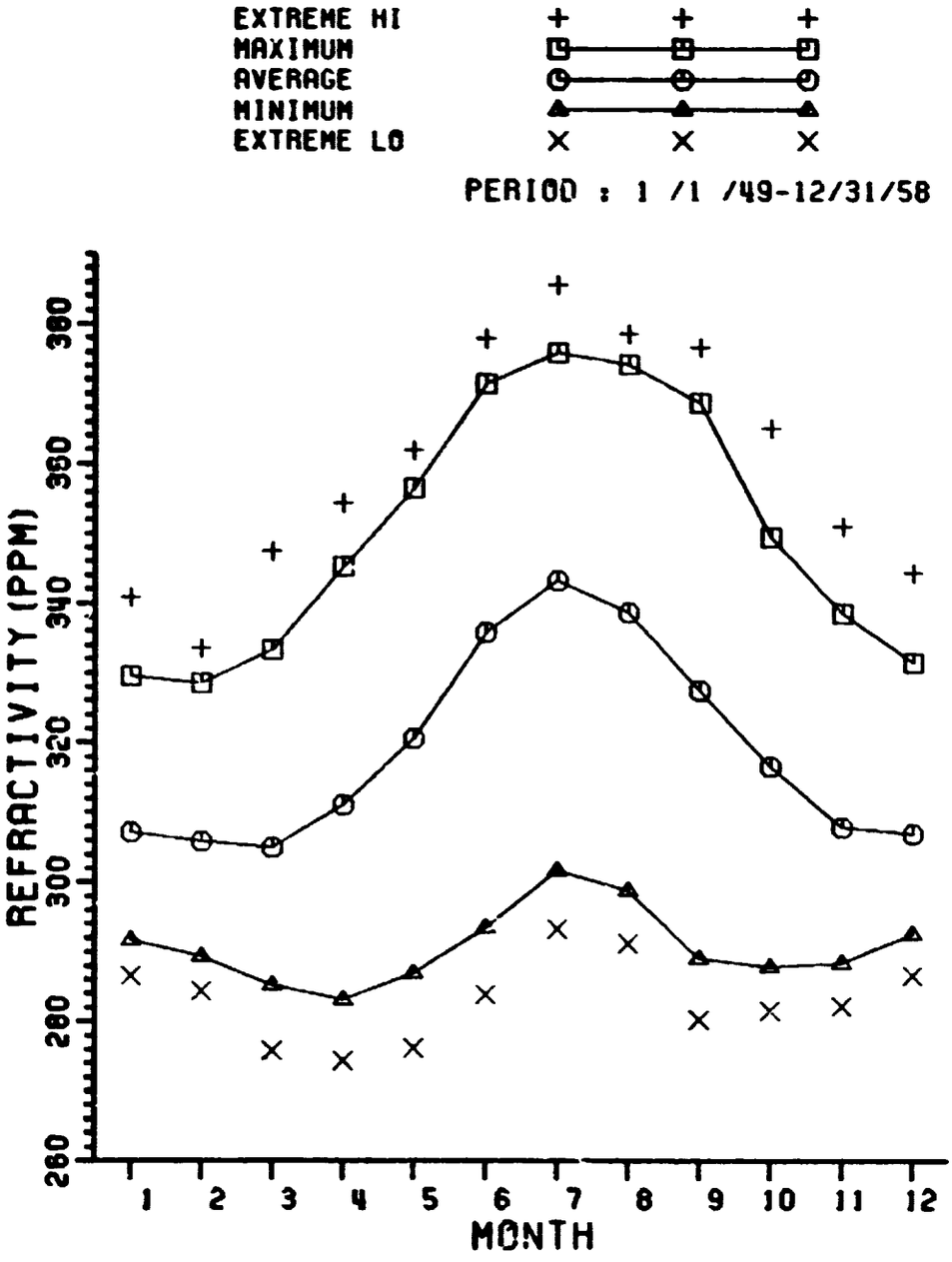

Figure 32. Daily maximum, average, minimum, and extreme N_o by months for the period 1949-1958.

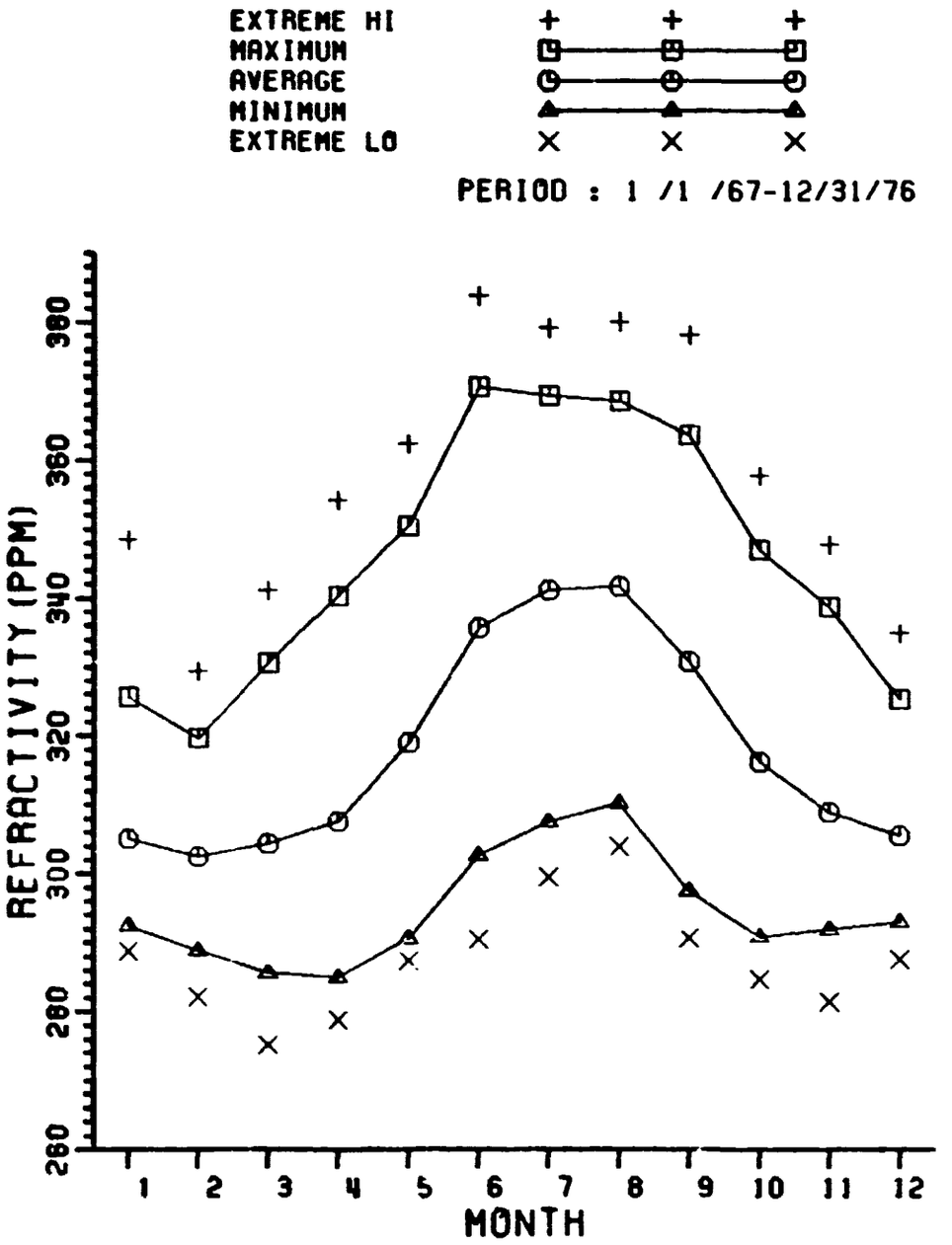

Figure 33. Daily maximum, average, minimum, and extreme N_o by months for the period 1967-1976.

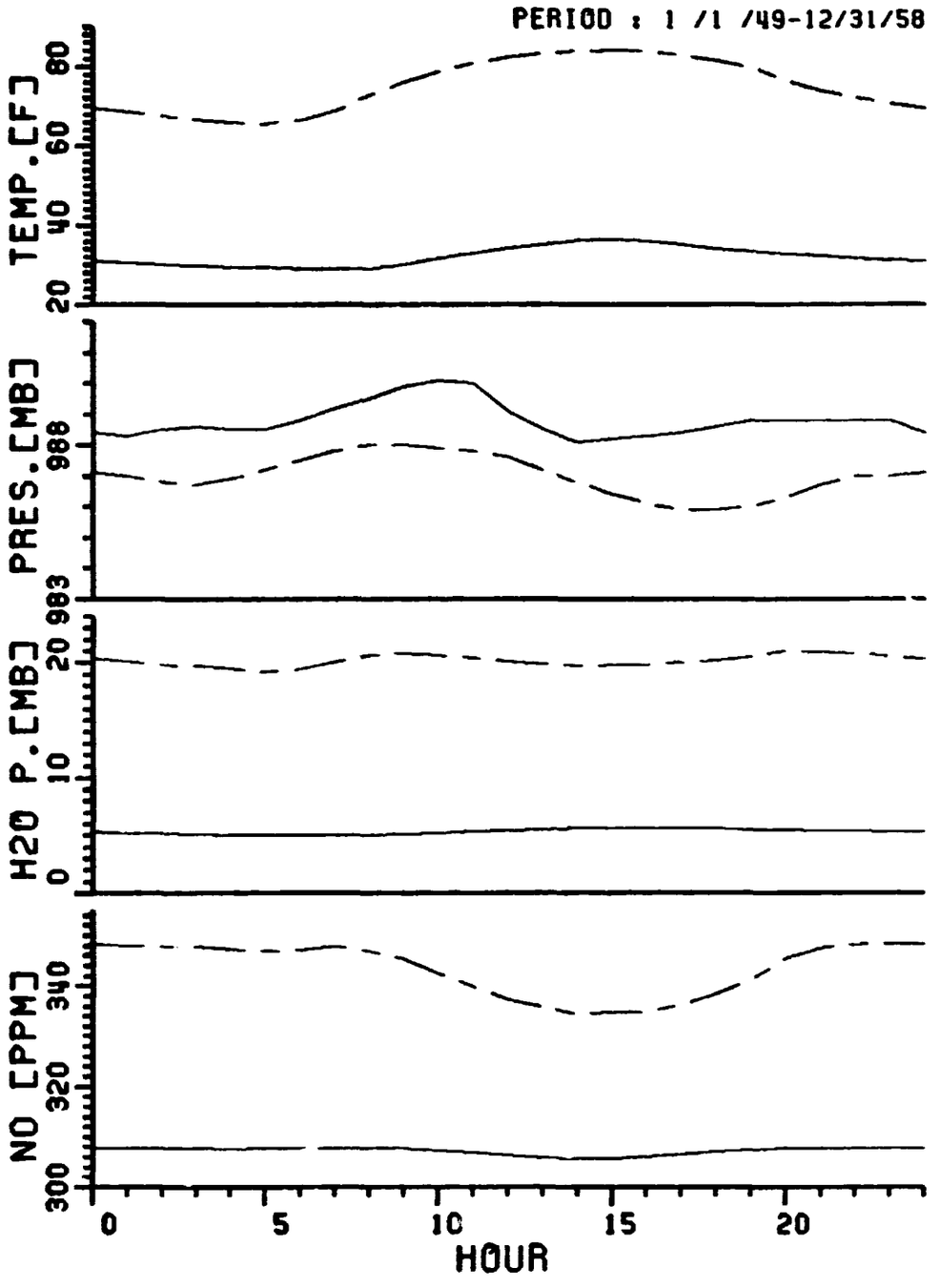

Figure 34. Average diurnal variations of temperature, pressure, water vapor pressure, and N_o for the period 1949-1958.

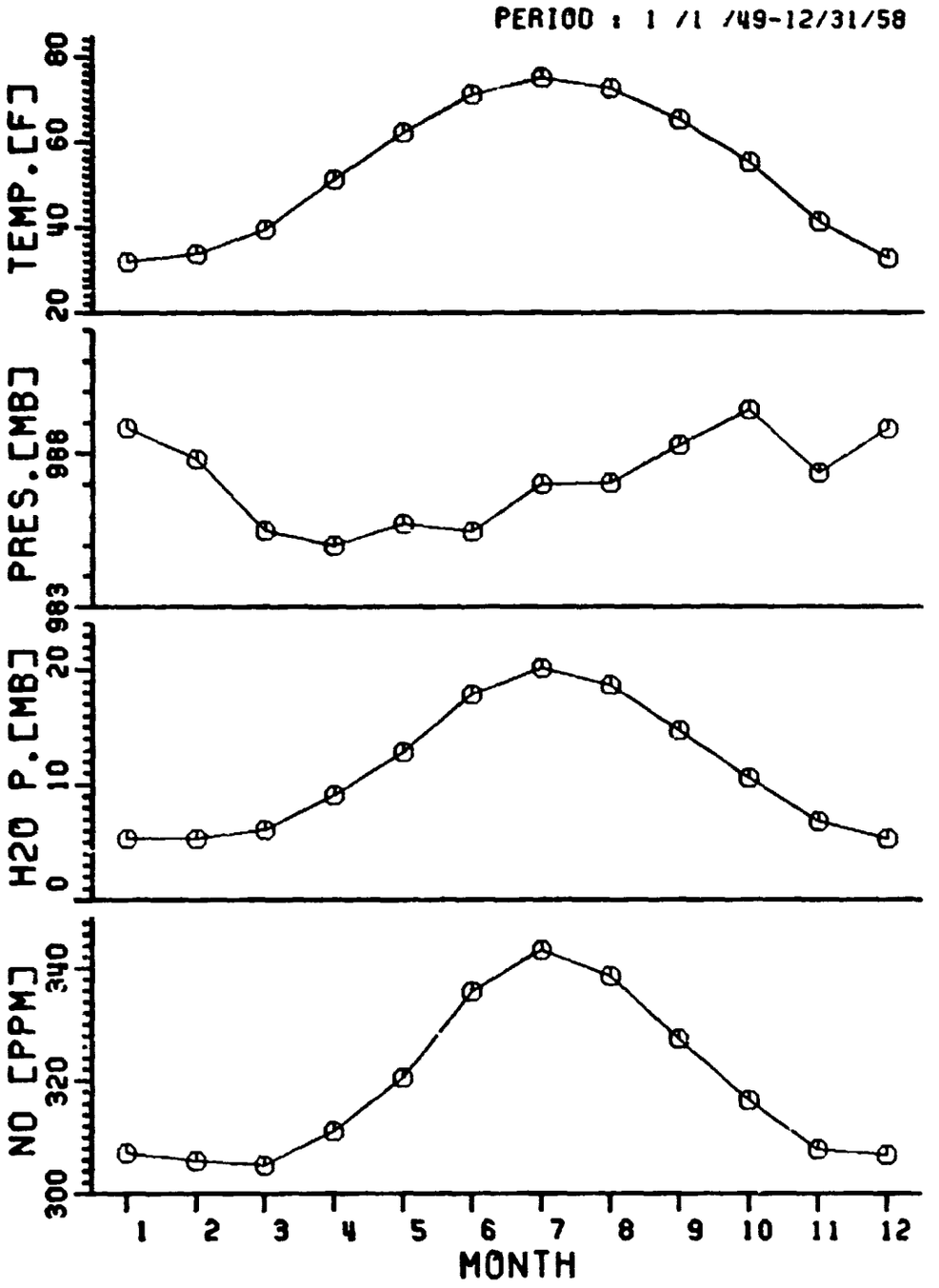

Figure 35. Daily averages of temperature, pressure, water vapor pressure and N_o by months for the period 1949-1958.

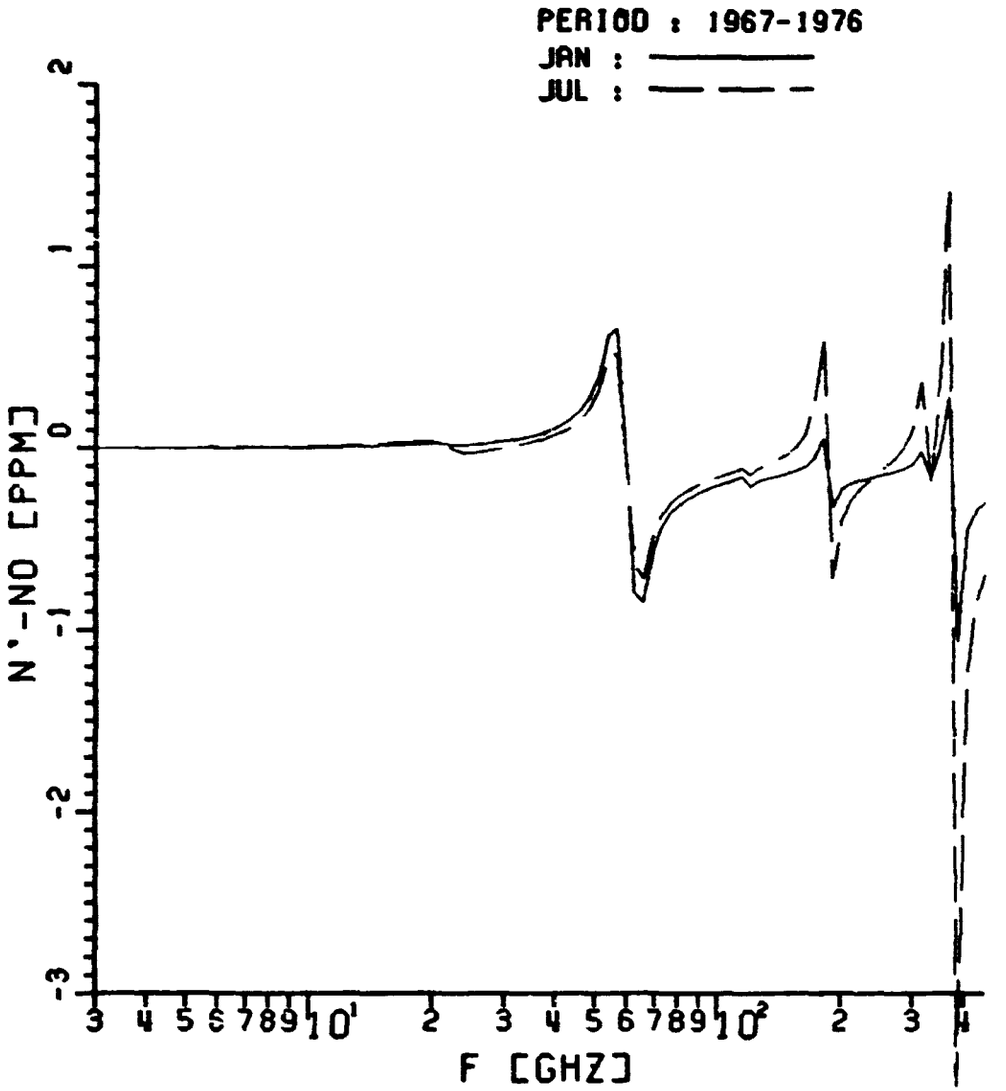

Figure 36. Average deviation of the real part of refractivity from N_o.

The imaginary part of the refractivity is shown as a function of frequency in Figure 37. Since the oxygen molecule's contribution to the imaginary part of refractivity does not depend on water vapor pressure (see Equation (4-1.14)), its value in the vicinity of the oxygen absorption lines (60 and 118.75 GHz) is not affected much by the change of the atmospheric state (see Figure 37). For clarity of the plot only January and July have been shown in these cases.

Since communications engineers are more interested in attenuation than in the refractivity, the attenuation variation has also been plotted in Figure 38. This may be used to estimate the variation of attenuation for the clear sky.

Because of current interest in propagation effects at twenty and thirty GHz, refractivity statistics were derived for these frequencies and are presented in Figures 39 through 41. Although the most probable values of specific attenuation at these frequencies are 0.05 and 0.03 dB/km, respectively, we note that these values can exceed 0.2 and 0.1 dB/km, respectively, during the humid summer season. The excursion at 20 GHz is much larger than at 30 GHz due to the strong influence of the 22 GHz water vapor absorption line.

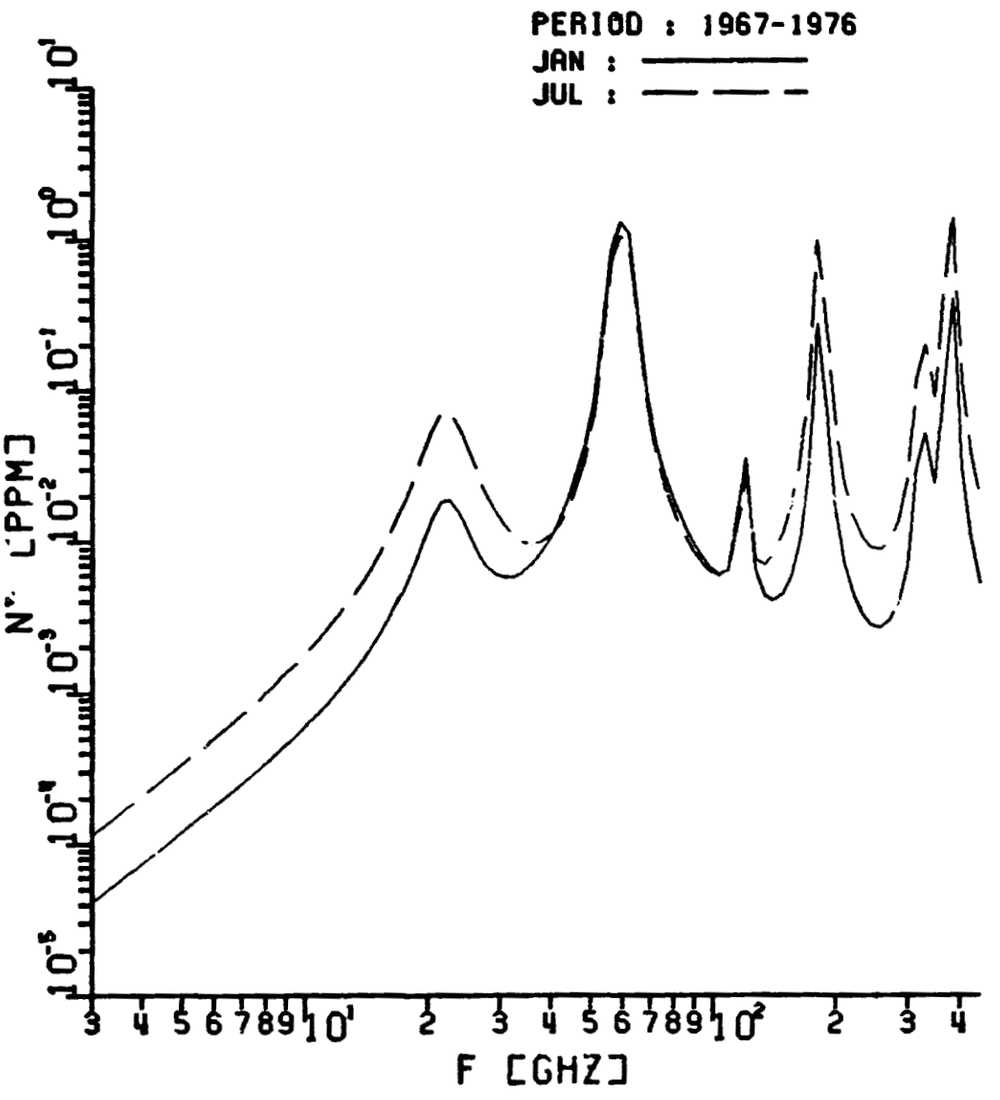

Figure 37. Average imaginary part of refractivity.

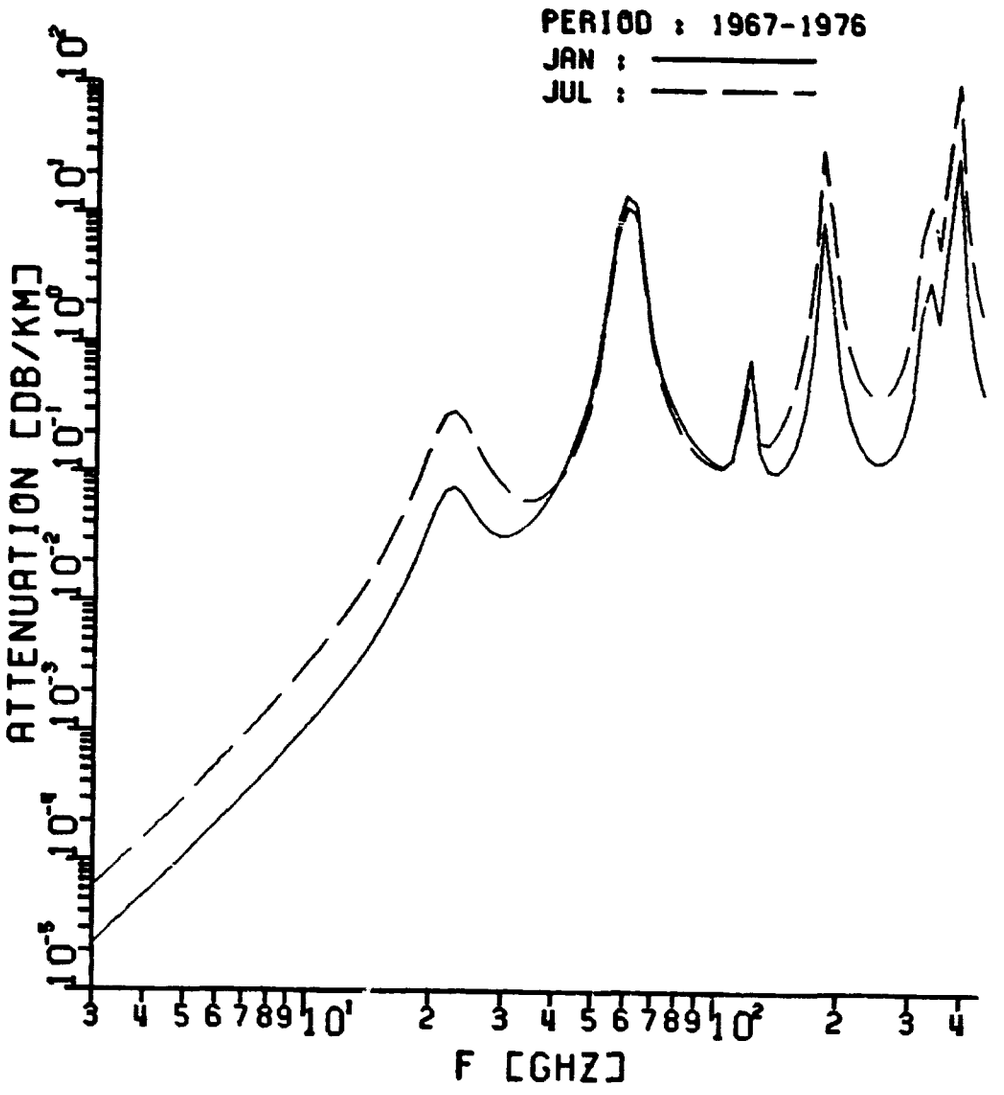

Figure 38. Average attenuation.

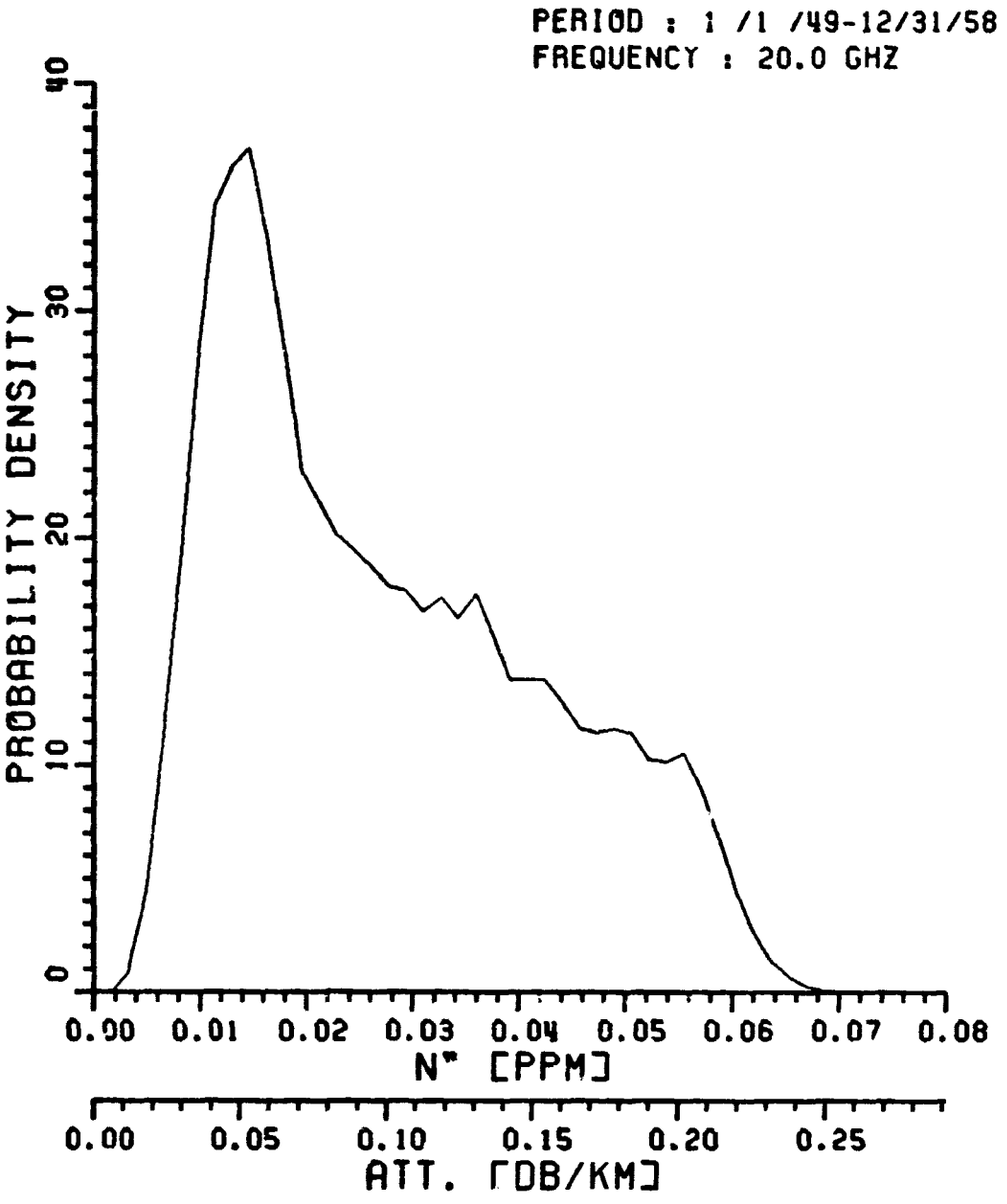

Figure 39. Probability density function of N" at 20 GHz; $\Delta N" = 1.6 \times 10^{-3}$ [ppm].

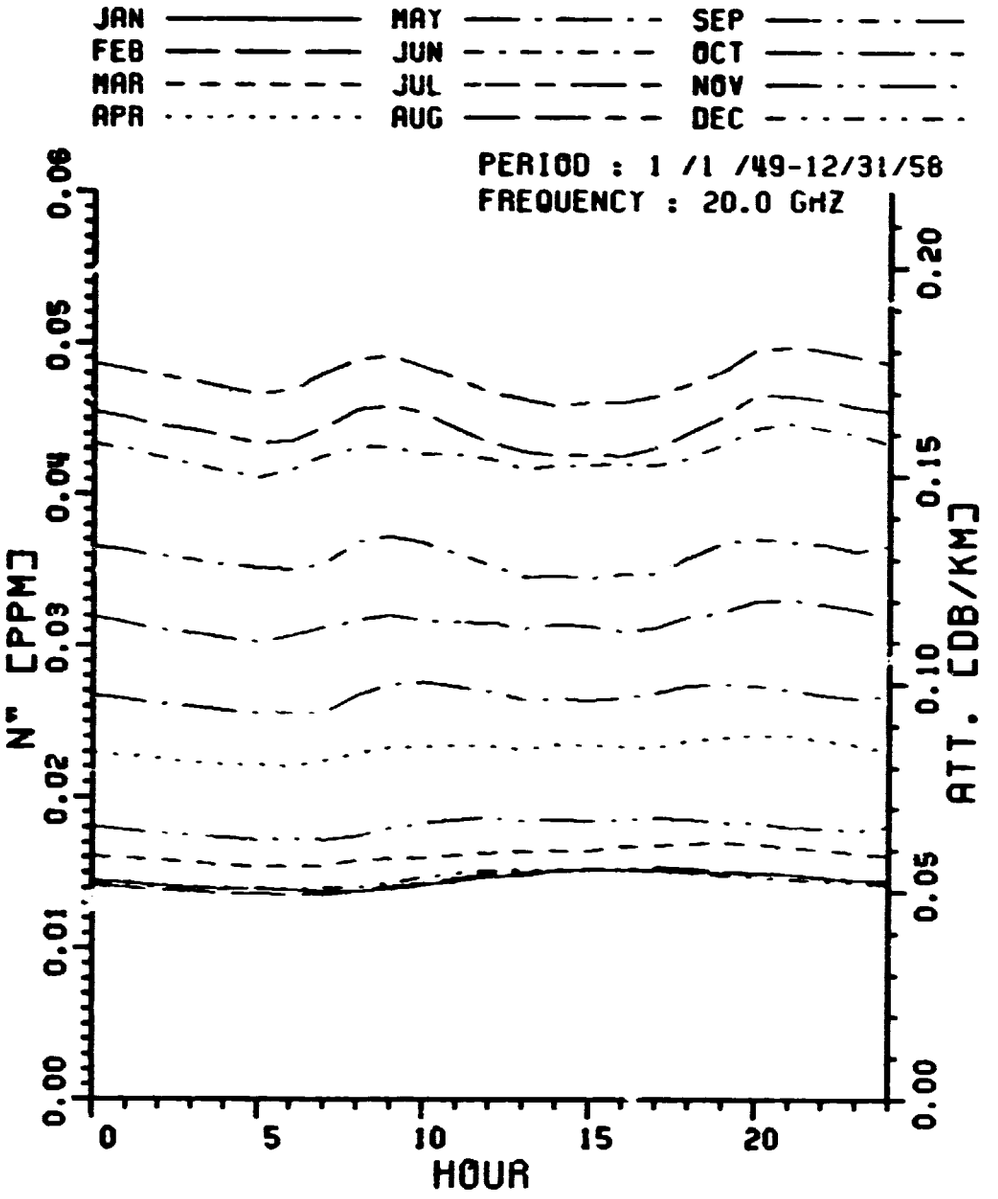

Figure 40. Average diurnal variation of N'' at 20 GHz.

Figure 41. Daily maximum, average, minimum, and extreme N" at 20 GHz by months.

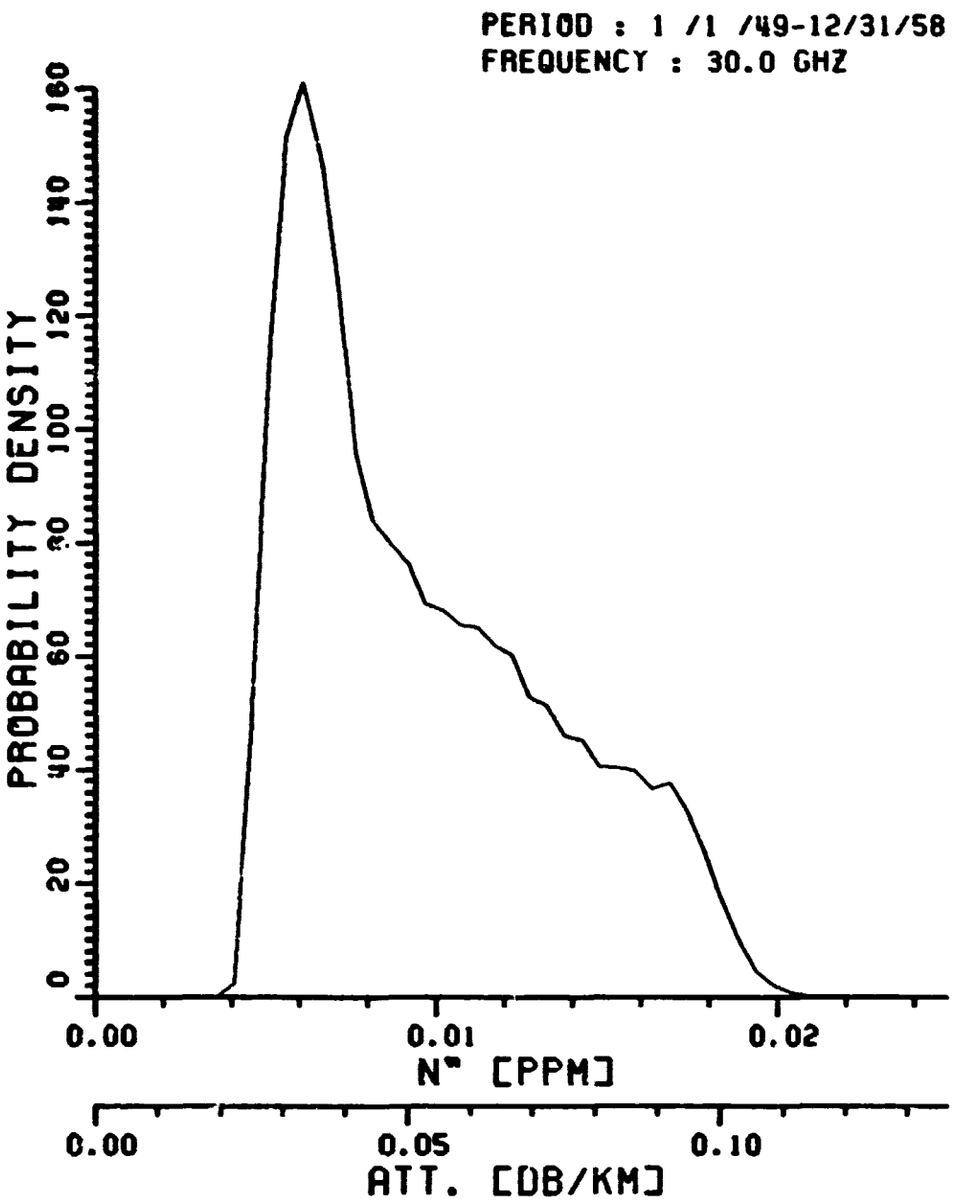

Figure 42. Probability density function of N" at 30 GHz; $\Delta N" = 5 \times 10^{-4}$ [ppm].

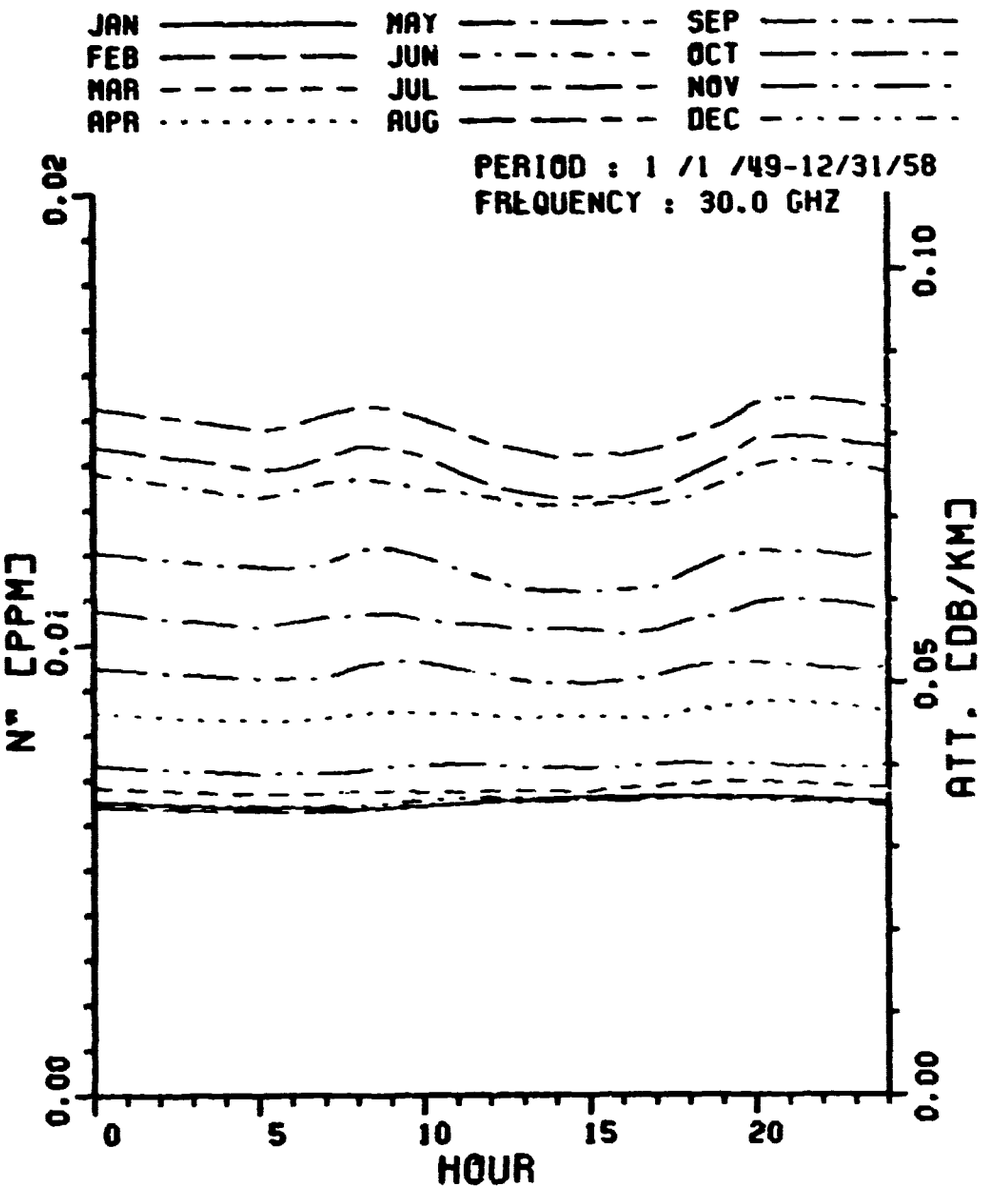

Figure 43. Average diurnal variation of N" at 30 GHz.

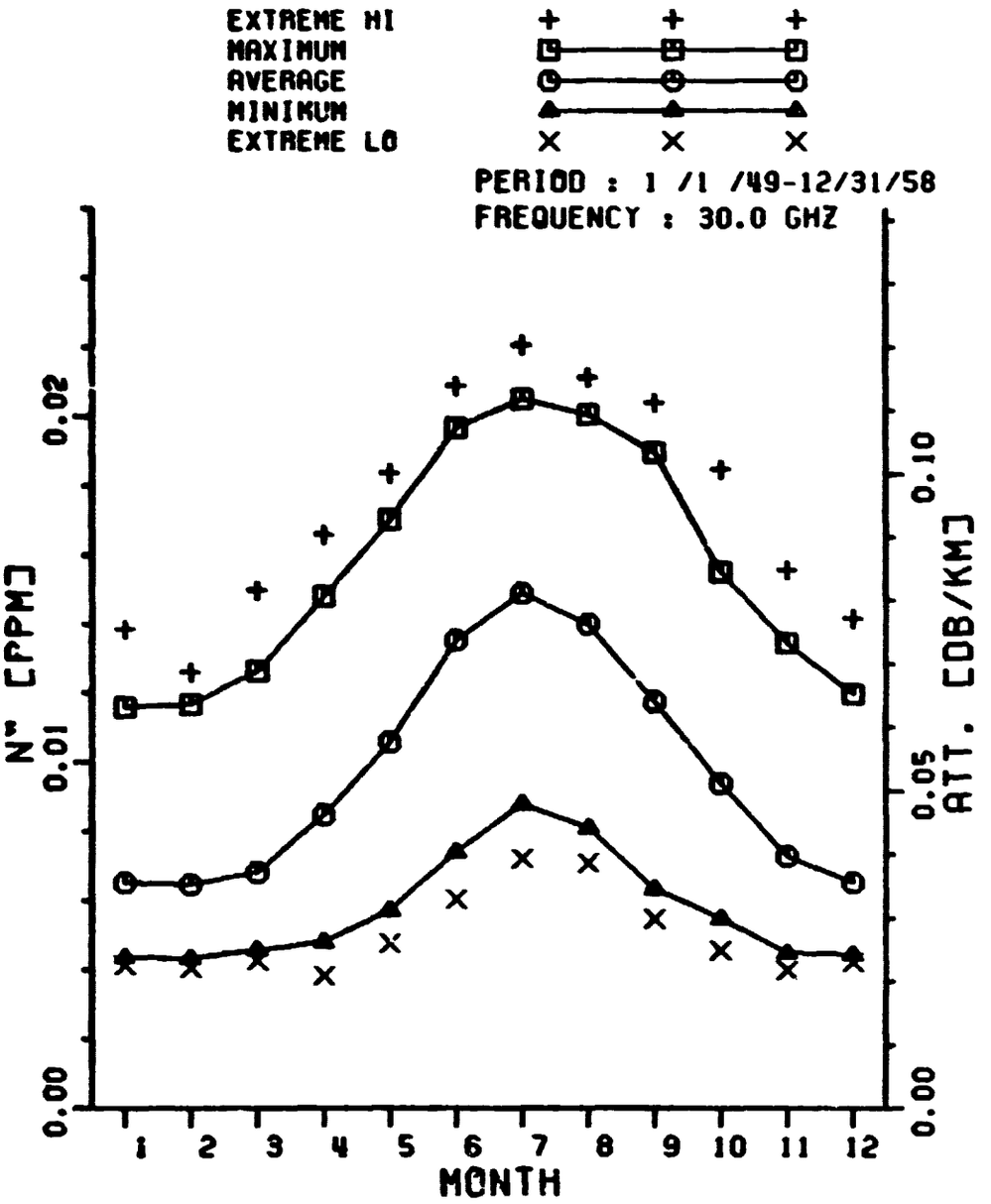

Figure 44. Daily maximum, average, minimum, and extreme N" at 30 GHz by months.

CHAPTER V

ATMOSPHERIC REFRACTION

In a standard atmosphere, pressure and water vapor decrease rapidly with height, while temperature decreases slowly with height from the ground level to the troposphere. It is evident in such an atmosphere that the refractive index of the atmosphere decreases approximately in an exponential fashion with height; and, as a result, waves travelling in the atmosphere are bent downward under normal atmospheric conditions. The effects of this atmospheric refraction of radio waves are usually expressed in terms of the angle through which a radio ray turns as it passes through the atmosphere. To the radar engineer, it is important to estimate the elevation angle error which is a measure of the difference between the apparent elevation angle as indicated by radar and the true elevation angle. Usually the calculation of the effects of the atmospheric refraction depends on the refractive index profile model used and the numerical integration techniques.

In this chapter, we will develop analytic expressions for the bending angle, elevation angle error, and range error in an exponentially tapered spherical atmosphere.

A. Refractive Index Profile

In atmospheric refraction studies, it is necessary to have a knowledge of the behavior of the refractive index as a function of position.

It is common to assume that the refractive index of the atmosphere is spherically stratified with respect to the surface of the earth. Neglecting the effect of horizontal variations seems quite reasonable in the tropospheric region because of the relatively slow horizontal change of refractive index in contrast to the rapid decrease with height under normal conditions.

An examination of long term climatic data of N_s and of ΔN, where ΔN is the decrease in refractivity over the first kilometer in the atmosphere and N_s is the refractivity at the surface of the earth, reveals that a high correlation exists between these two parameters. The empirically derived relationship (7) is,

$$\Delta N = 7.32 \exp [0.005577 \ N_s] \qquad (5\text{-}1.1)$$

This relationship between ΔN and N_s suggests that a model of the atmospheric refractivity structure in the first kilometer above the earth's surface may be obtained from N_s alone. A consideration of the standard atmosphere (Figure 1) and Equation (4-1.7) indicates that the refractivity generally decreases exponentially with height.

The exponential model specified by assuming a single exponential distribution of N is

$$N = N_s \exp \{-c \ (r-r_s)\} \qquad (5\text{-}1.2)$$

where N_s = refractivity at radius r_s

$$C = \ln \left(\frac{N_s}{N_s - \Delta N} \right) = - \ln \left(\frac{N_s - \Delta N}{N_s} \right)$$

Even though this exponential model does not give a good representation of

refractivity above 5km, it is widely used in theoretical studies because of the advantage of being an entire function. Furthermore, since most of the refraction effects occur in the lower portion of the troposphere where the refractivity is largest, the accuracy of the model for larger heights is of less importance.

If we assume $\frac{\Delta N}{N_s} << 1$ (typically $\frac{\Delta N}{N_s} = \frac{39}{301} = 0.13$), then $C = -\ln\left(1 - \frac{\Delta N}{N_s}\right) \approx \frac{\Delta N}{N_s}$. Hence, our simplified exponential model will be described as:

$$N = N_s \exp\left[-\frac{\Delta N}{N_s}(r-r_s)\right] \qquad (5\text{-}1.3)$$

This exponential model and Equation (5-1.1) will be used in the following section to develop the bending angle.

B. Bending Angle

If it is assumed that the refractive index is a function only of a height, then the path of a radio ray (Figure 45) will obey Snell's law for polar coordinates:

$$n_1 r_1 \cos\theta_1 = nr\cos\theta = n_2 r_2 \cos\theta_2 \qquad (5\text{-}2.1)$$

The classical expression for the angular change, τ, or the bending of a ray travelling from a point where the refractive index is n_1 to a second point where the refractive index is n_2 is given by (7)

$$\tau_{1,2} = -\int_{n_1}^{n_2} \cot\theta \frac{dn}{n} \qquad (5\text{-}2.2)$$

where θ is the local elevation angle. The differential equation for τ will be:

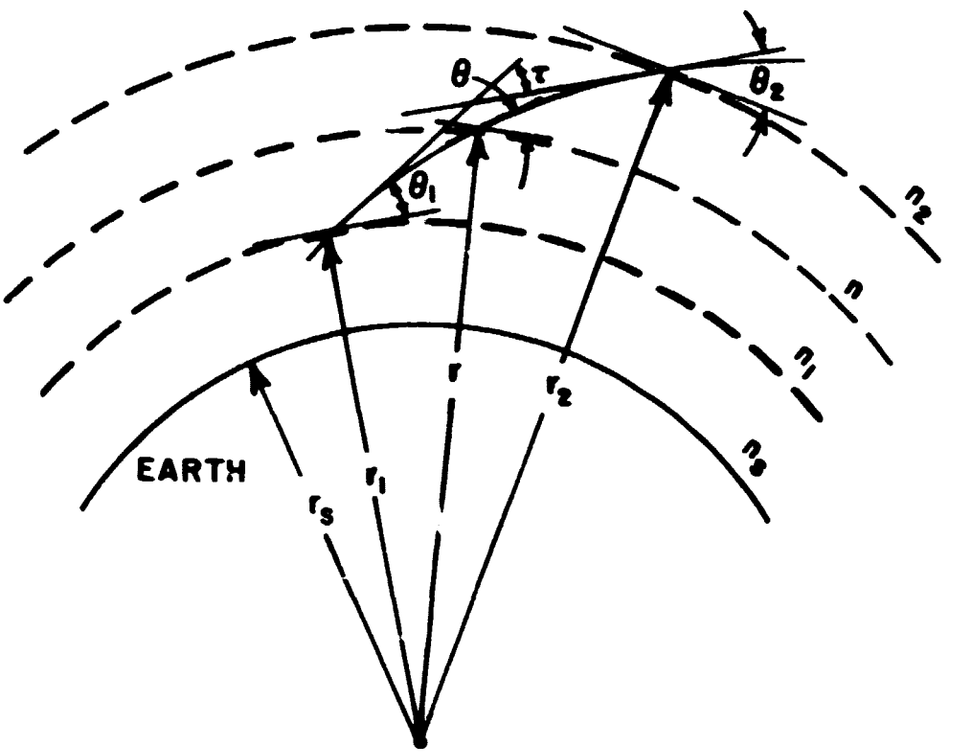

Figure 45. Geometry of the refraction of radio waves.

$$d\tau = - \cot \theta \frac{dn}{n} \tag{5-2.3}$$

Since n ranges from about 1.0000 at very high altitude to about 1.0003 at the surface of the earth, Equation (5-2.1) can be approximated as

$$r_1 \cos \theta_1 = r \cos \theta$$

or

$$\cos \theta = \frac{r_1}{r} \cos \theta_1 \tag{5-2.4}$$

Now, by using trigonometry,

$$\cot \theta = \frac{r_1 \cos \theta_1}{\sqrt{r^2 - r_1^2 \cos^2 \theta_1}} \tag{5-2.5}$$

Substituting Equation (5-2.5) into Equation (5-2.3) yields,

$$d_\tau = - \frac{r_1 \cos \theta}{\sqrt{r^2 - r_1^2 \cos^2 \theta_1}} \cdot \frac{1}{n} \cdot \frac{dn}{dr} dr \tag{5-2.6}$$

and, since $\frac{1}{n} \simeq 1$,

$$d_\tau \simeq - \frac{r_1 \cos \theta_1}{\sqrt{r^2 - r_1^2 \cos^2 \theta_1}} \frac{dn}{dr} dr$$

or

$$\tau = -r_1 \cos \theta_1 \int_{r_1}^{r_2} \frac{1}{\sqrt{r^2 - r_1^2 \cos \theta_1^2}} \frac{dn}{dr} dr \tag{5-2.7}$$

If $\frac{dn}{dr}$, the rate of change of the index of refraction with radius, is known, the bending angle, τ, may be calculated. In Section A, we developed an exponential model for refractive index structure:

$$N = N_s \exp\left[-\frac{\Delta N}{N_s}(r - r_s)\right] \tag{5-2.8}$$

So, the derivative of refractive index is

$$\frac{dn}{dr} = -\Delta N \exp\left[-\frac{\Delta N}{N_s}(r - r_s)\right] \times 10^{-6} \tag{5-2.9}$$

where

$\Delta N = 7.32 \exp[0.005577\ N_s]$

N_s = refractivity at the surface of earth

r_s = radius of the earth

Combining Equation (5-2.9) with Equation (5-2.8) gives

$$\tau = r_1\ \Delta N \cdot 10^{-6} \cos\theta_1 \exp\left[\frac{\Delta N}{N_s}\ r_s\right]$$

$$\int_{r_1}^{r_2} \frac{\exp\left[-\frac{\Delta N}{N_s} r\right]}{\sqrt{r_2 - r_1^2 \cos^2\theta_1}}\ dr \tag{5-2.10}$$

Let us now change variables, $h = r - r_1$, so that h represents the height above the starting point, r_1. And let $H = r_2 - r_1$ be the total increase in height when moving from point 1 to point 2. The Equation (5-2.10) will be

$$\tau = r_1\ \Delta N \cdot 10^{-6} \cos\theta_1 \exp\left[-\frac{\Delta N}{N_s}(r_1 - r_s)\right]$$

$$\int_0^H \frac{\exp\left(-\frac{\Delta N}{N_s} h\right)}{\sqrt{(h + r_1)^2 - r_1^2 \cos^2\theta_1}}\ dh \tag{5-2.11}$$

Now we note that, even for a large H, the integrand is forced to zero by the exponential in the numerator. It is apparent that almost all of the refraction occurs within the lowest twenty km of the atmosphere. With h = 19km, the numerator, $\exp\left(-\frac{\Delta N}{N_s}h\right)$, drops to 0.1. So the second order term in the denominator of the integrand may be ignored:

$$\tau = \Delta N \cdot 10^{-6} \cos\theta_1 \exp\left[-\frac{\Delta N}{N_s}(r_1 - r_s)\right]$$

$$\int_0^H \frac{\exp\left(-\frac{\Delta N}{N_s}h\right)}{\sqrt{2\frac{h}{r_1} + \sin^2\theta_1}}\, dh \qquad (5\text{-}2.12)$$

Introducing another change of variables, $2\frac{h}{r_1} + \sin^2\theta_1 = \chi^2$, gives:

$$\tau = r_1 \Delta N \cdot 10^{-6} \cos\theta_1 \exp\left[-\frac{\Delta N}{N_s}(r_1 - r_s)\right] \exp\left[\frac{\Delta N}{N_s}\frac{r_1}{2}\sin^2\theta_1\right]$$

$$\int_{\sin\theta_1}^{\sqrt{\frac{2H}{r_1} + \sin^2\theta_1}} \exp\left[-\frac{\Delta N}{N_s}\frac{r_1}{2}\chi^2\right] d\chi \qquad (5\text{-}2.13)$$

And, with yet another change of variables, $\frac{\Delta N}{N_s}\frac{r_1}{2}\chi^2 = t^2$, Equation (5-2.13) reduces to:

$$\tau = \sqrt{2r_1 \Delta N \cdot N_s}\; 10^{-6} \cos\theta_1 \exp\left[-\frac{\Delta N}{N_s}(r_1 - r_s)\right] \exp\left[\frac{\Delta N}{N_s}\frac{r_1}{2}\sin^2\theta_1\right] \int_{\sqrt{\frac{\Delta N}{N_s}\frac{r_1}{2}\sin\theta_1}}^{\sqrt{\frac{\Delta N}{N_s}\left(H + \frac{r_1}{2}\sin^2\theta_1\right)}} \exp(-t^2)\, dt \qquad (5\text{-}2.14)$$

Since the error function is defined as $\Phi(\chi) = \frac{2}{\sqrt{\pi}} \int_0^{\chi} \exp(-\chi^2)\, d\chi$, we have

$$\tau = \sqrt{\frac{\pi}{2} r_1 \Delta N \cdot N_s}\ 10^{-6} \cos\theta_1 \exp\left[-\frac{\Delta N}{N_s}(r_1 - r_s)\right] \exp\left[\frac{\Delta N}{N_s}\frac{r_1}{2} \sin^2\theta_1\right] \left\{\Phi\left(\sqrt{\frac{\Delta N}{N_s}\left(H + \frac{r_1}{2}\sin^2\theta_1\right)}\right) - \Phi\left(\sqrt{\frac{\Delta N}{N_s}\frac{r_1}{2}}\sin\theta_1\right)\right\} \quad (5\text{-}2.15)$$

This is the general expression for the bending angle in a single exponential model defined by Equation (5-1.3).

We can calculate the bending angle for various situations by using the following rational approximation of the error function (8):

$$\Phi(\chi) = 1 - \frac{1}{[1 + a_1\chi + a_2\chi^2 \ldots\ldots + a_6\chi^6]^{16}} + \varepsilon(\chi) \quad (5\text{-}2.16)$$

where

$|\varepsilon(\chi)| \leq 3 \times 10^{-7}$

$a_1 = 0.0705230784$ $\qquad$ $a_2 = 0.0422820123$

$a_3 = 0.0092705272$ $\qquad$ $a_4 = 0.0001520143$

$a_5 = 0.0002765672$ $\qquad$ $a_6 = 0.0000430638$

But for a large initial elevation angle, θ_1, the error functions converge to 1 and $\frac{\Delta N}{N_s}\frac{r_1}{2}\sin^2\theta_1$ becomes a very large value. So in this case, we must use the asymptotic relation for the error function (8):

$$\Phi(\chi) = 1 - \frac{1}{\sqrt{\pi}\,\chi} \exp(-\chi^2) \quad (5\text{-}2.17)$$

The criteria for this will be:

$$\sqrt{\frac{\Delta N}{N_s}\frac{r_1}{2}}\ \sin\theta_1 \gg 1$$

This condition corresponds to $\theta_1 >> 2.89°$ for typical values of ΔN, N_s, and r_1. Then, the bending angle for high initial elevation angle is given by:

$$\tau = N_s \cdot 10^{-6} \cos\theta_1 \exp\left[-\frac{\Delta N}{N_s}(r_1 - r_s)\right] \left[\sin\theta_1 - \frac{\exp\left[-\frac{\Delta N}{N_s} H\right]}{\sqrt{\frac{2H}{r_1} + \sin^2\theta_1}}\right] \quad , \theta_1 >> 3° \qquad (5\text{-}2.18)$$

Figures 46 and 47 show the bending angle versus refractivity for 70km and 35,785km heights. The nominal height of a geosynchronous satellite above the earth of radius r_s = 6,378 km is 35,785 km (9). Since most of the refraction occurs in the region below twenty km, there is no noticeable difference between these two figures.

C. Elevation Angle Error

For earth-satellite communication links, where narrow beamwidth antennas are often used, the elevation angle error, ε, cannot be ignored. To find this error, consider the geometry shown in Figure 48. Summing all the angles about the quadrilateral defined by two radii r_1 and r_2 and two local tangents at points ① and ② gives the relationship:

$$\phi = \tau + \theta_2 - \theta_1 \qquad (5\text{-}3.1)$$

From the geometry shown in Figure 48,

$$\tan\beta = \frac{r_1 \cos\theta - r_2}{r_2 \sin\phi} \qquad (5\text{-}3.2)$$

Since $\varepsilon = \theta_1 - \beta$, substituting Equation (5-3.1) in Equation (5-3.2)

Figure 46. Bending angle versus refractivity for various initial elevation angles; H = 70 km.

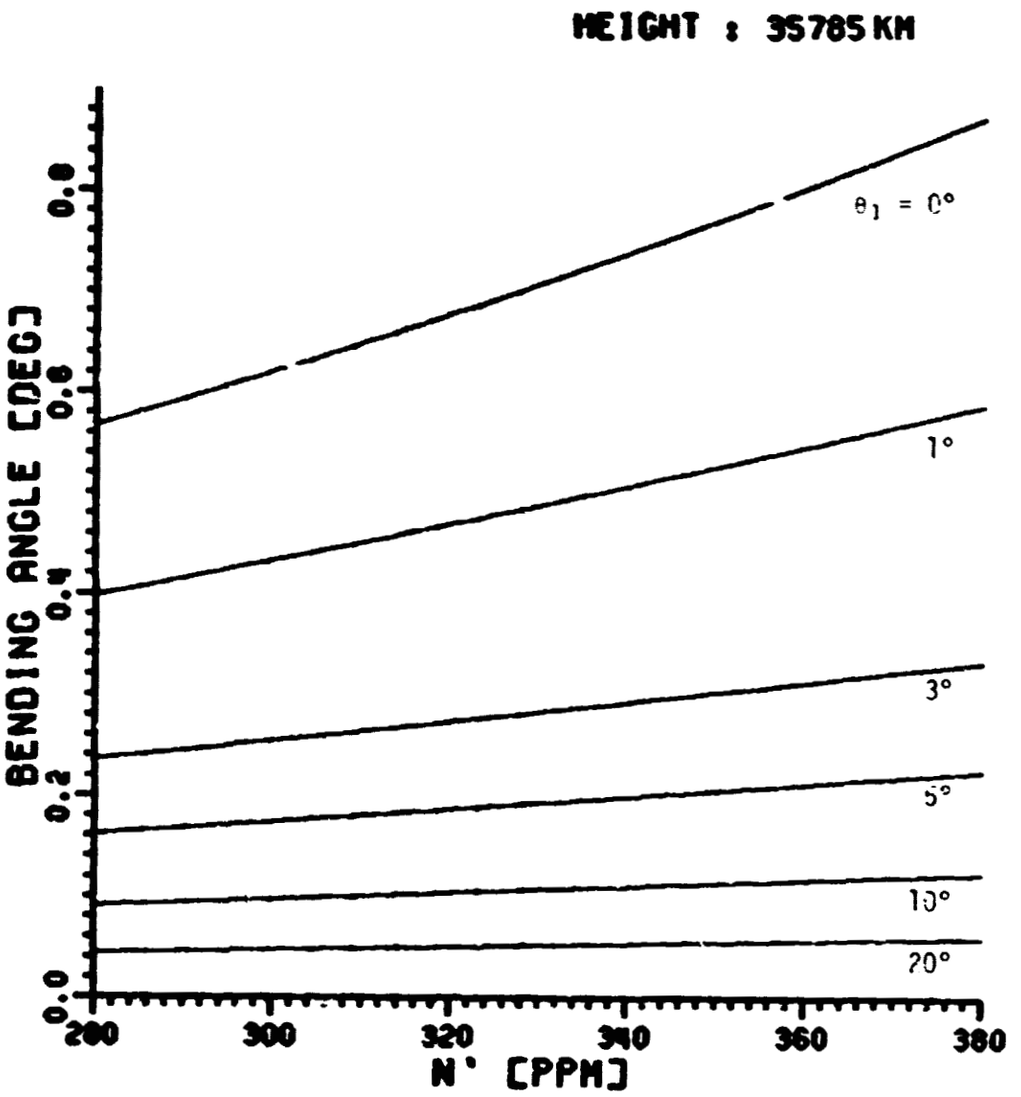

Figure 47. Bending angle versus refractivity for various initial elevation angles; H = 35,785 km.

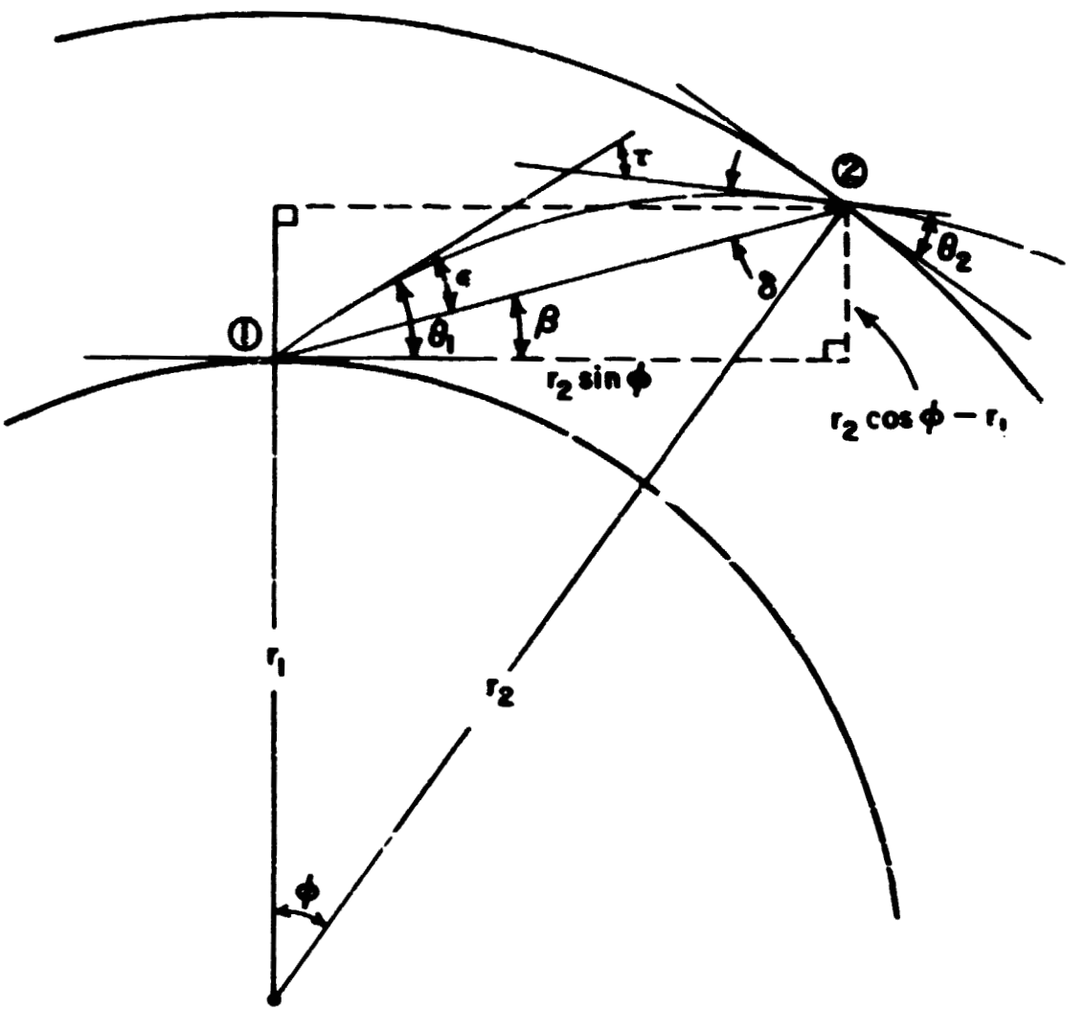

Figure 48. Geometry for elevation angle error.

yields:

$$\tan\epsilon = \frac{\tan\theta_1 - \tan\beta}{1 + \tan\theta_1\tan\beta}$$

$$= \frac{-r_2\cos\tau\cos\theta_2 + r_2\sin\tau\sin\theta_2 + r_1\cos\theta_1}{r_2\sin\tau\cos\theta_2 + r_2\cos\tau\sin\theta_2 - r_1\sin\theta_1} \qquad (5\text{-}3.3)$$

From Equation (5-2.1),

$$r_1\cos\theta_1 = \frac{n_2}{n_1} r_2\cos\theta_2 \qquad (5\text{-}3.4)$$

Dividing denominator and numerator of the right hand side of Equation (5-3.3) by $r_1\cos\theta_1$ gives:

$$\tan\epsilon = \frac{-\cos\tau + \sin\tau\tan\theta_2 + \frac{n_2}{n_1}}{\sin\tau + \cos\tau\tan\theta_2 - \frac{n_2}{n_1}\tan\theta_1}$$

or

$$\epsilon = \text{Arctan}\left(\frac{-\cos\tau + \sin\tau\tan\theta_2 + \frac{n_2}{n_1}}{\sin\tau + \cos\tau\tan\theta_2 - \frac{n_2}{n_1}\tan\theta_1}\right) \qquad (5\text{-}3.5)$$

Here, the bending angle, τ, can be obtained from the expressions in Section A, and the angle between the local ray tangent and the local horizontal at point ②, θ_2, can be obtained using Equation (5-3.4) if we know r_1, r_2, and θ_1.

In Figures 49 and 50, we plot the elevation angle error for 70 and 35,785 [km], respectively. Comparison of these figures shows that the elevation angle error increases with the height of the end of the ray path.

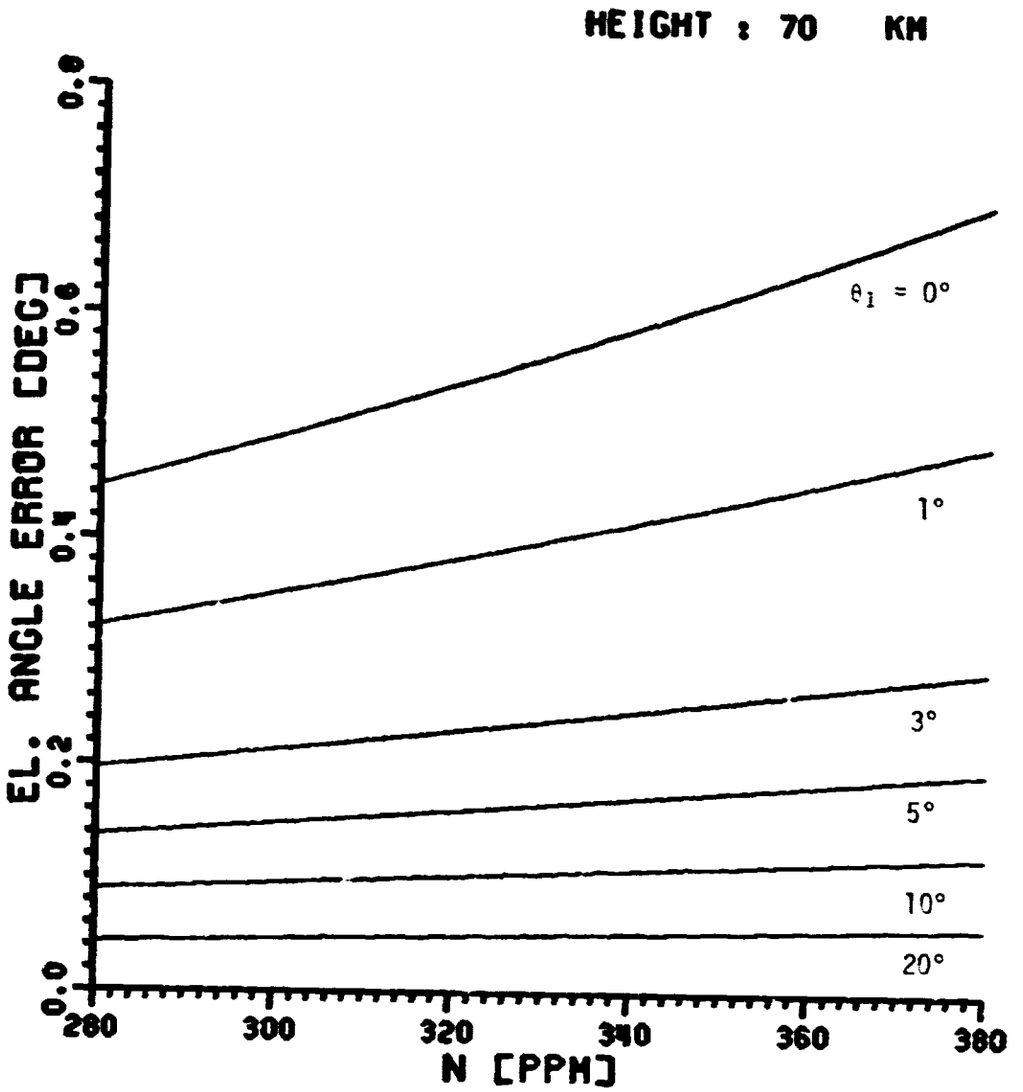

Figure 49. Elevation angle error versus refractivity for various initial elevation angles; H = 70km.

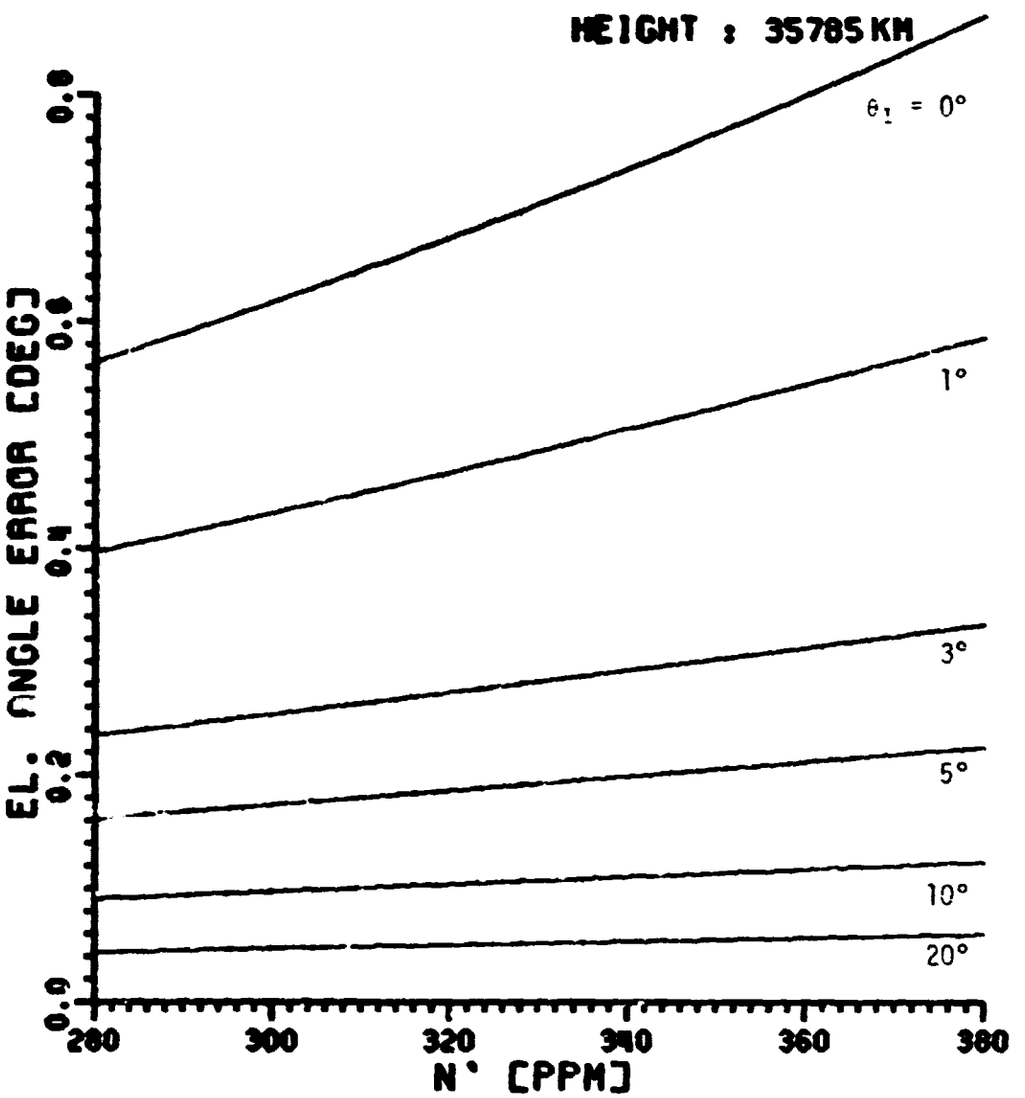

Figure 50. Elevation angle error versus refractivity for various initial elevation angles; H = 35,785km.

D. Range Error

When a radio signal travels from point ① to point ② (see Figure 48), the time delay is longer than would be expected if the signal traveled through a free space for two reasons. First, the path is longer due to the ray bending. And, second, the velocity of propagation is lower in a refractive medium. The true slant distance, R_{true}, may be obtained from the geometry of Figure 48.

$$R_{true} = \sqrt{r_1^2 + r_2^2 - 2r_1r_2\cos\phi} \qquad (5\text{-}4.1)$$

Since $\phi = \tau - \theta_1 + \cos^{-1}(\frac{r_1}{r_2}\cos\theta_1)$, we can calculate R_{true} if we know r_1, r_2, and θ_1. The bending angle, τ, may be obtained from Equation (5-2.15) or (5-2.18). The apparent distance is given by:

$$R_a = cT = \int_{r_1}^{r_2} n\,ds \qquad (5\text{-}4.2)$$

where T is the time delay for the signal travelling from point ① to ② and c is the velocity of light in free space. Since $ds = \frac{1}{\sin\theta}\,dr$ and $n = 1 + N \times 10^{-6}$, the above equation will be:

$$R_a = \int_{r_1}^{r_2} \frac{1}{\sin\theta}\,dr + 10^{-6}\int_{r_1}^{r_2} \frac{N}{\sin\theta}\,dr \qquad (5\text{-}4.3)$$

Thus, the total apparent range error, $\Delta R = R_a - R_{true}$, is given by:

$$\Delta R = \int_{r_1}^{r_2} \frac{1}{\sin\theta}\,dr + 10^{-6}\int_{r_1}^{r_2} \frac{N}{\sin\theta}\,dr - R_{true} \qquad (5\text{-}4.4)$$

The first term represents the length of the curved ray path. Since the difference in length between the straight path and the curved ray path does not represent a significant portion of the total range error except

at very small initial elevation angles, below about 3° (7), the range error for elevation angles greater than about 3° may be given by

$$\Delta R \cong 10^{-6} \int_{r_1}^{r_2} \frac{N}{\sin\theta} \, dr \qquad (5\text{-}4.5)$$

Substituting Equation (5-1.3) into Equation (5-4.5), and changing variables, $r = r_1+h$ and $r_2 = r_1+H$, yields:

$$\Delta R = N_s \times 10^{-6} \exp\left[-\frac{\Delta N}{N_s}(r_1-r_s)\right]$$

$$\int_0^H \frac{(1+\frac{h}{r_1}) \exp\left[-\frac{\Delta N}{N_s} h\right]}{\sqrt{1+\frac{2h}{r_1}+\frac{h^2}{r_1^2}-\cos^2\theta_1}} \, dh \qquad (5\text{-}4.6)$$

Note that the integrand is significant only when h is very small. Neglecting the higher order terms in $\frac{h}{r_1}$, and from Equation (5-2.12), the range error can be related to the bending angle, τ, by

$$\Delta R = \frac{N_s}{\Delta N} \frac{\tau}{\cos\theta_1} \qquad (5\text{-}4.7)$$

The range errors versus the surface refractivity are plotted in Figures 51 and 52 for H = 70 km, H = 35,785 km, respectively. These may be used for the first order approximation of the range error. It should be emphasized that the difference between the straight and the curved path contributes nearly thirty percent of the total range error at zero elevation angle (7).

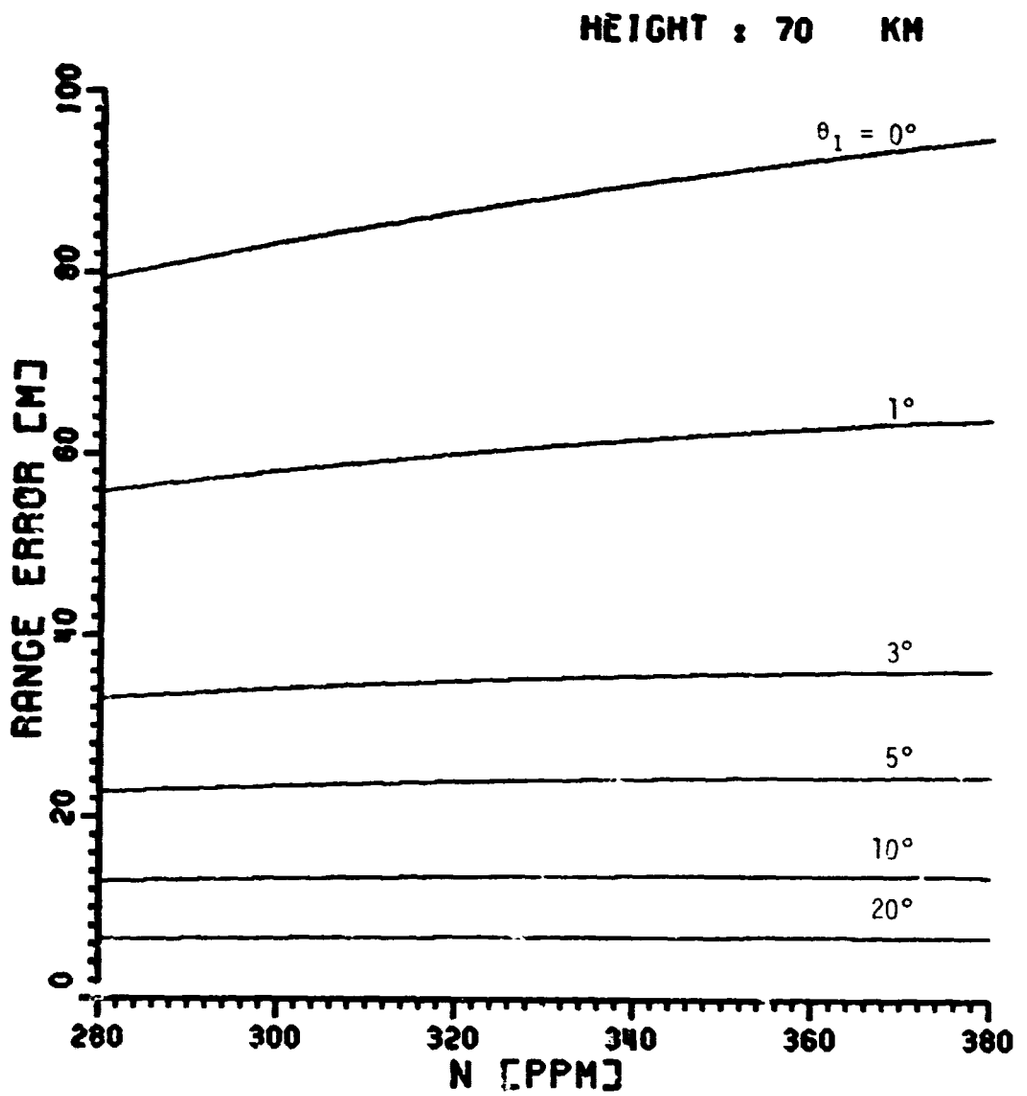

Figure 51. Range error versus refractivity for various initial elevation angles; H= 70km.

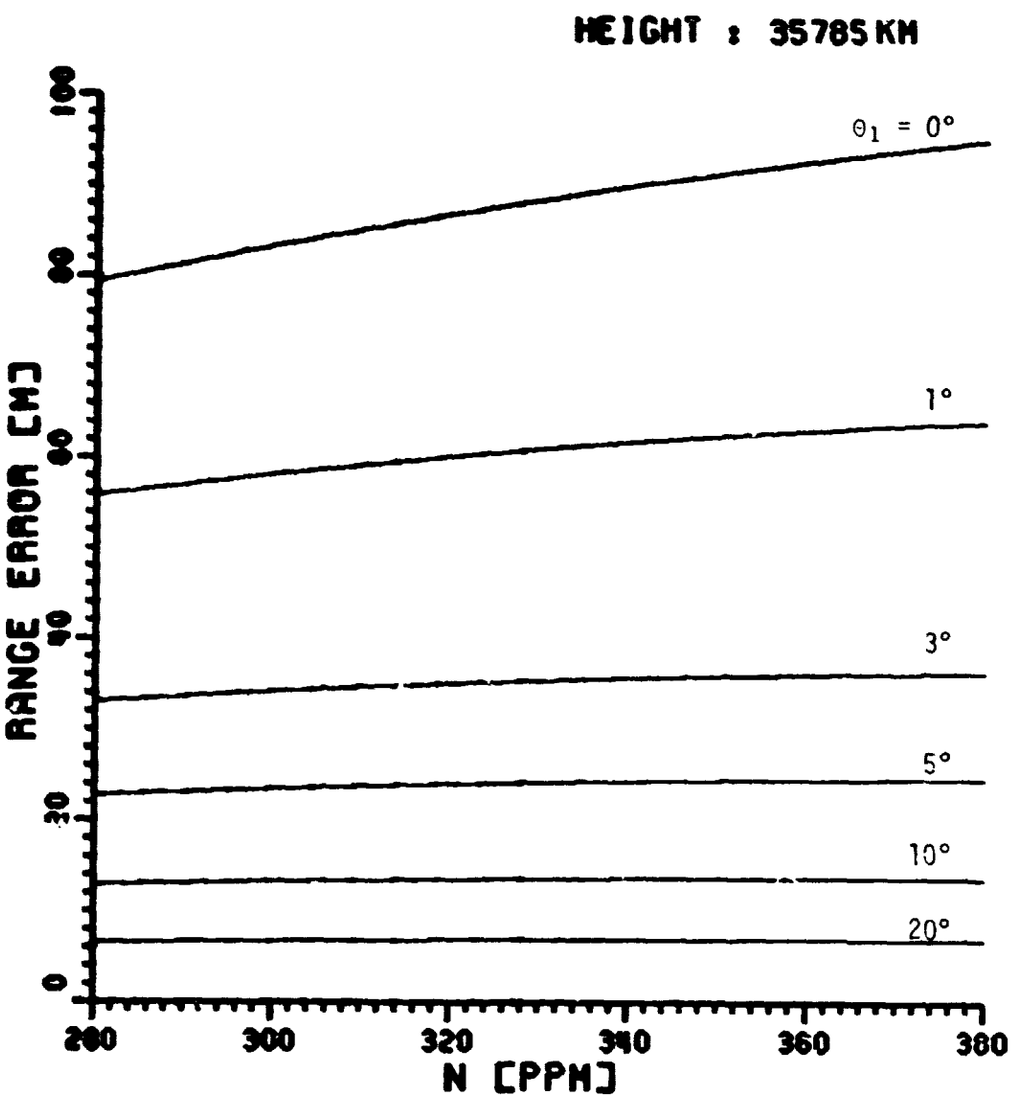

Figure 52. Range error versus refractivity for various initial elevation angles; H = 35,785 km.

CHAPTER VI

SUMMARY

The atmosphere is a most changeable propagation media; and its electrical characteristic, microwave refractivity, is dependent on temperature, pressure, and water vapor content. The statistics of these meteorological quantities at Columbus, Ohio, were generated using two ten-year period weather data bases from the National Weather Service.

The microwave refractivity was calculated using these meteorological data bases and its variations were plotted and analyzed. In the calculation of the microwave refractivity for the EHF range, the Gross line shape was used. The frequency independent refractivity varies from about 280 to 380 [ppm] and the average seasonal variation is about 35 [ppm]. The average seasonal variation of attenuation due to the atmospheric gases is about 0.13 dB/km at 20 GHz, and 0.05 dB/km at 30 GHz. The maximum variations of these are 0.2 and 0.1 db/km, respectively.

Based on a single exponential model for the atmospheric refractivity structure, bending angle, elevation angle error, and range error were developed and plotted. Most of refraction occurs in the lower region of troposphere because the refractivity decays exponentially with height. For small elevation angles, below about 5°, the refraction effects are very sensitive to the refractivity at the earth's surface.

REFERENCES

1. J.H. Van Vleck, "The Absorption of Microwave by Oxygen," Phys. Rev., Vol. 71, pp. 413-424, April 1947.

2. T.L. Oliver, "Atmospheric Attenuation and Sky Noise Temperature in the Microwave and mm Wave Spectrum," Report 2440-2, May 1968, The Ohio State University ElectroScience Laboratory, Department of Electrical Engineering; prepared under Contract F33615-67-C-1663 for Air Force Avionics Laboratory.

3. W.I. Thomson, III, "Atmospheric Transmission Handbook," Nat. Aeron. and Space Adm., p. 27, Washington, D.C., 1971.

4. A. Miller and J.C. Thomson, "Elements of Meteorology," C.E. Merrill Publishing Company, pp. 30, Columbus, Ohio, 1970.

5. H.J. Liebe and G.G. Gimmestad, "Calculation of Clear Air EHF Refractivity," Rad. Science, Vol. 13, pp. 245-251, April 1978.

6. A.I. Omoura and D.B. Hodge, Microwave Dispersion and Absorption due to Atmospheric Gases," Technical Note No. 10, August 1979, The Ohio State University ElectroScience Laboratory, Department of Electrical Engineering, pp. 16-17, 24-25.

7. B.R. Bean and E.J. Dutton, "Radio Meteorology," Dover Publication, Chapter 1, New York, 1968.

8. M. Abramowitz and I.A. Stegun, "Handbook of Mathematical Functions," Dover Publications, pp. 297-299, 1970.

9. H.T. Dougherty, "A Consolidated Model for UHF/SHF Telecommunication Links Between Earth and Synchronous Satellites," U.S. Department of Commerce, pp. 66, August 1980.

10. National Climatic Center, "Local Climatological Data, Columbus, Ohio," U.S. Department of Commerce, 1973.

APPENDIX A

CODING AND FORMAT OF METEOROLOGICAL DATA

Character Set

		HEXADECIMAL	OCTAL
	1	F1	01
	2	F2	02
	3	F3	03
	4	F4	04
	5	F5	05
	6	F6	06
	7	F7	07
	8	F8	10
	9	F9	11
	0	F0	12
	Δ (blank)	40	20
	-	60	40
	*	5C	54
	&	50	60
	A	C1	61
	B	C2	62
	C	C3	63
	D	C4	64
*	E	C5	65
	F	C6	66
	G	C7	67
	H	C8	70
	I	C9	71
	J	D1	41
	K	D2	42
	L	D3	43
	M	D4	44
**	N	D5	45
	O	D6	46
	P	D7	47
	Q	D8	50
	R	D9	51
*		C0	72
**		D0	52
		E0	32

* C0 through C9 in hexadecimal represent positive decimal numbers.
** D0 through D9 in hexadecimal represent negative decimal numbers.

Record Format

TAPE FIELD NUMBER	TAPE POSITIONS	ELEMENT
001	001 - 004	Tape deck number
002	005 - 009	Station number
003	010 - 011	Year
004	012 - 013	Month
005	014 - 015	Day
101	016 - 017	Hour
102	018 - 021	Ceiling height and indicator
103	022 - 025	Horizontal visibility and indicator
104	026 - 027	Wind direction - 16 points
105	028 - 030	Wind speed
106	031 - 033	Dry bulb (air) temperature
107	034 - 036	Wet bulb temperature
108	037 - 039	Dew point temperature
109	040 - 043	Relative humidity and indicator
110	044 - 048	Sea level pressure
111	049 - 052	Station pressure
112	053 - 057	Sky condition and indicator
113	058	Total sky cover
114	059	Total opaque sky cover
115	060	Amount of lowest cloud layer
116	061	Type of lowest cloud or obscuring phenomena
117	062 - 064	Height of base of lowest cloud layer or obscuring phenomena
118	065	Amount of second cloud layer
119	066	Type of cloud - second layer
120	067 - 069	Height of base of second cloud layer
121	070	Summation amount of first two cloud layers
122	071	Amount of third cloud layer
123	072	Type of cloud - third layer
124	073 - 075	Height of base of third cloud layer
125	076	Summation amount of first three cloud layers
126	077	Amount of fourth cloud layer
127	078	Type of cloud - fourth layer
128	079 - 081	Height of base of fourth cloud layer
129	082	Occurrence of thunderstorm, tornado, or squall
130	083	Occurrence of rain, rain showers, or freezing rain

TAPE FIELD NUMBER	TAPE POSITIONS	ELEMENT
131	084	Occurrence of rain squalls, drizzle, or freezing drizzle
132	085	Occurrence of snow, snow pellets, or ice crystals
133	086	Occurrence of snow showers, snow squalls or snow grains
134	087	Occurrence of sleet, sleet showers or hail
135	088	Occurrence of fog, blowing dust, or blowing sand
136	089	Occurrence of smoke, haze, smoke and haze, dust, blowing snow, blowing spray
137	090 - 091	Wind direction - 36 points
138	092 - 094	Blank
139	095	Record mark
201 - 239	096 - 175	Second observation } These observations
301 - 339	176 - 255	Third observation } follow the same
401 - 439	256 - 335	Fourth observation } format as fields
501 - 539	336 - 415	Fifth observation } 101-139 (Tape Posi-
601 - 639	416 - 495	Sixth observation } tions 016-095).

C-2

TAPE FIELD NUMBER	TAPE POSITIONS	ELEMENT	TAPE CONFIGURATION	CODE DEFINITIONS AND REMARKS
001	001 - 004	Tape deck number	1400 - 1499	Used to distinguish different data sources. See current list at beginning of manual.
002	005 - 009	Station number	01001 - 98999	Unique number used to identify each station. Usually a WBAN number but occasionally a WMO number.
003	010 - 011	Year	00 - 99	Year of observation. 00-99 = 1900-1999
004	012 - 013	Month	01 - 12	Month of observation. 01-12 = Jan.-Dec.
005	014 - 015	Day	01 - 31	Day of month
101	016 - 017	Hour	00 - 23	Hour of observation in local standard time. 00-23 = 0000-2300 LST
	⋮			
106	031 - 033	Dry bulb (AIP) temperature	00$\bar{1}$ - 13$\bar{0}$	Specified temperature in whole degrees fahrenheit. 00$\bar{1}$-13$\bar{0}$ = -1° - -130°F 00$\dot{0}$-14$\dot{0}$ = 0° - +140°F ΔΔΔ = Unknown ΔΔ* = Original value invalid
	⋮			
109	041 - 043	Relative humidity	001 - 100 ΔΔΔ, ΔΔ*	Relative humidity in whole percentage ΔΔΔ = Unknown ΔΔ* = Original value invalid
	⋮			
111	049 - 052	Station pressure	1900 - 3999 ΔΔΔΔ, ΔΔΔ*	Pressure at station level in inches and hundredths of hg. 1900-3999 = 19.00 - 39.99 in hg. ΔΔΔΔ = Uknown ΔΔΔ* = Invalid